NKS-461
ISBN 978-87-7893-554-0

Source Term And Timing Uncertainty in Severe Accidents

Sergey Galushin[1], Anders Riber Marklund[1]

Dmitry Grischenko[2], Pavel Kudinov[2]

Tuomo Sevón[3], Sara Ojalehto[3], Ilona Lindholm[3]

Patrick Isaksson[4], Elisabeth Tengborn[4]

Naeem Ul-Syed[5]

[1] Vysus Sweden AB

[2] KTH Royal Institute of Technology

[3] VTT Technical Research Centre of Finland Ltd

[4] SSM Swedish Radiation Safety Authority

[5] DSA Norwegian Radiation and Nuclear Safety Authority

July 2022

Abstract

One set of representative accident scenarios and one set of relevant deterministic modelling parameters that can affect Nordic boiling water reactor (BWR) severe accident progression and the magnitude of the source term released to the environment were identified. To achieve this, a set of activities was performed, including review of the safety design of the Swedish and Finnish BWRs; review of the PSA L2 for a typical Nordic BWR and identification of risk significant accident sequences; review of severe accident phenomena and respective modelling in the MELCOR code as well as identification of epistemic modelling parameters that can affect severe accident progression and the source term.

The scenario set was based on review of PSA L2 for a typical Nordic BWR design, as well as insights from the emergency preparedness and response and national regulators, including accident scenarios that lead to acceptable release (diffuse leakage from the intact containment, filtered containment venting in case of transient or LOCA), as well as scenarios that lead to unacceptable release (either due to containment rupture due to ex-vessel phenomena or unfiltered containment venting in case of failed containment isolation, or containment bypass sequences).

In total, 50 MELCOR code parameters were selected for further analysis based on the review of the MELCOR modelling of severe accident phenomena and uncertain epistemic (phenomenological) modelling parameters that can affect severe accident progression and the source term released to the environment. These parameters involved in the modelling of core degradation and relocation, fission products release from fuel, debris behaviour in the core region and vessel lower head, vessel lower head failure, fission products behaviour in the RCS and the containment, as well as modelling of the filter trapping, containment sprays and pool scrubbing.

Best-estimate and bounding assessments of the magnitude of fission products released to the environment were performed for the set of selected scenarios and parameters using MELCOR simulations performed at KTH, VTT and Vysus Group. A preliminary screening of the parameters and scenarios was performed using the obtained results and proposals for further study in phase two of the project were made.

Key words

Severe accident, Source term, PSA L2, Boiling Water Reactor, MELCOR, Uncertainty analysis

NKS-461
ISBN 978-87-7893-554-0
Electronic report, July 2022
NKS Secretariat
P.O. Box 49
DK - 4000 Roskilde, Denmark
Phone +45 4677 4041
www.nks.org
e-mail nks@nks.org

Source Term And Timing Uncertainty in Severe accidents

Final Report from the NKS-R STATUS activity

(Contract: AFT/NKS-R(21)133/5)

Sergey Galushin[1], Anders Riber Marklund[1]

Dmitry Grischenko[2], Pavel Kudinov[2]

Tuomo Sevón[3], Sara Ojalehto[3], Ilona Lindholm[3]

Patrick Isaksson[4], Elisabeth Tengborn[4]

Naeem Ul-Syed[5]

[1] Vysus Sweden AB

[2] KTH Royal Institute of Technology

[3] VTT Technical Research Centre of Finland Ltd

[4] SSM Swedish Radiation Safety Authority

[5] DSA Norwegian Radiation and Nuclear Safety Authority

The views expressed in this document remain the responsibility of the author(s) and do not necessarily reflect those of NKS. In particular, neither NKS nor any other organisation or body supporting NKS activities can be held responsible for the material presented in this report.

NKS conveys its gratitude to all organizations and persons who by means of financial support or contributions in kind have made the work presented in this report possible.

Table of contents

1. Introduction

Analyzing and estimating risks is an integral part of both the industrial use and the public debate on nuclear power. At the same time, global climate change is increasing the demand for low-carbon sources of electricity, and the nuclear industry strives to maintain and expand its share of the global energy production. With these observations in mind it is reasonable to expect that the need for technological advances and reduction of uncertainties in both financial and radiological risks related to nuclear power will be as big as ever in the coming decades.

An important part of the risk profile of nuclear power relates to so-called severe accidents – i.e. events leading to a partly or fully damaged (melted) reactor core. State-of-the-art assessments of radiological risks related to such events relies on estimations of two fundamental quantities; their frequency and their consequence. As simple as these notions may seem, their quantification depends heavily on input data as well as on scope and complexity in the mathematical modelling used.

In so-called level 2 probabilistic safety assessments (L2 PSA), the main frequency estimate of interest is the large release frequency, (LRF), or sometimes the large early release frequency, (LERF). Assessing these frequencies based on summation over a large number of possible event sequences implies, among other things, that radioactive releases (the source term) need to be calculated for a set of representative scenario classes and compared to a pre-defined threshold to classify them as large or not large. These assessments are typically performed with integral plant response codes, such as ASTEC, MAAP or MELCOR, and are in themselves subject to uncertainty, both regarding the accident scenarios (aleatory uncertainty) and in the modelling of phenomena (epistemic uncertainty). Aleatory uncertainty arises from the natural variability of stochastic processes and cannot be reduced beyond this level, while epistemic uncertainty relates to our knowledge on systems, processes or parameters and can therefore be reduced by gathering more knowledge.

Typically, the source term evaluation is performed for a limited set of accident scenarios, using point-estimate values of epistemic uncertain parameters in the code used. Furthermore, such analyses typically do not consider the effect of epistemic uncertainty on interactions between physical phenomena or processes and transient accident scenarios, i.e. when different samples on the epistemic uncertainty range can significantly affect the course of the accident progression.

For some accident sequences, the standard practice, for the sake of conservatism, is to define the source term as everything escaping the containment. This creates a situation where a potentially very diverse family of realistic scenarios is represented by a set of assumed sequences that may contribute substantially to the LRF in a typical PSA L2. In this case, the uncertainty lies in the level of applied conservatism.

In both cases described above, source term uncertainty presents a challenge for any attempt to develop, use or increase the level of detail in L2 PSA results and merits targeted research solely on the basis of this.

Within the field of nuclear emergency preparedness towards severe accidents, the main goal is ultimately to be able to perform relevant and efficient actions to protect the public. The International Atomic Energy Agency (IAEA) states on the one hand that decisions on these actions should be based on observations of plant conditions, and on the other hand that decisions or protective actions should not be delayed by attempts to perform detailed source term estimates [1][2]. It is acknowledged that performing source term assessments with integral plant response codes is sufficiently complicated outside of accident conditions, which creates a need for simpler and faster tools for assessment of plant condition and source term estimation. One such tool is the Rapid Source Term Prediction (RASTEP) methodology, developed by Vysus Group. This method relies on a database on pre-calculated source term scenarios together with a probabilistic Bayesian Belief Network (BBN) model. The tool has the ability to take observed plant conditions and rescale results from L1-L2 PSA using conditional probabilities, logical relations and expert judgements. The output is a complete list of scenarios ranked by likelihoods, which is continuously updated with any new observations. In this way, current plant conditions can always be mapped to a representative class of scenarios. A problem arises if a RASTEP model (or any approach based on pre-calculated source terms) is used with overly conservative or uncertain data. Within emergency preparedness planning, source term uncertainties therefore also come with an operational aspect, directly impacting decisions taken in a stressful situation.

Within this project, the analysis of severe accident progression and fission products release to the environment are performed using MELCOR. MELCOR is a fully integrated, engineering-level computer code that models the progression of severe accidents in light water reactor nuclear power plants. A broad spectrum of severe accident phenomena in both boiling and pressurized water reactors is treated in MELCOR in a unified framework. These include thermal-hydraulic response in the reactor coolant system, reactor cavity, containment, and confinement buildings; core heatup, degradation, and relocation; core-concrete attack; hydrogen production, transport, and combustion; fission product release and transport behavior. Current uses of MELCOR include estimation of severe accident source terms and their sensitivities and uncertainties in a variety of applications [10][11].

It is our hope that this project will be able to shine some light on all of the abovementioned aspects of the source term uncertainty, for the first year of the project limited to nordic Boiling Water Reactors (BWR).

2. Project scope and goals

The overall goal of the project is to generate a body of knowledge regarding the uncertainty in the magnitude of fission products release in case of a potential severe accident in Nordic nuclear power plants. The work aims to provide insights into the effect of various types of uncertainty on the source term predictions. Results of the work will be useful both for probabilistic and deterministic safety assessments as well as for emergency response applications.

The work is planned to be performed in two phases, where the first phase corresponds to the work performed in the 2021-2022 period, as presented in this report.

The goal of the first phase of the project has been to identify, for the Nordic BWR, a set of representative accident scenarios as well as relevant deterministic modelling parameters that can affect accident progression, phenomena and the magnitude of the fission products release. The selection is based on the state-of-the-art review of the major contributors to the uncertainty in source term prediction and include the following tasks:

Task 1. Review of the safety design of Nordic BWR. This work is described in section 3.

Task 2. Identification of accident sequences for study. This work combines information from PSA with additional insights related to the views of national regulators, in particular with respect to offsite consequence analysis, emergency preparedness and response. This work is described in section 4.

Task 3. Identification of epistemic (phenomenological) modelling uncertainties in different stages of severe accident progression that can affect severe accident progression, release paths and magnitude of the release. This work is described in section 5.

Task 4. Preliminary assessment of release magnitude spans using MELCOR code simulations of the set of accident scenarios identified in Task 2, assuming best-estimate and bounding assumptions regarding the values of epistemic uncertain parameters identified in Task 3. This work is described in section 7. The results of this analysis can be used to screen-out parameters that have negligible impact on the results.

The main outcome of the above is a set of accident scenarios that are of interest from both frequency and consequence standpoints, as well as a set of deterministic modelling parameters that can have a major effect on the magnitude of the fission products release and offsite consequences, including preliminary assessments of the effect of epistemic uncertain parameters on the magnitude of the fission products in various accident scenarios.

The goal of phase 2 of the project will be evaluation of the sensitivity of the magnitude of the fission products release in different accident scenarios to the variability in deterministic modelling parameters (epistemic uncertainty), identification of the major contributors to the uncertainty, as well as quantification of the uncertainty in the results.

3. Background on Nordic Boiling Water Reactors

Designed by ASEA/ABB Atom, a total of 10 BWRs have been commissioned in Sweden and Finland since the first unit, Oskarshamn 1, was brought online in 1972. Two of the original design families, BWR69 and BWR75, are in operation today, distributed as four units in Sweden and two units in Finland, all with planned lifetimes extending to around 2040.

Over time, these reactors have evolved in partly different directions. The configurations of the sister reactors Forsmark 1/2 as well as Olkiluoto 1/2 are still more or less identical within the sites, while the differences between the sites are more marked.

3.1. Safety design

The Nordic Boiling Water Reactor (NBWR) will hereby be used as a common name for ~3300 MW_{th} BWRs designed by ASEA/ABB Atom. A summary of main technical data for the currently operational NBWRs is given in [3].

Table 3-1. Main technical data for operating NBWRs, some numbers rounded.

	O3/F3 (BWR75)	F1/2 (BWR69)	OL1/2 (BWR69)
Thermal power [MW]	3900/3300	3000/3250	2500
Reactor operating pressure [MPa]	7.0	7.0	7.0
Number of fuel elements [-]	700	676	500
Number of control rods [-]	169	161	121
Gas volume in containment [m^3]	8300/8500	6800	7600
Capacity of system [kg/s]:			
Containment drywell spray	300	360	250
Containment wetwell spray	400	N/A	120
Containment design pressure [MPa]	0.6	0.5	0.5
Containment operating pressure [MPa]	<0.1	<0.1	<0.1
Filtered containment venting pressure setpoint [MPa]	0.5	0.57	0.2/0.5-0.6*
Unfiltered containment venting pressure setpoint [MPa]	0.65		
Containment rupture pressure [MPa]	~1	~1	~1

*For wetwell venting in OL1/2, the drywell pressure needs to exceed the defined overpressure that depends on drywell gas temperature (total pressure 0.5-0.6 MPa). The drywell venting takes place if the water level in the wetwell is too high to allow venting from there, and the drywell pressure is higher than 0.2 MPa.

The safety design of the NBWRs is described further in the following.

The reactor pressure vessel (RPV) consists of carbon steel clad by stainless steel on the inside. The reactor containment is of the pressure suppression (PS) type with vertical blowdown pipes, and its outer cylindrical shell is made of pre-stressed concrete. It is sealed at the top by a large steel cupola which sits at the bottom of the reactor service pool. The containment also functions as a radiological shield to the environment. During normal operation, the containment gas volume is filled with nitrogen to prevent ignition of hydrogen if generated during a severe accident.

Details on the NBWR safety systems relevant for severe accident progression (and source term) are provided below:

- Hydraulic control rod insertion: The hydraulic actuating power shut-off system gives full insertion of all control rods within a few seconds after initiation. Should this system fail, an electromechanic system inserts the rods within a few minutes. If this also fails, boric acid can be added to the reactor vessel via a dedicated injection system.
- Pressure control and relief system: This system has several operating modes and can operate with battery backup only:
    - TA Function: The spring-operated part of the overpressure protection system will open valves stepwise, starting at slightly above 7 MPa to release steam and protect the RPV from catastrophic failure. After a properly controlled pressure transient, the system will continue to control the pressure to around 7 MPa.
    - TB Function (ADS): Activation of TB initiates steam discharge into the wetwell (WW) on setpoint 1 m below top of active fuel (TAF). The pressure is reduced to a level sufficient for water injection by the emergency core cooling system (ECCS) or the independent core cooling system. The TB function is at the same time leading to coolant being lost from the primary system quite rapidly, which leads to core uncover.
- Emergency core cooling system (ECCS): This is an AC power driven, low-pressure coolant injection system comprised of four independent trains, which can pump water to the reactor from the suppression pool. The system has activation setpoints on water level 2 m above TAF and low reactor pressure. Actual water injection will not occur unless the pressure difference between WW and downcomer (DC) is less than 1.25 MPa and the injection capacity is, in general, dependent on this pressure difference.
- Independent core cooling system: This is, in the Swedish configuration, an AC power driven injection system comprised of one independent train with one or several separate water sources as well as a dedicated diesel generator. In the Finnish configuration, this is a separate steam turbine driven injection system, taking suction from water storage tanks in the system for distribution of demineralised water.
- Auxiliary feedwater system (AFW): This is an AC power driven high-pressure coolant injection system comprised of four independent trains, which provides water to the reactor from the wetwell or from a separate storage tank into the downcomer. The system activation logics includes several different setpoints. Water injection is more or less independent of reactor pressure.

- Drywell flooding system: Flooding of drywell from the wetwell is initiated to provide cooling of melt fragmentation and debris in case of melt release from the reactor pressure vessel. . The system is typically actuated on downcomer water level 2 m below the TAF for more than 10 minutes, or 30 minutes after containment isolation, depending on plant.
- Non-filtered containment venting system: This is a pressure relief directly to the ambient atmosphere designed for LOCA events with failing PS function. It is activated by the opening of a rupture disc at around 0.65 MPa containment pressure. The line is automatically closed by a shut-off valve 20 minutes after containment isolation signal. It should be noted that this containment isolation signal is triggered individually by any of the typical conditions that are indicative of a serious event e.g. low reactor water level, high containment temperature, high containment pressure or triggered TB function.
- Filtered containment venting system: In the Swedish configuration, this is achieved from the upper drywell to the atmosphere via a multi-venturi scrubbing system situated in a separate building, equipped with a dedicated stack. Venting is activated by a rupture disc opening around 0.55 MPa containment pressure. In parallel with this rupture disc, two valves for manual depressurization are also installed for cases where additional capacity is required, e.g. when manual operation of the filtered venting is an option due to for instance favourable weather conditions.

  In the Finnish configuration, filtered venting can be done both from the wetwell and drywell to the atmosphere via a SAM-scrubber placed inside the reactor building. Wetwell venting is possible if the water level is below 14.5 m. The drywell pressure needs to exceed the defined overpressure that depends on drywell gas temperature. At a drywell temperature of 293 K, the threshold overpressure is 0.5 MPa.
  The drywell venting through a rupture disk takes place if the water level in the wetwell has been higher than 14.5 m for longer than a specified time (which precludes possibility of venting from wetwell) and the drywell pressure is higher than 0.2 MPa.

- Suppression pool: The suppression pool, located in the wetwell, is an inherently passive system designed to limit the containment pressure by use of the so-called PS function; Steam leaking or blown out from the primary system to the drywell will be pushed through blowdown pipes ending in the wetwell pool where the steam is condensed. Vacuum valves in large pipes between wetwell and lower drywell ensure that the wetwell pressure will not be higher than that of the drywell.
- Residual heat removal and containment spray system (RHR and CSS): This is an AC power driven system, comprised of four independent trains with heat exchangers, all recirculating water from the suppression pool. All four loops are connected to feed spray nozzles located in the containment. The safety functions of the system are to reduce the containment pressure by condensing steam in case of a LOCA, to remove heat from the suppression pool through a series of heat exchangers and to provide scrubbing of airborne fission products from the containment atmosphere in case of core damage.
- Independent containment heat removal and spray system: This is an EOP/SAMG spray system in the upper drywell (UDW) that takes water from an independent external

water source. It can be used to reduce pressure in the containment as well as to provide scrubbing of airborne fission products. Water level control is provided in order to not damage the containment.

3.2. MELCOR models

3.2.1. Swedish MELCOR modelling of NBWR

The MELCOR model of the NBWR used in this project is the further development of the input deck originally developed for the analysis of accidents in power uprated plants [4], mainly maintained by KTH. In this model, the core is represented by five non-uniform radial rings and eight axial levels. The 6^{th} ring represents the downcomer region (Figure 3-1).

The reactor pressure vessel (Figure 3-2) and the containment (Figure 3-3) are represented by 27 control volumes (CV), connected with 45 flow paths (FL) and 73 heat structures (HS). The vessel is represented by 6 rings and 19 axial levels, with the first 10 axial levels representing the lower plenum; the 11^{th} axial level represents the core support plate; levels 12 and 19 represent the core inlet and outlet regions and structures; and levels 13-18 represent the active core region. Lower head penetrations for 66 instrumentation guide tubes (IGTs) are distributed between rings 1-5 proportionally to the cross-sectional area of these rings. Containment leakage is modelled from the drywell directly to the environment.

The containment is subdivided into control volumes for upper and lower drywell, wetwell, blowdown pipes and overflow pipes from lower drywell to wetwell.

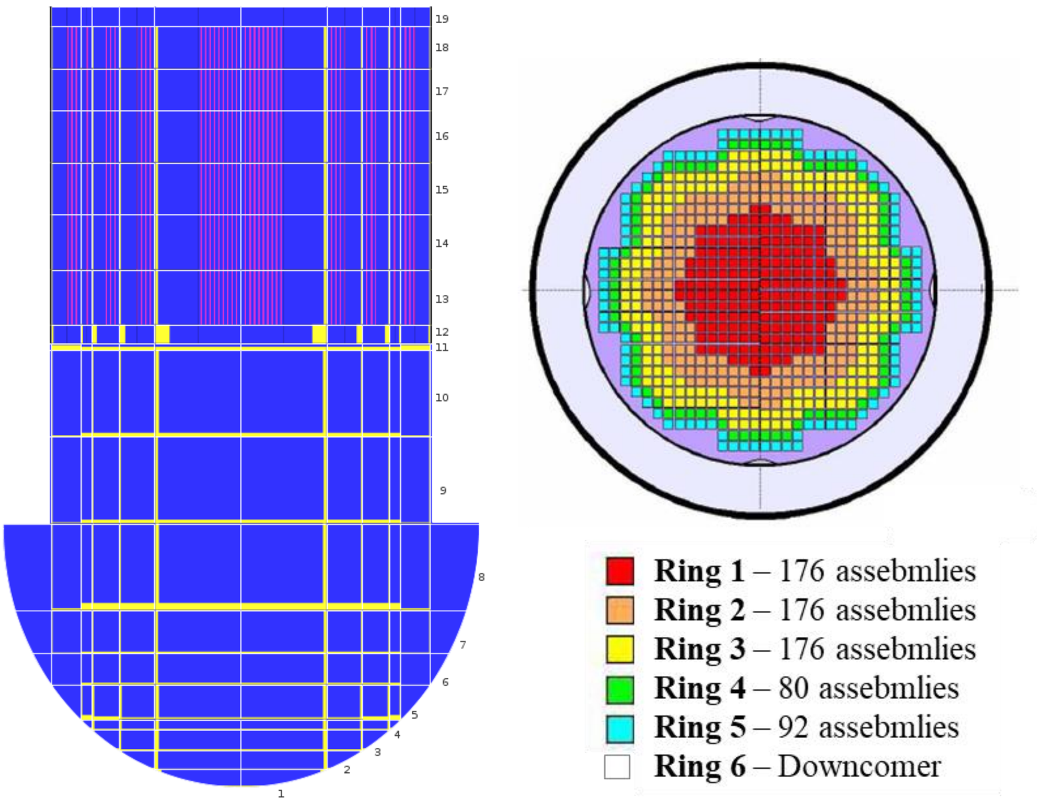

Figure 3-1. Swedish NBWR model COR nodalization.

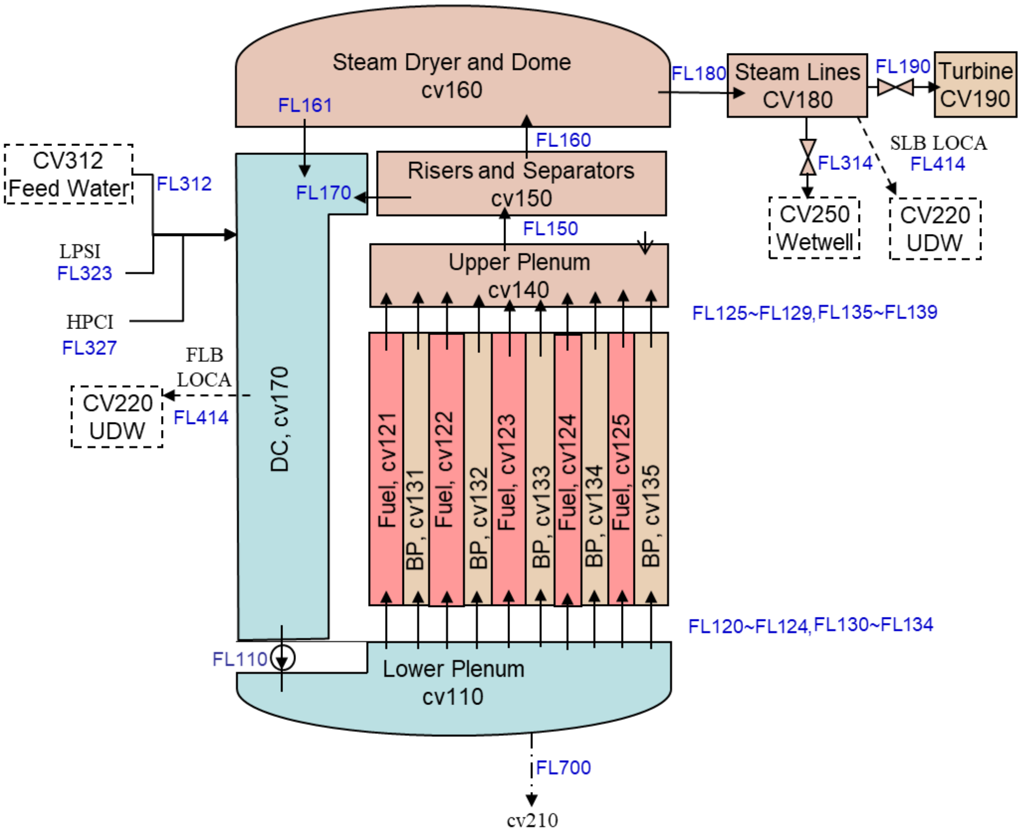

Figure 3-2. Swedish NBWR model CVH nodalization of the core.

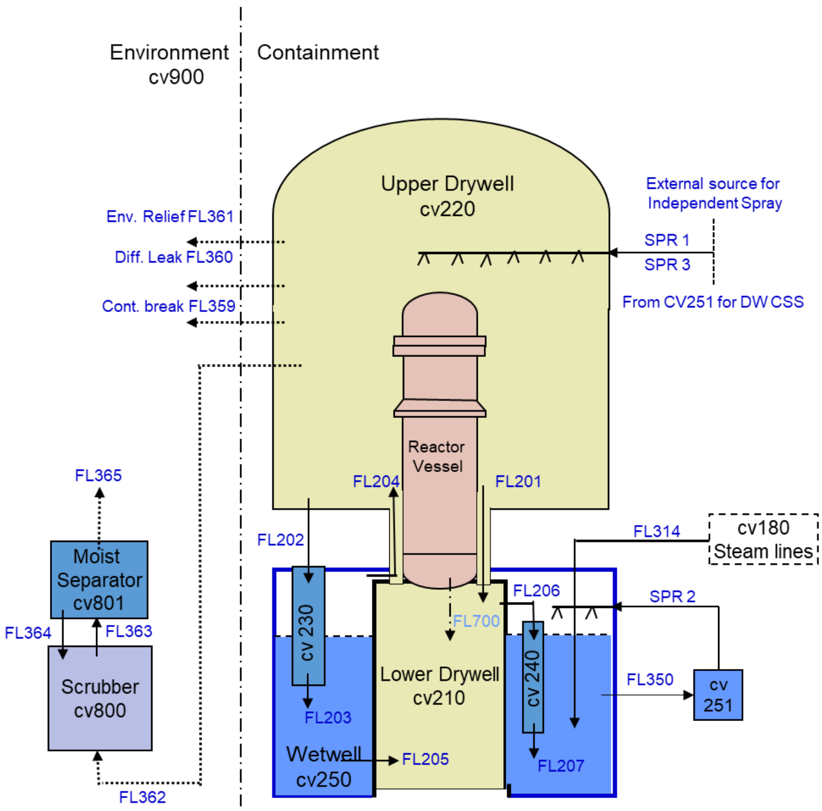

Figure 3-3. Swedish NBWR model containment nodalization.

The following safety systems are implemented in the model:

- Hydraulic control rod insertion
  - The effect of this system is modeled in MELCOR by fission power decrease (during 3.5 s) according to a tabular function at time zero.
- Pressure control and relief system
  - Both TA and TB valves as well as pipelines are implemented as a single flow path (FL314) from the steamlines to the wetwell, controlled by a set of control and tabular functions. SPARC pool scrubbing model is activated at the pool discharge end of the 314-pipes.
- Emergency core cooling system
  - All 4 trains are modeled by a single flow path (FL323) to the downcomer, with the number of trains and flow managed by a set of control functions. Flow rate vs. back pressure is controlled by a tabular function. The wetwell is used as water source for the system in the model and the injection is stopped on high suppression pool temperature.
- Auxiliary feedwater system.
  - All 4 trains are modeled by a single flow path (FL171) to the downcomer, with the number of trains and flow managed by a set of control functions. It is assumed that the system injects water with constant flow rate of 26 kg/s regardless of the pressure difference between DW and WW. The wetwell is used as water source for the system in the model and the injection is stopped on high suppression pool temperature.
- Drywell flooding system.
  - The system is implemented as a single flow path (FL205) from the wetwell to the lower drywell; the valves are controlled by a set of control functions. Together with the drywell flooding system an overflow pipe is modelled connecting the lower drywell and the wetwell to prevent lower drywell overfilling.
- Drywell blowdown pipes
  - A total of 24 drywell blowdown pipes are modelled from the drywell floor to the suppression pool. The diameter of the pipes is about 60 cm. The SPARC pool scrubbing model is activated at wetwell discharge at the end of the blowdown pipe. The blowdown pipes are purposed for the LOCA situations, when rapid and large steam release is able to clear the water in the pipes, and steam is driven into the suppression pool for condensation.
- Vacuum breakers
  - Vacuum breakers are modelled as a single flow path (FL204) that connects wetwell gas space with upper drywell to prevent wetwell pressure exceeding the drywell pressure.
- Non-filtered containment venting system.

- Implemented as a single flow path (FL361) from the upper drywell to the environment, the rupture disk and shut-off valves are modelled as a set of control functions.

- Filtered containment venting system.
  - Implemented by a set of flow paths and control volumes (c.f. Figure 3-3). The rupture disk and valves are controlled by a set of control functions. The actual filtering of substances containing radionuclides is modelled by simple filter factors based on system requirements.
- Residual heat removal and containment spray system.
  - Currently modelled as two sprays (SPR2 in the wetwell and SPR3 in the drywell). The wetwell spray (SPR2) represents up to 4 trains of the containment spray system with 100 kg/s per train, with a possibility to reroute up to 3 spray trains to the upper drywell. Control volume CV251 represents the heat exchangers in the residual heat removal system and used as a water (and temperature) source by the containment spray system and enthalpy source for the residual heat removal system.
- Independent containment spray system
  - Implemented as a single train system with flow path (SPR1) ending in the upper drywell. The capacity is 100 kg/s assuming a constant water source temperature at 293.15 K.

The MELCOR model does not include the newly implemented independent core cooling system. As the aim is to study source terms of severe accidents, i.e. cases where all core cooling fails, this is judged to be acceptable.

The MELCOR model is not built to treat cases with failing hydraulic control rod insertion, as sequences with failing reactor shutdown also require the electromechanical insertion and the boron injection to fail, thereby rendering this core damage mode a very small contributor in the PSA.

Note that steam lines, condenser and turbine plant are not modelled, as is also the case for the reactor building and its ventilation system. This implies that containment rupture or bypass cases will be conservative in terms of the source term, as any retention and delay in the turbine system or building structures will not be taken into account.

In the last few years, KTH has developed and demonstrated a systematic approach to quantification of uncertainty in severe accident scenarios and phenomena based on the Risk Oriented Accident Analysis Methodology framework (ROAAM+). The approach combines the most recent development in the areas of sensitivity analysis, uncertainty quantification and surrogate modeling approaches. In the previous ROAAM+ work the focus was on the quantification of uncertainty in containment failure probability. The next step in the ROAAM+ development is application to quantification of uncertainty in the source term.

3.2.2. Finnish MELCOR modelling of NBWR

VTT's MELCOR model of Olkiluoto 1&2 was developed for code version 1.8.2 in 1994. The model has been updated several times when new code versions have been taken into use. The latest update was made in 2017 by Magnus Strandberg who converted the model to MELCOR 2.1 with funding from the SAFIR2018 research program [5]. Systematic checking of the input deck or comparisons to current plant configuration have not been made for at least 19 years. The model is somewhat outdated because it does not follow current best modelling practices, and plant modifications are not included in the model.

The core nodalization is presented in Figure 3-4 (left). The core is modelled with five uniform radial rings; the sixth ring represents the downcomer region. The first three axial levels represent the lower plenum; the fourth axial level represents the core support plate; levels 5–14 represent the active core region; and level 15 represents the core outlet region.

The reactor thermal-hydraulic nodalization is presented in Figure 3-4 (right). There are 7 control volumes and 10 flow paths, plus one flow path from the core to the bypass that is opened upon failure of the channel boxes. The steam lines are not modelled as a separate volume. Instead, the steam to the safety relief valves is taken directly from the downcomer volume. The instrument guide tube penetrations in the lower head were added to the model during the current project.

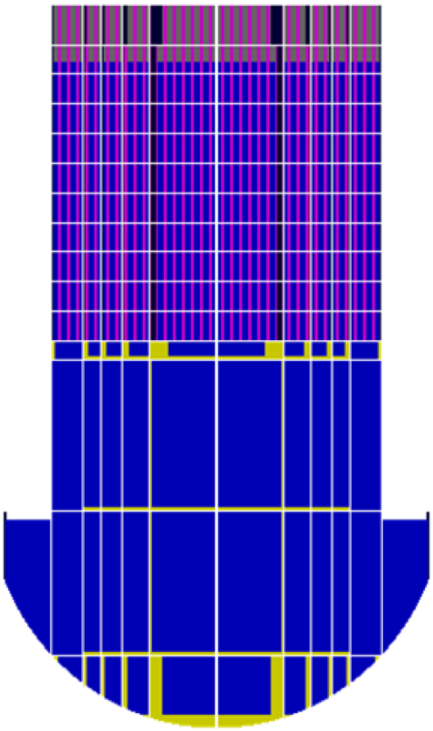

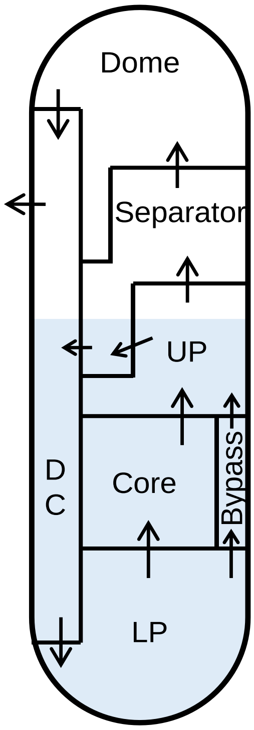

Figure 3-4. Finnish NBWR core model COR (left) and CVH (right) nodalization.

The containment is modelled with four control volumes, see Figure 3-5. The biological shield volume represents the space between the RPV and the concrete wall around it. The RPV lower head is interfaced with the biological shield volume. In addition, the model has six volumes representing rooms in the reactor building and a time-independent volume representing the environment. The control volumes of the reactor building represent major potential leakage routes from the containment to the reactor building and were purposed for hydrogen spreading and combustion analyses. The reactor building model is not purposed to model the entire complex RB configuration. Containment leakage is modelled from the drywell to the reactor building.

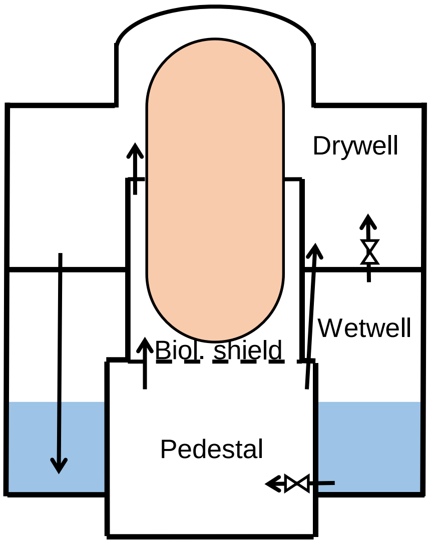

Figure 3-5. Finnish NBWR model containment nodalization.

The following systems are implemented in the Finnish NBWR MELCOR model:

- Hydraulic control rod insertion
  - Reactor scram is assumed to take place at time zero.
- Containment isolation
  - Closure of the main steam isolation valves (system 311) is activated by I-isolation or at a predefined time.
- Reactor main recirculation,
  - Modelled as a coast-down curve during the first 9.1 s of the calculation
- Pressure control and relief system
  - Relief valves controlled by downcomer pressure are modelled to discharge from the RPV downcomer to the suppression pool in the wetwell as four different groups: Group 1 opens when the downcomer pressure exceeds 8 MPa and closes when the pressure decreases below 7.4 MPa. The second group opens at 7.4 MPa and close at 7.1 MPa, the third group of valves opens at 8.5 MPa and closes at 7.6 MPa and the fourth group is open at pressure higher than 7.0 MPa and otherwise closed. The vertical discharge lines are submerged 4.5 meters in the suppression pool. SPARC pool scrubbing model is activated at the pool discharge end of the 314-pipes.
  - Automatic depressurization system of the reactor (314-ADS)

    Automatic depressurization is initiated on any of the following three signals:

    1) automatic TB signal

    2) manual TB signal

    3) on L4 signal lasting for the delay of 906 s.

    The automatic TB signal is generated if L4 signal is obtained and drywell pressure simultaneously exceeds 95 kPa and the drywell pressure increases faster than 130 Pa/s. The valve opening generates a delay of 15 s. The

ADS blowdown takes place from the downcomer to the suppression pool at water submergence of 4.5 m. SPARC model is activated at the pool discharge end of the 314 pipes by input parameter.

- Emergency core cooling system
  - The system 323 injects water to the Upper Plenum (UP node) and takes suction from the suppression pool. The injection starts when L4 signal is obtained (downcomer water level goes below 28.25 m (0.5 meters above TAF)) and the 323 pumps run until the water level in the downcomer reaches 32.25 m (= 4.5 meters above TAF). There are four (4) pumps with each having the capacity ranging from a maximum of 115 kg/s to zero at respective downcomer counter pressure range from 0.1 MPa to 1.0 MPa. The initiation of 323 injection to core spray requires also that suppression pool heat removal recirculation mode (system 322) is first locked-off.
- Auxiliary feedwater system
  - System 327 injects coolant to downcomer (50%) and to upper plenum via core spray spargers (50%). The system incorporates four (4) piston-driven pumps that produce constant water flow rate of 25 kg/s per pump independently of counter-pressure up to the pressure 2.0 MPa. The signals L2 and L3 are received when the collapsed water level in the downcomer becomes less than 2.9 m and less than 1.8 m above the top of active fuel (TAF), respectively (i.e. DC water height is less than 30.65 m and 29.55 m). Two 327 pumps start to inject water to downcomer when L2 signal is reached and a 10-s pump delay has elapsed. The DC injection continues until the collapsed water height in the DC reaches 4.0 meters above TAF. The 327 injection with two pumps through core spray spargers initiates from L3 signal with a 10-s pump delay and continues until the DC collapsed level reaches 4.5 meters above TAF.
- Failure of reactor lower head
  - A flow path from the reactor lower plenum to the pedestal is opened when MELCOR calculates lower head failure. The flow area is determined by MELCOR.
- Vacuum breaker between wetwell and drywell
  - Vacuum breakers are modelled as valves between the wetwell and the drywell near the ceiling of the wetwell. The vacuum breakers are purposed to relief wetwell pressure in situations where non-condensable gases accumulate in the wetwell thus diminishing steam suppression in the wetwell pool. The valves open when the pressure in 10 kPa higher in the wetwell than in the drywell. After pressure balancing to the level 1000 Pa the valves are fully closed.
- Drywell-wetwell leak
  - A small leakage between the wetwell and drywell is modelled, the leak area is assumed to increase with drywell pressure being at least 0.01 m2 at drywell pressure higher than 0.5 MPa.
- Drywell blowdown pipes

- A total of 16 drywell blowdown pipes are modelled from the drywell floor to the suppression pool with a submergence depth of 6.5 m. The diameter of the pipes is about 60 cm. The SPARC pool scrubbing model is activated at wetwell discharge at the end of the blowdown pipe. The 316 pipes are purposed for the LOCA situations, when rapid and large steam release is able to clear the water in the pipes, and steam is driven into the suppression pool for condensation.

- Containment heat removal and spray system
  - Drywell spray starts on I-isolation signal or by manual activation of the operator. The 322 system is also used for wetwell pool cooling in recirculation mode. A heat exchanger aligned in the 322 recirculation loop removes 172 kJ/K/kg from the pool water with flow capacity of 45 kg/s. The cut-off pool temperature for recirculation cooling is 291 K. Manual starting of spray requires that the water level in the drywell is lower than 2.5 m. The drywell spray flow rate is 60 kg/s.
  - The 322 spray can also be aligned to sprinkle wetwell airspace. The flow rate is then 30 kg/s. The initiation signal is I-isolation or manual start.
- Drywell flooding.
  - Assumed within 30 minutes in a station blackout situation.
- Filtered containment venting system
  - Wetwell venting is possible if the water level is below 14.5 m. The vent line elevation in the wetwell is 17.5 m. The drywell pressure needs to exceed the defined overpressure (to ambient pressure) that depends on drywell gas temperature in the following way: at a drywell temperature of 293 K, the threshold overpressure is 0.5 MPa and at 453 K the threshold is 0.4 MPa. The actual filtering of substances containing radionuclides is modelled by simple filter factors based on system requirements.
  - The drywell venting through a rupture disk takes place if the water level in the wetwell has been higher than 14.5 m for longer than a specified time (which precludes possibility of venting from wetwell) and the drywell pressure is higher than 0.2 MPa.
- Reactor building blow-off panel
  - opening at a pressure difference of 2.5 kPa to the environment.

4. Selection of accident sequences of interest

The PSA represents the state-of-the-art methodology to systematically identify and evaluate the effect of failure combinations in the safety functions and barriers of a nuclear power plant. To this end, Level 1 (L1) PSA focuses on core damage, while Level 2 (L2) PSA is focused on releases to the environment. In L2 PSA, the identified set of accident sequences is used as analysis specifications for integral response codes, such as MAAP or MELCOR, typically to qualify releases as acceptable or unacceptable with regards to some pre-defined threshold.

In this way, the L2 PSA will create a categorization of accident sequences with qualitatively similar behaviour, so-called release categories, which can be used as a starting point to assess source terms and their uncertainties. It should however be noted that, when simulations over the uncertainty ranges of the modelling parameters are performed, it is possible that extreme values of these parameters may trigger threshold effects, or simply surpass an absolute criterion on release magnitude, leading to the simulation ending up in another release category. Identifying occurrences of such effects would in itself be an important result of this study.

PSA results are generally plant specific. As the NBWR plants are relatively similar in design, and since reviewing several PSA models would be time consuming, it has been judged acceptable for this project to base the selection of accident sequences on one single example of an NBWR PSA model. The release categorization should be more or less equal for different NBWR plants, while frequency results may differ.

The selection of qualitatively different NBWR accident sequences is described further in the following. The present work is limited to sequences starting from power operation, i.e. outage events are excluded from the scope.

4.1.Accident sequence categorization in PSA

The output of L1 PSA is typically core damage frequency and the sequences of events that lead to core damage are then divided into a number of sub-categories representing important features for L2 PSA accident progression, the so-called plant damage states (PDS). These describe, not only the reason of core damage, but also the conditions of the primary system and the containment. The main attributes that are considered relevant for modelling of the continued accident progression in L2 PSA are:

- Core damage cause (failure of shutdown, core cooling or residual heat removal).
- Initiating event (transient or LOCA).
- Time of core melt (early, late).
- Reactor pressure (low, high).
- Containment atmosphere (inert, air).
- Containment spray system status.
- Unfiltered containment venting status (activated, not activated).
- Filtered containment venting status (activated, not yet activated, failed).
- Bypass of containment (bypass, intact).
- Suppression pool temperature (warm if pool cooling fails, else cool).

The events that are represented in L2 PSA are those that may change the conditions for retaining/mitigating of releases within the RPV or the containment. For each of the PDSs, a subsequent containment event tree (CET) is defined, modelling the continued accident progression. The accident progression sequences are influenced both by manual actions and by various physical phenomena that can affect containment integrity and magnitude of the release to the environment. Their end-states are named release categories (RC).

The RCs can be defined in different ways, for example by release size or type of sequence. The usual approach is to use the sequence type, because then only a limited amount of verifying deterministic calculations needs to be considered in the underlying deterministic analysis. For the sequence type approach, the characterization is typically based on:

- Release path (containment bypass, containment rupture, filtered release, leakage).
- Timing of release (early, late).
- Initiator (pipe rupture, transient).
- Containment spray established (yes/no).

The main outcomes of L2 PSA analysis are the estimates of the frequencies and magnitudes of different types of releases of radioactive materials to the environment for each release category. Typical NBWR release categories are summarized in Table 4-1.

Table 4-1. Summary of release categories for the Nordic BWR.

Release Category	Description
RC1	Severe accident initiated by a transient. Containment sprays. Early containment failure.
RC2	Containment bypass due to IS-LOCA.
RC3	Containment bypass due to unisolated RPV (failure to close main steam or main feedwater isolation valves).
RC4	Severe accident initiated by a transient or LOCA. Containment failure due to a containment phenomenon.
RC5	Severe accident initiated by a LOCA. Early containment failure[1]. No containment sprays.
RC6	Severe accident initiated by a transient. Early containment failure[2]. No containment sprays.
RC7	Intact containment. Release through FCV
RC8	Diffuse leakage.
RC9	Containment melt-through.

It should be noted that RC7 and RC8 together make up the vast majority of typical PSA L2 outcomes.

Furthermore, the L2 PSA provides insight into severe accident progression and plant specific vulnerabilities in the safety design, i.e. it determines how severe accidents can challenge the containment and identify major containment failure mechanisms.

[1] Containment failure due to overpressurization or failure to isolate the containment.

[2] Containment failure due to overpressurization or failure to isolate the containment.

4.2.Level 2 PSA overview for NBWR

In a typical NBWR power operation L2 PSA, there are mainly 6 release categories that contribute to the unacceptable release frequency - URF[3], see Figure 4-1. Furthermore, 5 out of 6 URF RCs also have significant contribution to the large early release frequency - LERF[4], see Figure 4-2.

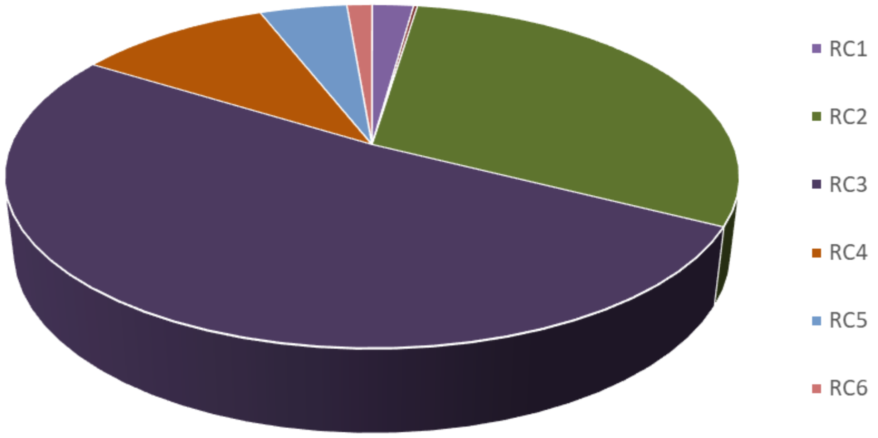

Figure 4-1. NBWR unacceptable release frequency distribution example.

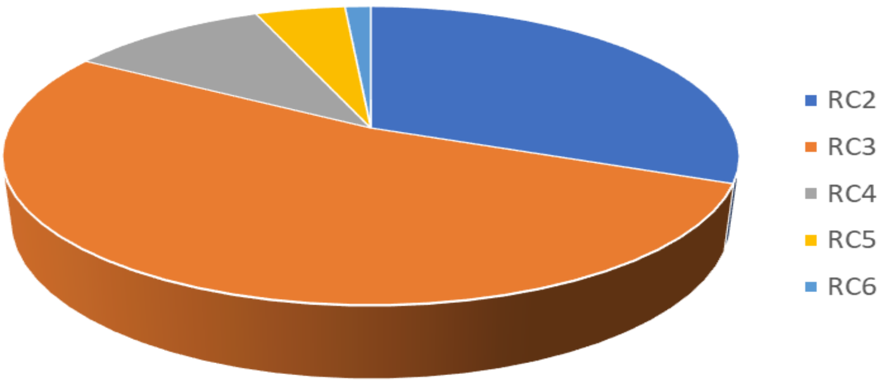

Figure 4-2. NBWR LERF distribution example.

From these pie charts, it is clear that these results for both URF and LERF are majorly represented by the sequences where containment is bypassed, either due to an interfacing system LOCA (IS-LOCA) or due to an unisolated reactor pressure vessel (e.g. transients or LOCAs with open MSIVs).

It should be noted that for the bypass sequences, a standard practice is to define the source terms as everything escaping the containment. This creates a situation where a potentially very diverse family of realistic containment bypass scenarios is represented by a set of assumed sequences that contribute substantially to LERF in a typical PSA L2.

---

[3] Releases over 0,1 % of the inventory of the caesium isotopes Cs-134 and Cs-137 in a core of 1800 MW_{Th}, excluding noble gases, which corresponds to a release of 160 TBq of Cs-134 and of 103 TBq of Cs-137 [6].

[4] Unmitigated releases from the containment in such a time frame prior to effective evacuation of the close-in population such that there is a potential for early health effects [7]**Error! Reference source not found.**.

The RCs that have significant contribution to the acceptable release frequency are represented in Figure 4-3. The major contributors to acceptable releases are the sequences where release of radioactive materials will occur through the filtered containment venting system (FCV) or via diffuse leakage. It should be noted that the identification of these RCs as acceptable releases is dependent on integral response code and other modelling assumptions, e.g. regarding the extent of diffuse leakage and the efficiency of the filtered containment venting system.

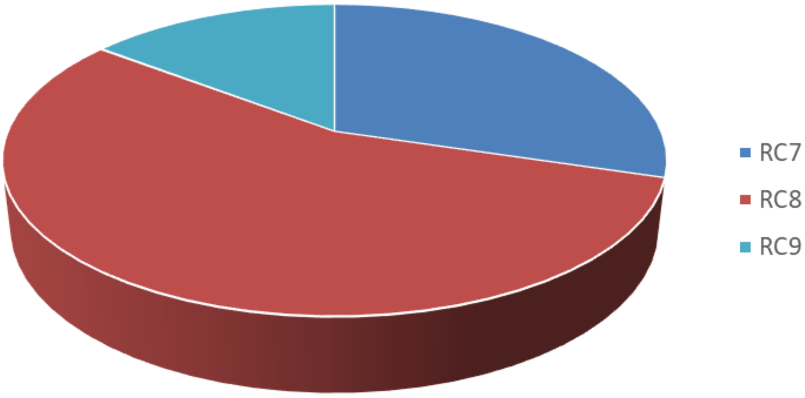

Figure 4-3. NBWR acceptable release frequency example.

4.3. Release categories and sequences

The studied release categories and their typical accident sequence progressions are described in detail in the following. Sequence specific areas of interest regarding source term uncertainty are identified. Also, it is stated whether typical integral plant response codes model the full release path to the environment or not.

4.3.1. Acceptable releases - Diffuse leakage & basemat melt-through (RC8 & RC9)

RC8 – Diffuse leakage. Typical sequence: Station blackout with recovery of water injection.

The accident is initiated by a station blackout that results in complete loss of all safety equipment that requires AC power, i.e. all water injection to the core and residual heat removal systems are considered unavailable during the whole sequence. Reactor shutdown, containment isolation, safety relief valves and automatic depressurization systems are assumed to work, activated according to the control logic. Flooding of the lower drywell (LDW) from the wet well for ex-vessel debris coolability is initiated according to the control logic. Water injection to the core is recovered early enough to prevent the need for containment depressurization.

Uncertainties of interest:

Uncertainties relating to timings and margin to onset of phenomena and/or need for containment depressurization are of interest.

Typical PSA supporting integral plant response code models *do not represent* the full release path to the atmosphere, since retention in the reactor building or building ventilation systems are not explicitly modelled.

RC9 – Basemat melt-through. Typical sequence: Station blackout with non-coolable debris in lower drywell.

The accident is initiated by a station blackout that results in complete loss of all safety equipment that requires AC power, i.e. all water injection to the core and residual heat removal systems are considered unavailable during the whole sequence. Reactor shutdown, containment isolation, safety relief valves and automatic depressurization systems are assumed to work, activated according to the control logic. Flooding of the lower drywell (LDW) from the wet well for ex-vessel debris coolability fails or is insufficient. Independent containment sprays can be credited in the sequence.

In principle, any sequence with RPV melt-through where flooding of the lower drywell (LDW) from the wet well fails or ex-vessel debris coolability is not achieved will ultimately lead to the melt penetrating the containment floor.

Uncertainties of interest:

Uncertainties relating to timing and possible need for containment depressurization are of interest. Uncertainties related to FCI phenomena at RPV melt through. Debris behaviour in the lower drywell. Effect of water pool temperature at RPV melt through (e.g. delayed SBO sequences).

Typical PSA supporting simulations *do not represent* the full release path to the atmosphere, since retention in the reactor building or building ventilation systems after basemat melt-through are not explicitly modelled.

4.3.2. Acceptable releases - Filtered containment venting (RC7)

RC7. Typical sequence A: Station blackout with filtered containment venting.

The accident is initiated by a station blackout that results in complete loss of all safety equipment that requires AC power, i.e. all water injection to the core and residual heat removal systems are considered unavailable during the whole sequence. Reactor shutdown, containment isolation, safety relief valves and automatic depressurization systems are assumed to work, activated according to the control logic. Flooding of the lower drywell (LDW) from the wet well for ex-vessel debris coolability is initiated according to the control logic. No containment failure due to FCI phenomena at RPV melt-through. The filtered containment venting system (FCV) rupture disc will burst around 0.55 MPa pressure in the upper drywell, depending on exact conditions in the relief line.

Independent containment spray system may or may not be credited.

Uncertainties of interest: Uncertainties relating to timing of events (such as FCV opening), potential effect of independent containment sprays and RCS depressurization are of interest. Effect of FCI phenomena at RPV melt-through.

Typical PSA supporting simulations *do represent* the full release path to the atmosphere if the filtered containment venting system is explicitly modelled.

RC7. Typical sequence B: Large break LOCA with filtered containment venting.

The accident is initiated by a large break LOCA. All water injection to the core and residual heat removal systems are considered unavailable during the whole sequence. Reactor shutdown, containment isolation, safety relief valves and automatic depressurization systems are assumed to work, activated according to the control logic. Flooding of the lower drywell (LDW) from the wet well for ex-vessel debris coolability is initiated according to the control logic. No containment failure due to FCI phenomena at RPV melt-through. The filtered containment venting system (FCV) rupture disc will burst around 0.55 MPa pressure in the upper drywell, depending on exact conditions in the relief line.

Independent containment spray system may or may not be credited.

Uncertainties of interest: Uncertainties relating to timing of events (such as FCV opening), potential effect of independent containment sprays. Effect of FCI phenomena at RPV melt-through.

Typical PSA supporting simulations *do represent* the full release path to the atmosphere if the filtered containment venting system is explicitly modelled.

RC7. Typical sequence C: ATWS with main and auxiliary feedwater systems unavailable – filtered release

ATWS in this context refers to any initiating event followed by failed insertion of control rods and failed boric acid injection. Safety relief valves and automatic depressurization systems are activated according to the standard control logic. Containment sprays and emergency core cooling systems are available initially but switched off due to elevated temperature in the suppression pool. Successful isolation of the containment. Flooding of the lower drywell (LDW) from the wet well for ex-vessel debris coolability is initiated according to the standard control logic. No containment phenomena at RPV melt through. Automatic activation of FCV via rupture disk with manual opening of an additional valve in the FCV system in order to prevent overpressurization.

Uncertainties of interest: Uncertainties relating to timing of events (such as manual FCV opening) and the effect of containment sprays are of interest.

Typical PSA supporting simulations *do represent* the full release path to the atmosphere.

RC7. Typical sequence D: Loss of ultimate heat sink – filtered release.

A loss of the ultimate heat sink leads to reactor shutdown and initially operating auxiliary feedwater system. The suppression pool is however heated due to deposited residual heat and the loss of ultimate heat sink. When the temperature of the water in the suppression pool reaches the setpoint value, the auxiliary feedwater stops automatically. Thereafter, connection failure (or depletion) of the auxiliary feedwater external water source is assumed. The automatic depressurization system and flooding of the lower drywell (LDW) from the wetwell for ex-vessel debris coolability are initiated according to the standard control logic.

If no phenomena fail the containment at RPV melt-through, the sequence typically leads to opening of the filtered containment venting system. The independent containment spray system may or may not be used.

Uncertainties of interest: Uncertainties relating to timing of events (such as FCV opening) and the effect of containment sprays are of interest.

Typical PSA supporting simulations *do represent* the full release path to the atmosphere.

4.3.3. Large releases (RC1, RC2, RC3, RC4, RC5, RC6)

RC1. Typical sequence A (B): SBO with failed isolation of containment overpressure protection line, with independent containment spray.

The accident is initiated by a station blackout that results in complete loss of all safety equipment that requires AC power, i.e. all water injection to the core and residual heat removal systems are considered unavailable during the whole sequence. Reactor shutdown and safety relief systems are activated according to the standard control logic (activation of automatic depressurization system in *Sequence B*). Failed isolation of the containment overpressure protection line. Flooding of the lower drywell (LDW) from the wetwell for ex-vessel debris coolability is initiated according to the standard control logic. No containment failure due to FCI phenomena at RPV melt-through but the rupture disk in the containment overpressure protection line is assumed to open at RPV melt-through. The independent containment spray system is started and operated in accordance with EOP/SAMG instructions.

Uncertainties of interest: Transition from high pressure to low pressure scenario (e.g. due to safety relief valves stuck open[5]), number of trains of containment spray in the drywell (in case of recovery), FCI phenomena at RPV melt through and its effect on containment pressure response (is it possible to avoid rupture disk opening at RPV melt through?). Potential effect on RC category: Transition of RC category from RC1 to RC7 or RC8 (with sprays[6]).

Typical PSA supporting simulations *do represent* the full release path to the atmosphere.

RC2. Typical sequence: Unisolated break outside the containment in the shutdown cooling system (IS-LOCA).

An unisolated pipe break occurs outside of the containment, in the shutdown cooling system creating an IS-LOCA. Coolant is lost through the break until all available water sources are depleted. The exact source term release path will depend on the location of the break.

Uncertainties of interest:

Uncertainties regarding timing are of interest.

Typical PSA supporting simulations *do not model* the full release path to the atmosphere (typical representative deterministic calculations are performed for an unisolated LOCA in the main steamlines outside the containment).

RC3. Typical sequence: SCRAM with failed main feedwater, auxiliary feed water system available, failed ADS and failure to isolate main steam lines.

Uncertainties of interest:

For PSA, these sequences are typically added to the large release frequency. In reality, the release will (at least initially) end up in the condenser and feedwater system.

---

[5] Note that in typical PSA applications no positive credit is given for failed safety functions.

[6] RC8 with sprays is a separate release category according to PSA L2 for Nordic BWR, but the contribution to URF is below the cut-off frequency used in the analysis.

Uncertainties regarding fission product retention in the condenser and feedwater system are of interest.

Typical PSA supporting simulations *do not model* the full release path to the atmosphere (typical representative deterministic calculations are performed for an unisolated LOCA in the main steamlines outside the containment).

RC4. Typical sequence: A Large Break LOCA (B SBO with RCS depressurization), containment failure due to phenomena at RPV melt-through.

The accident is initiated by (a) a LBLOCA (b) station blackout, that results in complete loss of all safety equipment that requires AC power, i.e. all water injection to the core and residual heat removal systems are considered unavailable during the whole sequence. Reactor shutdown, safety relief, automatic depressurization system and flooding of the lower drywell (LDW) from the wetwell for ex-vessel debris coolability are all initiated according to their standard control logic. The containment fails due to an ex-vessel steam explosion at RPV melt-through.

Uncertainties of interest: Uncertainties regarding timing of events, probability and magnitude of phenomena are of interest.

Typical PSA supporting simulations *do not model* the full release path to the atmosphere.

RC5. Typical sequence A (B): Large LOCA with failing PS function and early containment failure due to overpressurization.

A large or medium size LOCA occurs with the PS function being severely deteriorated. This leads to an early overpressurization of the containment.

Sequence A: The rupture disc in the containment overpressure protection line will open around 0,65 MPa. Core cooling systems and isolation of the containment overpressure protection line (normally closing 20 minutes after containment isolation signal) are assumed to fail.
Sequence B: The rupture disk in the containment overpressure protection line fails to open (due to mechanical failure of the rupture disk, erroneous base position or spurious closure of the isolation valves), leading to early containment failure due to overpressurization. Containment spray may or may not be used.

Uncertainties of interest:

Uncertainties relating to timings are of interest in case of containment rupture due to overpressure, as well as the effect of the filtered containment venting system and degree of PS function deterioration needed to lead to overpressurization of the containment.

Typical PSA supporting simulations *do represent* the full release path to the atmosphere for sequence A but *do not* for sequence B.

RC6. Typical Sequence A: SBO with failed isolation of containment overpressure protection line and failed independent containment spray

The accident is initiated by a station blackout that results in complete loss of all safety equipment that requires AC power, i.e. all water injection to the core and residual heat removal systems are considered unavailable during the whole sequence. Reactor shutdown, safety relief systems and automatic depressurization system are activated according to the standard control logic. Failed isolation of the containment overpressure protection line. Flooding of the lower drywell (LDW) from the wetwell for ex-vessel debris coolability is initiated according to the standard control logic. No containment failure due to FCI phenomena at RPV melt-through but the rupture disk in the containment overpressure protection line assumed to open. Independent containment sprays are considered unavailable.

Uncertainties of interest:

Transition from high pressure to low pressure scenario (e.g. due to safety relief valves stuck open[7]), FCI phenomena at RPV melt-through and its effect on containment pressure response, i.e. regarding whether the opening of containment overpressure protection line at RPV melt-through can be avoided.

RC6. Typical Sequence B: SBO with failed containment depressurization via FCV system and failed independent containment spray

The accident is initiated by a station blackout that results in complete loss of all safety equipment that requires AC power, i.e. all water injection to the core and residual heat removal systems are considered unavailable during the whole sequence. Reactor shutdown, safety relief systems, containment isolation and flooding of the lower drywell (LDW) from the wetwell for ex-vessel debris coolability are all initiated according to the standard control logic. The filtered containment venting system is assumed to fail (due to mechanical failure of the rupture disk, erroneous base position, or spurious closure of the isolation valves, together with failed or too little time available for manual actions). Containment assumed to fail early due to overpressurization. Independent containment sprays are considered unavailable.

Uncertainties of interest:

Timing of events. Transition from HP to LP scenario (e.g. due to safety relief valves stuck open[8]).

Typical PSA supporting simulations *do not model* the full release path to the atmosphere.

RC6: Typical Sequence C: ATWS with failed isolation of main feed water lines.

ATWS (failed insertion of control rods and boric acid injection) with available main feedwater system (due to failed isolation of main feed water lines). Automatic depressurization, auxiliary feed water and emergency core cooling systems are activated according to control logic. The auxiliary feedwater is switched to external water source after a while due to elevated suppression pool temperature. Successful isolation of the main steam lines and containment overpressure protection line.

After a while, all systems using the suppression pool as a water source will stop due to high temperature. Core cooling is lost due to this or due to depletion of the external auxiliary feedwater source, whichever occurs last. Independent containment spray may be used but it is

---

[7] Note that in typical PSA applications no positive credit is given for failed safety functions.

[8] Note that in typical PSA applications no positive credit is given for failed safety functions.

assumed that both this and the filtered venting fails to prevent containment overpressurization, which occurs before the onset of core damage.

Uncertainties of interest:

Timing of manual activation of an additional valve in the filtered venting system on pressure development in the containment together with the effect of water injection systems (e.g. sequences with main feed water (due to IM isolation) and/or auxiliary feed water systems unavailable typically lead to RC7 release category in PSA L2 for Nordic BWR).

Typical PSA supporting simulations *do not model* the full release path to the atmosphere.

4.4. Views of national regulators

4.4.1. DSA

In general, DSA has interest in accident sequences initiated by large break LOCAs and/or station blackout. Associated to (and depending on) these initiating events, DSA proposed that the project should consider uncertainty in the following functions and phenomena:

- Status of the primary circuit and automatic depressurization. Flow blocking by core melt.
- Availability and timing of emergency core cooling and auxiliary feedwater, including auxiliary water storage tanks.
- Core heat transfer after uncovered fuel
- Status of the containment isolation – unfiltered release via containment overpressure protection system line
- Containment spray system unavailable
- Status of the containment integrity – Containment pressures above 0,65 MPa

Furthermore, DSA expressed interest in differences between the Swedish SSM-KTH MELCOR model for Nordic BWR and the Finnish VTT model for OL1/2.

4.4.2. SSM

General

From a general knowledge standpoint, relating to studies typically performed as part of the safety analysis report (SAR) deterministic analysis sections, SSM are interested in sequences that may enhance understanding of source term uncertainties which relate specifically to core degradation and containment phenomena.

PSA

From a PSA perspective, SSM notes that typical release categories cover many possible scenarios, with possibly quite different source terms. This motivates some focus on “cliff-edge studies” of how large parameter variations (and resulting source term variations) can be made without making the sequence “jump” to another release category. Examples:

- How large can a diffuse leakage scenario be before changing to a filtered release scenario?

- How large can a filtered release scenario be before surpassing design capacity of the filtered venting system? (E.g. after failed reactor shutdown, extensive containment water filling or other deteriorating conditions.)
- How much source term overlap is there between sequences with and without containment spray when varying other parameters?
- How much PS function deterioration is needed for opening of containment overpressure protection in case of LOCA?

Emergency preparedness & response

In Sweden new emergency planning zones and distances will become operational as of 1 July 2022. These emergency planning zones and distances are based on the report *2017:27e Review of Swedish emergency planning zones and distances*. Two scenarios form the basis for the emergency planning zones and distances. The two scenarios both represent severe accidents involving core meltdown and vessel melt-through. In the first scenario (FILTRA), the mitigation systems function in accordance with regulatory requirements and releases pass via the filtered containment venting system. In the second scenario (100xFILTRA), the mitigation systems malfunction and the reactor containment leak tightness is lost in connection with vessel melt-through. The later scenario corresponds to a conceivable worst-case scenario in terms of release magnitude from a Swedish nuclear power reactor.

The scenarios were analysed by both GRS in Germany using MELCOR and the licensees of Swedish nuclear power plants using MAAP. The differences between source terms for different reactor types (BWR and PWR), produced using the same computer code for analysis, are comparable with the differences between source terms produced using different computer codes for the same reactor type. With the exceptions of release height and distribution of iodine forms in the release, the assessment is that it is unwarranted to use different representative source terms for BWR and PWR. Moreover, the differences in thermal power between the reactors that will remain in operation over the next few years in Sweden are not of a magnitude warranting production of different representative source terms for reactors with different thermal power output. Thus, the overall conclusion is that all Swedish reactors can be represented by the same source terms in relation to emergency preparedness and response.

The scenarios and the associated source terms are believed to be reasonably conservative. The source term for the worst-case scenario (100xFILTRA) is on a par with the source terms used by IAEA in EPR NPP Public protective action (2013) and Germany in their review of emergency response management in the vicinity of NPPs (H. Walter et.al, 2015). This is despite the fact that the German scenario is quite different from the one used in Sweden. The source term for the worst-case scenario (100xFILTRA) is also on a par with the total atmospheric release from reactors 1 to 3 at Fukushima Daiichi (IAEA, The Fukushima Daiichi Accident, 2015). The source term for the scenario with functioning mitigation systems (FILTRA) is also thought to be reasonably conservative. The filtered containment venting systems are designed to be substantially more efficient in reducing the release of key nuclides as compared to the regulatory requirements used by SSM in the assessment. The two scenarios and the development of the source terms are described in detail in *Appendix 3 to the report 2017:27e Review of Swedish emergency planning zones and distances*.

To determine the radial extension of the new emergency planning zones and distances, a reference level of 20 mSv effective dose was used for the scenario with functioning mitigation systems (FILTRA) and a reference level of 100 mSv effective dose was used for the worst-case scenario (100xFILTRA). As it turned out, the worst-case scenario (100xFILTRA) and a reference level of 100 mSv annual effective dose is limiting for the radial extension of all planning zones and distances. This opens up possibilities to develop emergency arrangements within the zones and distances enabling a lower reference level of 20 mSv to be used for lower release magnitudes.

In practice, three release magnitude intervals are used FILTRA, 10xFILTRA and 100xFILTRA. The release magnitudes for all nuclides with the exception of noble gases are 10 and 100 times larger for 10xFILTRA and 100xFILTRA respectively as compared to FILTRA. All noble gases are always assumed to be released. The reason not to use more release magnitude intervals is twofold. First, emergency arrangements within the emergency planning zones cannot be too fragmented and still be efficient. The second reason to use a limited number of release magnitude intervals is the large uncertainties associated with severe nuclear emergencies. Placing a possible release magnitude within one of the release magnitude intervals may, however, be possible under certain circumstances. An example would be an accident in which the filtered containment venting system is operational and where it is likely that a release will pass via the filter.

Sensitivity studies performed with scenarios that could be more challenging than the worst-case scenario indicate that the distances used before and during release are robust. The sensitivity studies include events having a brief period of forewarning, events affecting fuel pools and events involving simultaneous releases from several reactors at the same NPP. Common for these events is that more far-reaching protective actions are not feasible without jeopardizing the efficiency to implement protective actions at shorter distances. However, it may be more challenging to keep residual doses below 100 mSv annual effective dose for these events. The sensitivity studies are described in detail in *Appendix 3 to the report 2017:27e Review of Swedish emergency planning zones and distances*.

The fact that SSM uses three release magnitude intervals with regard to emergency preparedness and response has resulted in an intense focus on the time to release trying to answer the question: How much time does the rescue commander have to implement protective actions?

From an emergency preparedness and response perspective it would thus be interesting to perform sensitivity analysis that results in:

- changing the release magnitude from one interval to another e.g. from FILTRA to 10xFILTRA
- changing the time to release from e.g. 6 h to 12 h or 12 h to 24 h.

Large releases

SSM areas of interest relating to large releases include intersystem LOCAs, outside containment steam line breaks or bypass cases to the turbine. It is understood that these will however require structures and/or systems outside of the containment to be modelled in more detail compared to what has currently been done in typical MELCOR input decks.

4.5. Summary of selection of accident sequences

4.5.1. KTH

- Option 1 (RC4A – Large release due to containment failure due to phenomena)
  - Main assumptions:
    - § Containment fails due to FCI phenomena at/after RPV melt-through
    - § Flooding of the LDW is initiated according to standard control logic.
  - Sequence description:
    - Sequence initiated by a LB-LOCA. All water injection and containment spray systems are unavailable during the whole transient. Fission products pass trough the suppression pool until RPV melt-through. Containment fails due to ex-vessel steam explosion or basemat melt-through.
  - Suggestions for specific uncertainty studies (accident sequence variability):
    - Possibility of containment failure due to ex-vessel steam explosion.
    - Possibility of containment failure due to basemat melt-through, possibility of release via containment filtered venting system due to melt resolidification and plugging in the cable penetrations located in the LDW floor.
- Option 2 (RC4B – Large release due to containment failure due to phenomena)
  - Main assumptions:
    - § Containment fails due to FCI phenomena at/after RPV melt-through
    - § Flooding of the LDW is initiated according to standard control logic.
  - Sequence description:
    - Sequence initiated by a SBO with successful (unsuccessful) depressurization of the RCS. All water injection and containment spray systems are unavailable during the whole transient. Fission products pass trough the suppression pool until RPV melt-through. Containment fails due to ex-vessel steam explosion or basemat melt-through.
  - Suggestions for specific uncertainty studies (accident sequence variability):
    - Possibility of containment failure due to ex-vessel steam explosion.
    - Possibility of containment failure due to basemat melt-through, possibility of release via containment filtered venting system due to melt resolidification and plugging in the cable penetrations located in the LDW floor.

4.5.2. VTT

- Option 1 (RC3, Containment bypass via unisolated MSIVs – as per functionality of VTT MELCOR model for bypass sequences)
  - Main assumptions.

- Sequence description.
    - Any accident sequence with unisolated MSIVs.
- Suggestions for specific uncertainty studies (accident sequence variability):
    - as per functionality of MELCOR model

- Option 2 (RC7/8 – Diffuse leakage/filtered release in case of SBO)
    - Main assumptions:
        - Rupture disk in FCV opens at RPV melt-through.
    - Sequence description.
        - Accident initiated by a SBO with water injection/ containment spray systems are unavailable.
    - Suggestion for specific uncertainty studies (accident sequence variability):
        - Pressure spike generated at RPV melt-through is high enough to activated FCV (see main assumptions above)
        - Timing of recovery of water injection to avoid activation of FCV (release category transition from Filtered Release to Diffuse leakage).
        - Timing of recovery of containment sprays to avoid activation of FCV (release category transition from Filtered Release to Diffuse leakage).

4.5.3. Vysus Group

- Option 1 (RC7/8 – Filtered release/Diffuse leakage due to SBO or LOCA)
    - Main assumptions:
        - Rupture disk in FCV opens at RPV melt-through.
    - Sequence description.
        - Accident initiated by a SBO or LOCA with water injection/containment spray systems are unavailable.
    - Suggestion for specific uncertainty studies (accident sequence variability):
        - Pressure spike generated at RPV melt-through is high enough to activated FCV (see main assumptions above)
        - Timing of recovery of water injection to avoid activation of FCV (release category transition from Filtered Release to Diffuse leakage).
        - Timing of recovery of containment sprays to avoid activation of FCV (release category transition from Filtered Release to Diffuse leakage).
- Option 2 (RC5 – Large release due to containment failure in case of LOCA with “initially” degraded PS function).
    - Main assumptions:
        - PS function is degraded initially, due to covered blowdown pipes after maintenance outage.

- Sequence description:
    - Accident initiated by a large LOCA with degraded PS function. Early containment failure due to overpressurization.
- Suggestions for uncertainty study (accident sequence variability):
    - Degree of PS function degradation (amount of blocked blowdown pipes).

5. Identification of uncertainties of interest

5.1. Initial inventory and decay heat

The initial inventory of radionuclides and their respective decay heat power generated in the fuel represent the main hazards concerning reactor safety and severe accidents with successful reactor shutdown. The amount of decay heat generated in high power reactors with significant burn-up levels can lead to core uncovery and fuel damage in the time frame of minutes in case of a LB-LOCA or a transient with loss of effective coolant inventory makeup, or hours in case of a transient with loss of ultimate heatsink with subsequential loss of effective coolant inventory makeup. The decay power information is therefore one of the most important inputs for any severe accident simulation.

The production of radionuclides and the variation in their inventory during and after reactor irradiation are governed by the Bateman equations [8]. This system of equations is typically solved numerically by using specific computer codes (ORIGEN2/ORIGEN-S, DARWIN-PEPIN).

In the MELCOR code the fission products and associated decay heat are treated by the DCH (Decay heat) and RN (Radionuclide) packages:

- The MELCOR decay heat (DCH) package models the decay heat power resulting from the radioactive decay of fission products. Decay heat is evaluated for core materials in the reactor vessel and cavity and for suspended or deposited aerosols and gases. MELCOR couples thermal-hydraulic processes and fission product behaviour during the calculation [10][11].
- The RadioNuclide (RN) package models the behaviour of fission product aerosols and vapours and other trace species, including release from fuel and debris, aerosol dynamics with vapor condensation and revaporization, deposition on structure surfaces, transport through flow paths, and removal by engineered safety features. The package also allows for simplified chemistry controlled by the user. The RN package determines decay heat power for current radionuclide inventories from the Decay Heat (DCH) package when requested by each of these packages [10][11].

It is important to note that in the MELCOR code, both the radionuclides present in the reactor at the time of the accident and the radionuclide daughter products contribute to the decay heat. In the calculation of decay heat, MELCOR does not explicitly treat each decay chain, since detailed tracking of radionuclide decay chains would be too costly. When the RadioNuclide package is active, the decay heat is calculated for each radionuclide class by using pre-calculated tables from ORIGEN calculations. If the RadioNuclide package is not active, the whole-core decay heat is computed from one of several possible user-specified calculations [10][11].

The MELCOR code DCH package models the decay heat power as a function of time and the total initial inventories of individual elements. The default decay heat curves and inventories were obtained from ORIGEN calculations (see ref [1] in DCH Package manual [10]).

The base case ORIGEN run for a BWR used the following assumptions [10]:

- 3578 MWt General Electric BWR,
- five types of assembly groups,

- initial enrichment for assemblies, either 2.83% or 2.66% U-235, depending on assembly group,
- assemblies in core for either 3 or 4 years, depending on assembly group,
- refuelled annually,
- 80% capacity factor.

Within the RN package, daughter isotopes are assumed to be transported along with the parents. Thus, the daughter products are assumed to retain the physical characteristics of their parents. This assumption may not be appropriate in some cases, but the ORIGEN analyses showed that the decay heat from the parent elements is generally much greater than that of the daughter products. Because of these considerations, the decay heat of an element's daughter products is included in the decay heat tabulation for the parent element [10][11].

In general, mass inventories of elements are sensitive to fuel burnup and reactor design. Therefore, two default mass inventories are included in the DCH package for the representative BWR and PWR used in the ORIGEN calculations. The inventory masses of the elements, normalized to grams per unit of reactor operating power (for the PWR and for the BWR), were given by ORIGEN at four times in the equilibrium fuel cycle: start-of-cycle, one-third point, two-thirds point, and end-of-cycle [10][11].

The radioactive elements treated by the DCH package are further grouped into chemical classes for tracking by the RN package. Table 5-1 lists the default classes treated by the RN and DCH packages. The remaining elements that do not contribute significant decay heat (< 1%) are enclosed in parentheses [10][11].

Table 5-1. Default Radionuclide Classes and Member Elements [10][11].

Class number and name	**Member elements**
1. Noble gases	Xe, Kr, (Rn), (He), (Ne), (Ar), (H), (N)
2. Alkali Metals	Cs, Rb, (Li), (Na), (K), (Fr), (Cu)
3. Alkaline Earths	Ba, Sr, (Be), (Mg), (Ca), (Ra), (Es), (Fm)
4. Halogens	I, Br, (F), (Cl), (At)
5. Chalcogens	Te, Se, (S), (O), (Po)
6. Platinoids	Ru, Pd, Rh, (Ni), (Re), (Os), (lr), (Pt), (Au)
7. Transition Metals	Mo, Tc, Nb, (Fe), (Cr), (Mn), (V), (Co), (Ta), (W)
8. Tetravalents	Ce, Zr, (Th), Np, (Ti), (Hf), (Pa), (Pu), (C)
9. Trivalents	La, Pm, (Sm), Y, Pr, Nd, (Al), (Sc), (Ac), (Eu), (Gd), (Tb), (Dy), (Ho), (Er), (Tm), (Yb), (Lu), (Am), (Cm), (Bk), (Cf)
10. Uranium	U
11. More Volatile Main Group Metals	(Cd), (Hg), (Pb), (Zn), As, Sb, (Tl), (Bi)
12. Less Volatile Main Group Metals	Sn, Ag, (In), (Ga), (Ge)

Class number and name	Member elements
13. Boron	(B), (Si), (P)
14. Water	(H_2O)
15. Concrete	(CON)
16. Caesium Iodide	(classes 2 and 4)
17. CsM	(classes 2 and 7)

The decay heat power is computed for each class by weighting the elemental decay heats by the relative mass of each element in the class given by the ORIGEN calculations.

Total radioactive class masses are normally determined by the DCH package from the operating power of the reactor and the mass of each element in the class per unit of operating power, while RN package input generally defines only the initial distribution of these masses in the core (masses can be distributed among core cells according to radial and axial decay heat power profiles in the core. In addition, a fraction of the radionuclides in a core cell can be designated as residing in the fuel-cladding gap). Until released as vapors or aerosols, fission products within the fuel are transported with the fuel as it relocates from core cell to core cell or is ejected to the reactor cavity [10][11].

5.1.1. Swedish NBWR model

The Swedish NBWR MELCOR model employs:

- Sandia ORIGEN model for the whole-core decay heat power calculation, at the end of equilibrium fuel cycle (default) scaled to DCH_OPW = 3900 MWth.
- Gap fractions defined based on NUREG-1465 [41].
- SC3210 = 1 - multiplier for all ORIGEN elemental decay heat curves. This sensitivity coefficient is a multiplier that will be applied to all elemental decay heat power curves stored as default data in MELCOR.

The current model is sufficient for the research purposes. However, if the model would be used for plant-specific safety analyses, the decay heat curve should be updated.

Modelling parameters to be considered in sensitivity analysis:

- SC3210: Since the decay heat is one of the most important inputs for severe accident simulations, SC3210 multiplier for all ORIGEN elemental decay heat curves was considered in the separate effect analysis with (i) default value SC3210 = 1.0, and (ii) SC3210 = 1.15 to evaluate the effect of the decay heat power on code predictions.

5.1.2. Finnish NBWR model

VTT's MELCOR model of Olkiluoto 1&2 employs:

- The fission product inventories, where the decay heat of each element are based on an old ORIGEN calculation. They are outdated, as the fuel type and burnup have changed.

- The whole-core decay heat is presented as a tabular function, which is based on an old ORIGEN calculation. The decay heat curve is outdated, as the fuel type and burnup have changed. MELCOR normalizes the elemental decay heats so that their sum is equal to the whole-core decay heat, given in the tabular function.
- The gap fractions follow the MELCOR best practice recommendations [12] (5 % of noble gases, Cs, I and Te, and 1 % of Ba).

The current model is sufficient for the research purposes. However, if the model is used for actual safety analyses, the old decay heat curve should be updated.

Modelling parameters to be considered in sensitivity analysis:

- The decay power is one of the most important inputs for severe accident simulations. The NRC SOARCA study considers the uncertainty of the decay heat to be about 6 % at a fixed point in the fuel cycle [43]. The power can be easily changed by modifying the multiplier of the decay heat tabular function.

5.2. Gap release

As stated earlier, the RN package input defines the initial distribution of radionuclide masses in the core, specifically a fraction of the radionuclides in a core cell can be designated as residing in the fuel-cladding gap. Upon cladding failure, the gap inventory of the entire radial ring is released to the appropriate control volume. In addition, any release of radionuclides from the fuel is held up in the gap until cladding failure. Therefore, a puff-type release is usually seen when the cladding fails.

The default value (1173K) will be used and no modelling parameters will be considered in sensitivity analysis.

5.3. Early in-vessel release

During the early in-vessel phase of severe accident progression, the fuel and other structural materials in the core heat up and reach sufficiently high temperatures that the reactor core geometry is no longer maintained. The fuel and other materials start to degrade (melt, convert into particulate debris and relocate). During this phase, significant quantities of the volatile fission products in the core inventory as well as small fractions of less volatile fission products are expected to be released into the reactor coolant system and containment.

5.3.1. FP release kinetics from the fuel before the onset of fuel rod collapse

In the MELCOR code, the release of radionuclides can occur from the core fuel (with nonradioactive releases from other core structures), from the fuel-cladding gap, and from material in the cavity.

There are several options available to model release of radionuclides from the core fuel component: the CORSOR (ICRLSE=1), CORSOR-M (ICRLSE=2) or CORSOR-Booth (ICRLSE=3) (including revised CORSOR-Booth (Modified ORNL-Booth) model (ICRLSE=5,7). The CORSOR-BOOTH model contains low (ICRLSE=3,5,7) and high burn-up options (ICRLSE=-3,-5,-7). In addition, the CORSOR and CORSOR-M release rates can be modified to be a function of the component surface-to-volume ratio as compared to a base value, derived from the experimental data on which CORSOR is based (ICRLSE=-1,-2 for CORSOR and CORSOR-M) [10][12].

The CORSOR and CORSOR-M models are classified as fractional release rate models, differing only slightly in mathematical form, which specify the fractional release rate of the fission product inventory remaining unreleased up to that time. These are empirical models that are based largely on the small-scale horizontal induction (HI) and vertical induction (VI) experiments performed at Oak Ridge National Laboratory (ORNL). The CORSOR-Booth diffusion model is by comparison a physics-based model, albeit oversimplified, that describes the transport of fission products within fuel grains to the grain surface as a diffusion process [10][12].

Based on the assessment of MELCOR code fuel release models, performed in [12], the revised CORSOR-Booth (ICRLSE=5,-5) was accepted as the best practice for MELCOR code analysis of severe accidents.

Furthermore, based on the discussion in [13], a new revised ORNL-Booth (CORSOR-Booth-7) model was introduced in MELCOR (ICRLSE=7,-7). The original CORSOR-Booth model (CORSOR-Booth-5), which calculated the diffusion release fraction for all classes by scaling the diffusion release rate of caesium, while the modified version of the CORSOR-Booth, instead, scales the diffusion coefficient for each RN class based on the diffusion coefficient for caesium. For the analyses with especially long durations, such as spent fuel pool boiloff accidents, depletion of RN Class 2 (Cs) will no longer prevent other RN classes from releasing.

The results of MELCOR code simulations of Phebus FPT1 experiment using CORSOR-Booth-5 and CORSOR-Booth-7 show comparable results for release of Xe, Cs, Te, Ru. The release fraction of I_2 is comparable for both models in MELCOR 2.2.14959 and CORSOR-Booth-7 in MELCOR 2.2.17260, however slightly underestimate the experimental data. CORSOR-Booth-5 in MELCOR 2.2.17260 slightly overestimate I_2 release fraction compared to other models and experimental data. Although, CORSOR-Booth-7 and CORSOR-Booth-5 (in MELCOR 2.2.14959) have better agreement with the Phebus FPT1 experimental data during the transient simulation, the final release fraction of I_2 has better agreement with CORSOR-Booth-5 model in MELCOR 2.2.17260. Release fraction of Ba is overestimated by CORSOR-Booth-7 and underestimated by CORSOR-Booth-5, approximately by a factor of 5.

Based on the discussion above, it is suggested to use CORSOR-Booth-5 model (*RN1_FP00 'RCB_HBF'* – Revised CORSOR-BOOTH for high burnup fuel, by enabling ICRLSE=-5 on RN1_FP00 record) for sensitivity analysis, since (i) the model gives slightly better estimate of I_2 release, as well as (ii) MELCOR simulations will be performed for transients and LOCA scenarios at fuel reactor power (with successful reactor shutdown), thus we expect rather rapid accident progression from intact fuel rod geometry to degraded/collapsed core. For instance, previous MELCOR code simulations of an unmitigated SBO in Nordic BWRs (see [14][15]) suggest that the time frame between the onset of core oxidation and fuel rod collapse is ~20 min, and between the onset of fuel rod collapse and core support plate failure is ~45 min.

It is important to note that the corresponding time windows for high pressure scenarios (e.g., Case B in [14]), or scenarios with loss of ultimate heat sink can be sufficiently larger, so the effect of the differences between CORSOR-Booth-5 and CORSOR-Booth-7, mentioned above, can be of importance for the end result. Thus, it is suggested to perform a “separate effect” analysis, considering the CORSOR-Booth-5 and CORSOR-Booth-7 models with other MELCOR modelling parameters fixed to the default/best estimate values.

CORSOR-Booth Model

The CORSOR-Booth model considers mass transport limitations to radionuclide releases and uses the Booth model for diffusion with empirical diffusion coefficients for caesium releases. Release fractions for other classes are calculated relative to that of caesium.

Based on the analysis of the CORSOR-Booth modelling given in the MELCOR code reference manual [10], two sets of parameters was considered in sensitivity analysis:

- CORSOR-Booth Coefficients for cesium release presented in Table 5-2.
- CORSOR-Booth Class Scaling Factors presented in Table 5-3.

A Detailed description of the CORSOR-Booth model and modelling equations can be found in section 2.3.1.3 of the RN Package reference manual [10].

Table 5-2. CORSOR-Booth Coefficients for Caesium.

SC Coefficient	Default value [11]	SA Range	Units
C7106(1,1) - Low burn-up value of D_0.	1.0E-6	5.0E-8 – 1.0E-6	m2/s
C7106(2,1) - High burn-up value of D_0.	1.0E-6	2.5E-7 – 1.0E-6	m2/s
C7106(4,1) - Activation energy Q.	3.814E5	2.41E5 – 3.814E5	J/kg-mole
C7106(5,1) - Equivalent sphere radius of fuel grain.	6.0E-6	6.0E-6 – 1.0E-5	m

Table 5-3. CORSOR-Booth Class Scaling Factors: Nominal Values

RN Group	Sensitivity Coefficient	Value	Units
XE	C7103-XE	1.0	-
CS	C7103-CS	1.0	-
BA	C7103-BA	4.0E-4	-
I2	C7103-I2	6.4E-1	-
TE	C7103-TE	6.4E-1	-
RU	C7103-RU	2.5E-3	-
MO	C7103-MP	6.25E-2	-
CE	C7103-CE	4.0E-8	-
LA	C7103-LA	4.0E-8	-
UO2	C7103-UO2	3.2E-4	-
CD	C7103-CD	2.5E-1	-
AG	C7103-AG	1.6E-1	-

RN Group	Sensitivity Coefficient	Value	Units
CSI	C7103-CSI	6.4E-1	-
CSM	C7103-CSM	1.0	-

To reduce computational burden and number of model evaluations in sensitivity analysis, only CORSOR-Booth coefficients for cesium release was considered. The uncertainty in release of other RN groups will be included through variability of Cs release, since these are defined through scaling factors in sensitivity coefficients array - SC7103 [10][11].

5.3.2. Fuel rod collapse

Currently, the Swedish MELCOR model of the Nordic BWR employs the time-vs-temperature model for fuel rod collapse, presented in [12]. Fractional damage is accrued in this way locally by axial level and radial ring throughout the core. The best practice dependence of time-to-failure as a function of temperature, enforced through user input via tabular function is presented in Table 5-4.

Table 5-4. Best-estimate time to fuel rod collapse versus cladding oxide temperature.

Cladding Temperature (K)	Time to Failure (Sec)
2000.0	1.0E10
2090.0	8.64E5
2100.0	36000.0
2500.0	3600.0
2600.0	300.0
2700.0	30.0

Times to failure intermediate to entries in Table 5-4 are linearly interpolated. Infinite lifetime is assumed at cladding oxide temperatures below the melting point of Zircaloy. The relatively short time associated with 2500 K and the even shorter time associated with 2600 K reflect the melting tendencies of irradiated fuel inferred from the Phebus experiments. Damage function accumulation does not begin until unoxidized cladding thickness drops below 10% of nominal values [12].

VTT's MELCOR model of Olkiluoto 1&2 uses the default time-at-temperature model for fuel rod collapse. The MELCOR manuals do not specify the default time to failure as a function of temperature, so it is not possible to compare the default model with Table 5-4.

Based on [16], the information obtained from VERDON and VERCORS tests showed that the systematic fuel collapse has been observed for a temperature range of 2300-2800K irrespective of burnup. Furthermore, the analysis showed significant effect of the final atmosphere in the tests (VERCORS HT2 vs. VERCORS HT1/HT3, VERCORS RT6 vs. VERDON-1, VERDON-3 vs. VERDON-4). It was observed that in oxidizing conditions the relocation temperature was systematically lower (~200K) than in reducing conditions [16].

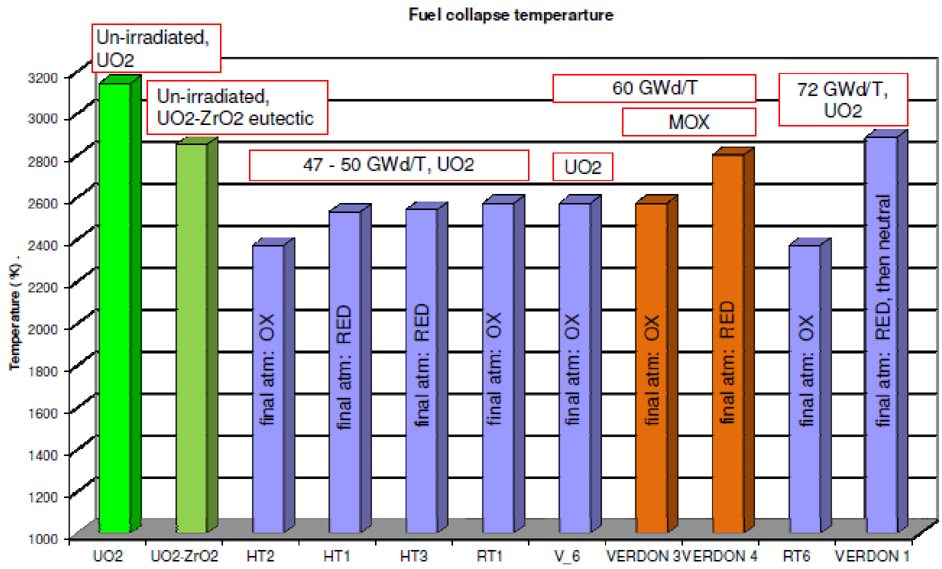

Figure 5-1. Fuel collapse temperature of VERCORS and VERDON tests compared with melting point of un-irradiated UO2 and UO2-ZrO2 eutectic [16].

Based on the considerations above, it is suggested to use the fuel rod collapse model presented in the NUREG/CR-7008 [12], with scaling coefficient applied on the tabular function to cover a wider range of temperatures of fuel rod collapse, as illustrated in Figure 5-2.

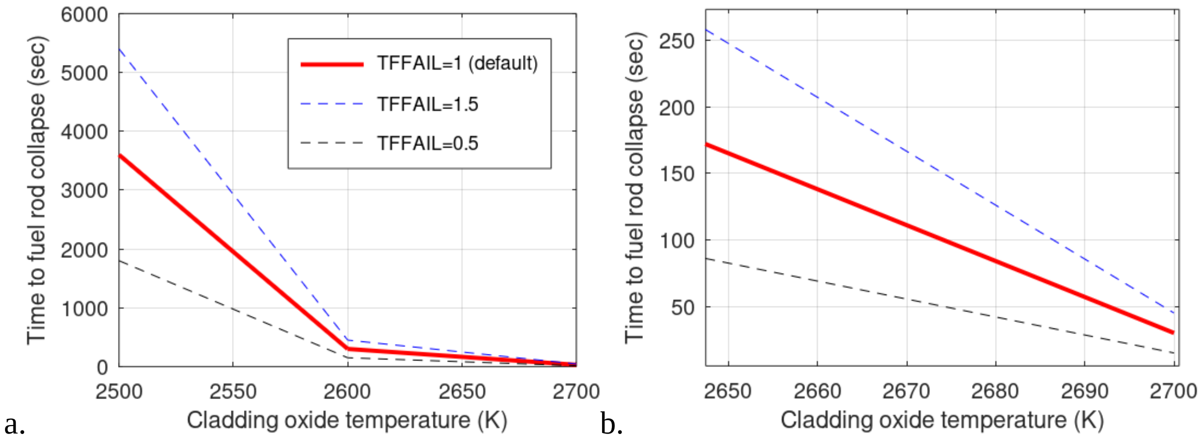

Figure 5-2. Time to fuel rod collapse versus cladding oxide temperature.

Modelling parameter (scaling coefficient of the tabular function for fuel rod collapse time vs. cladding oxide temperature, IRODDAMAGE record) *TFFAIL = 1* with range [0.5,1.5] (-).

5.3.3. Material interactions

In the current models of Nordic BWRs, the eutectics model is disabled, and all material interactions are captured via secondary material transport model (COR_CMT - a simple model that allows transport of unmolten secondary materials by melt, e.g., transport of UO2 or ZrO_2 by molten Zr, see COR package manuals in [10]).

Significant improvements in modelling of eutectic formations between zirconium and stainless-steel, zirconium and inconel, as well as between uranium oxide and zirconium oxide have been made during recent years [13]. Thus, it is suggested to perform a “separate effect” evaluation of the model on code predictions of in-vessel accident progression and vessel lower head failure.

The eutectics model can be activated by setting COR_EUT input record to ON or by specifying eutectic pairs (e.g. ZR/SS, ZR/INC, UO2/ZRO2), solidus temperatures for the eutectic pair (e.g. 1210K, 1210K, for ZR/SS and ZR/INC; 2450K for UO2/ZRO2 – all default values) and molar fraction of the first member in the pair at the eutectic temperature (default options are 0.76, 0.76 and 0.5 for ZR/SS, ZR/INC and UO2/ZRO2, respectively, see COR package manuals in [10] for more details).

The following parameters will be considered in sensitivity analysis (Table 5-5):

- Solidus temperatures for ZR/SS and ZR/INC eutectic pairs will be represented by a single parameter TZRSSINC.
- Solidus temperature for UO2/ZRO2 eutectic pair will be represented by TUO2ZRO2.

Table 5-5. Solidus temperature for eutectic pairs.

Parameter	Default [K]	Range [K]
TZRSSINC	1210	1210-1700
TUO2ZRO2	2450	2450-2800

VTT has observed that the new eutectics model causes calculations to crash frequently. Therefore VTT is using the 2014 best practice [12] of "interacting materials" UO_2-int and ZrO_2-int, with the melting temperature set to 2800 K.

5.3.4. Oxidation kinetics.

The MELCOR models of Nordic BWR employ a general oxidation model of structural materials (such as zircaloy and steel) which is discussed in detail in the COR reference manual [10]. The general oxidation model calculates the reacted metal mass using standard parabolic kinetics. Solid-state diffusion of oxygen through an oxide layer to unoxidized metal is represented by the parabolic rate equation (see eq (2-156) in [10]) where the rate constant is expressed as an exponential function of surface temperature multiplied by the low and high temperature range constants (see Chapter 2.5.1 in COR reference manual in [10] for details).

The default values of sensitivity coefficients SC1001-N-1 (N=1,2,3,4) for low temperature (SC1001-5-1 < 1853K) and high temperature (SC1001-6-1 > 1873K) oxidation of Zr by steam corresponds to the Urbanic-Heidrich model [18]). To address the uncertainty in Zr oxidation models and underlying parameters, different oxidation models were considered instead of considering variations in either rate coefficients or exponents (see COR package user´s manual for details [11]), which was inspired by the work done in [20].

Four correlations for the rate of zirconium–steam oxidation will be considered in sensitivity analysis, based on the work performed in [19][20]. The models to be used in the analysis are presented in Figure 5-3 and Table 5-6.

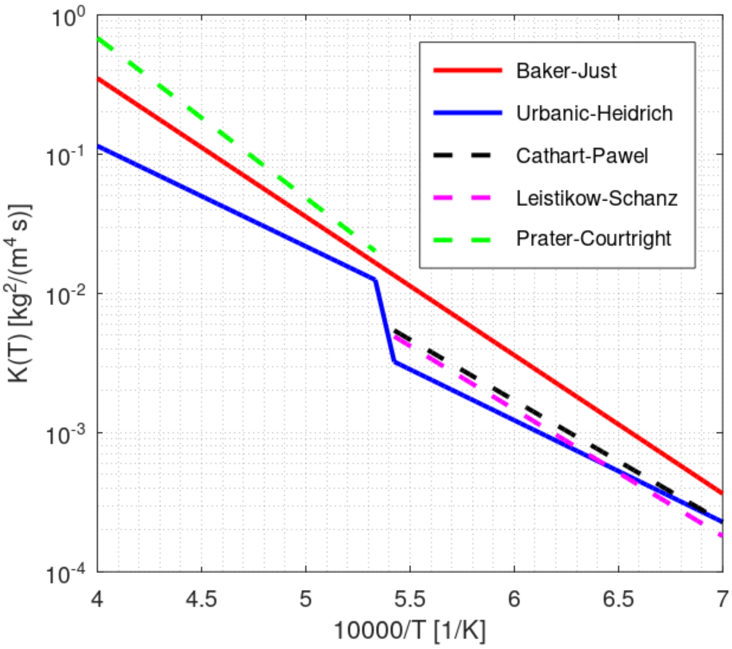

Figure 5-3. Zr oxidation rate as a function of temperature.

Table 5-6. Zr-steam oxidation models and parameters.

OXM	High temperature oxidation model		Low temperature oxidation model	
1	Urbanic-Heidrich	SC1001-1-1=29.6 SC1001-2-1=16820	Urbanic-Heidrich	SC1001-3-1=87.6 SC1001-4-1=16820
2	Prater-Courtright	SC1001-1-1=26763.6 SC1001-2-1=26440	Urbanic-Heidrich	SC1001-3-1=87.6 SC1001-4-1=16820
3	Prater-Courtright	SC1001-1-1=26763.6 SC1001-2-1=26440	Baker-Just	SC1001-3-1=3330 SC1001-4-1=22897
4	Prater-Courtright	SC1001-1-1=26763.6 SC1001-2-1=26440	Leistikow-Schanz	SC1001-3-1=425.8 SC1001-4-1=20962

The models will be switched using the parameter OXM = 1,2,3,4.

5.3.5. Radiative heat transfer

Radiative exchange factors for radiation radially outward and upward from the cell boundary to the next adjacent cell (FCELR and FCELA) affect inter-cell radiation, incorporating spatial information and view factors [10][11]. Based on the literature review [12], the following range will be used for both parameters: FCELRA = [0.1,0.25](-).

5.4.Fission products aerosol dynamics.

During severe accidents, fission products may be aerosolized as they are released from fuel early in the sequence and later expelled from the reactor coolant system. Other events and processes that occur later, such as core-concrete interactions, pool boiling, direct containment heating, deflagrations, and resuspension may also generate aerosols. High structural temperatures may also result in aerosolization of nonradioactive materials [10].

In the MELCOR code, the aerosol dynamics are based on the MAEROS computer code, but without direct inclusion of condensation or evaporation within the MAEROS solution framework. Vapor condensation on and evaporation from aerosol particles are handled separately to reduce the stiffness of the differential equation set and to ensure consistency with the calculation of these processes by other models and packages [10].

The MELCOR calculation of changes in aerosol distribution and location within a plant considers the following general processes [10]:

1) aerosol sources from other packages, such as release from fuel rods or during core-concrete interactions, and user-specified sources;
2) condensation and evaporation of water and fission products to and from aerosol particles;
3) particle agglomeration (or coagulation), whereby two particles collide and form one larger particle;
4) particle deposition onto surfaces or settling through flow paths into lower control volumes;
5) advection of aerosols between control volumes by bulk fluid flows; and
6) removal of aerosol particles by engineered safety features, such as filter trapping, pool scrubbing, and spray washout.

The RN package includes models to simulate each of these processes, but only user-defined aerosol sources and agglomeration and deposition processes are formally coupled in the MAEROS integrated solution framework. See MELCOR code RN package reference manual [10] for detailed description of MELCOR modelling of aerosol dynamics.

Based on the literature review [10][11][26][27][28][29], the modelling parameters described in sections 5.4.1 to 5.4.7 was considered in sensitivity analysis.

5.4.1. Agglomeration and dynamic shape factors.

The models describing aerosol dynamics have been traditionally developed for spherical, fully dense particles. Dynamic and agglomeration (collision) shape factors are introduced into the aerosol physics equations to describe the dynamics of non-spherical particles. These parameters are provided as MELCOR code inputs on RN1_MS00 record [11]. Real aerosol particles in the primary system or the containment are seldom either fully dense or spherical. So-called primary particles may agglomerate to form fractal structures but vapours condensing on them can change their shapes. Only at a very high humidity or with steam condensation in the bulk do the particles become spherical (droplets) [26].

In the SOARCA study, presented in [27], it has been assumed that agglomeration and dynamic shape factors are equal to 1 (which represents a perfectly spherical aerosol particle). The assumption is based on hygroscopic effects during the accident sequence, which will induce some condensation of moisture on the aerosol particles causing the particles to tend towards being spherical and limit the degree of non-spherical shapes.

The findings presented in [26] suggest that dynamic shape factors can range from 1 (for water filled voids) to 4 (dry voids), depending on accident conditions.

The analysis performed in [28] considered a range from 1 to 3. Furthermore it showed that variability in these parameters have high impact on the suspended aerosol mass in a control volume.

The following parameter ranges was considered [26][28][29]:

- Aerosol dynamic shape factor CHI = [1.0, 3.0] (-).
- Aerosol agglomeration shape factor GAMMA = [1.0, 3.0] (-).

5.4.2. Particle sticking probability

The rate of agglomeration is affected by the probability that a collision between two particles results in the two particles actually sticking together. Often this factor is taken as 1.0; however, this may depend on the wetness of the particles and could be influenced by electrostatic phenomena; like-charged particles that might otherwise collide and stick may instead fail to collide as their distance of separation closes [29]. This parameter is provided as a MELCOR code input on RN1_MS00 record [11]. The analysis performed in [28] suggest that this parameter has a strong influence on the suspended aerosol mass. The suggested range for this parameter is [0.25, 1] based on [29], and [0.5, 1] based on [28].

The following range was considered: STICK = [0.5, 1] (-).

5.4.3. Particle density

Gravitational deposition is often the dominant mechanism (especially for large control volumes). One of the sources of uncertainty within gravitational deposition is the particle density. This parameter is provided as a MELCOR code input on RN1_ASP record [11]. The default density used in MELCOR is 1000 kg/m^3, however the densities of materials represented in the RN classes of interest are in the range between 3700-4900 kg/m^3 [27].

The following range was considered: RHONOM = [1000, 4900] (kg/m^3).

5.4.4. Number of sections

Sections are particle size bins based on particle mass. This parameter is provided as a MELCOR code input on RN1_DIM record [11]. The MELCOR code default is 10 sections between 0.1 and 50.0 mm in geometric diameter.

The following range was considered: NUMSEC = [10, 20] (-).

5.4.5. Turbulence dissipation rate

The turbulent energy dissipation factor, [default 0.001 m^2/s^3] appears in the agglomeration coefficients in the turbulent shear and inertial terms [10]. This parameter is provided as a MELCOR code input on RN1_MS01 record [11]. The analysis performed in [28] suggests that this parameter has an important influence on the results and thus was considered in this study.

The following uncertainty range will be assumed: TURBDS = [7.5E-4, 1.25E-3] (m^2/s^3).

VTT's experience from the EU MUSA project shows that the turbulence dissipation rate has only a minor effect on the results. Therefore, VTT is not going to examine the effect of this parameter.

5.4.6. Chemisorption

MELCOR employs a set of models for chemisorption of fission product vapours on metallic surfaces. Based on a review of the MELCOR code manuals [10][11], when the chemisorption option is on (provided by MELCOR input card RN1_CAF ON), it uses default chemisorption classes defined in the reference manual (see RN package manual in [10]).

The parameters of the governing equations are implemented as sensitivity coefficient array SC7160.

Currently, due to modelling restrictions, such as no provision for revaporization of chemisorbed species, it is suggested to perform a separate effect evaluation of the chemisorption model on code results. This can be achieved by standalone MELCOR calculations for the best estimate model (default/BE values of modelling parameters and sensitivity coefficients) with chemisorption model being activated and deactivated.

5.4.7. Condensation, evaporation and hygroscopic behavior

Fission products and water can condense onto or evaporate from aerosols, heat structure surfaces, and water pools. Calculation of mass transfer due to condensation and evaporation of fission product vapours is performed in the MELCOR code using the TRAP-MELT2 equations [10][11], which employ vapour diffusivity for the fission product vapours in the bulk gas, calculated by the MP package, using the sensitivity coefficient array SC7111.

The sigma *C7111(1)* and E/K *C7111(2)* values are Lennard-Jones parameters, where sigma is a characteristic diameter of the molecule and E/K is the characteristic energy of interaction between the molecules divided by the Boltzmann constant [10][11]. The default values and proposed ranges of these parameters are presented in Table 5-7.

Table 5-7. Vapour diffusivity constants, from [11].

Class	Sigma C7111(1) (Å)	SA Range (default +/- 15%)	E/K C7111(2) (K)	SA Range (default +/- 15%)
Xe*	4.055	-	229	-
Cs, Ba	3.617	SC7111CS1= [3.0745,4.1595]	97	SC7111CS2= [82.450, 111.550]
I2	4.982	SC7111I1= [4.2347,5.7293]	550	SC7111I2= [467.50, 632.50]
Other (Te, Ru,…, CsI, CsM)	3.617	SC7111CS1= [3.0745,4.1595]	97	SC7111CS2= [82.450,111.550]

* The parameters will not be considered in SA/UA.

Aerosol particles (such as CsOH and CsI) that are soluble in water exhibit hygroscopic properties such that they can absorb moisture from an atmosphere with relative humidity less than 100%. This effect leads to a growth of the particle size as water vapor condenses onto the soluble particle. An important consequence of this growth in size (and mass) is an increase in the gravitational settling rate, and the subsequent depletion of airborne fission product aerosols.

In the MELCOR model of Nordic BWR the hygroscopic model is switched ON and uses default values of sensitivity coefficients (SC array 7170). The following parameters and ranges was considered:

- Saturation solubility at low temperature reference for Cs – RN Class Alkali Metals (CsOH) default value 3.95 +/-15%, SC7170CS = [3.3575, 4.5425] (kg/kg H2O).
- Saturation solubility at high temperature reference for Cs – RN Class Alkali Metals (CsOH) default value 3.95 +/-15%, SC7170CS = [3.3575, 4.5425] (kg/kg H2O).[9]
- Saturation solubility at low temperature reference for CsI – RN class CsI default value 0.44 +/-15%, SC7170CSI3 = [0.374, 0.5060] (kg/kg H2O).
- Saturation solubility at high temperature reference for CsI – RN class CsI default value 2.25 +/-15%, SC7170CSI4 = [1.9125, 2.5875] (kg/kg H2O).
- Saturation solubility at low temperature reference for CsM – RN class CsM default value 0.67 +/-15%, SC7170CSM = [0.5695, 0.7705] (kg/kg H2O).
- Saturation solubility at high temperature reference for CsM – RN class CsM default value 0.67 +/-15%, SC7170CSM = [0.5695, 0.7705] (kg/kg H2O).[10]

These parameters are entered as RN package sensitivity coefficients on the RN1_CSC record.

The Finnish NBWR MELCOR model does not consider cesium molybdate; all Cs is assumed to be CsOH and CsI.

5.5. Late in-vessel release

The release rate of fission products from the fuel and debris before core support plate failure is affected by several phenomena, such as formation of particulate debris in the core and debris relocation, molten material candling and refreezing on intact structures or debris, debris coolability above the core support plate as well as axial and radial debris relocation.

Based on the scoping analysis performed in [12][14] and [15] as well as review of recent modelling changes in the MELCOR code [13], a set of MELCOR modelling parameters was proposed to be addressed in sensitivity analysis, and discussed further in this section.

5.5.1. Debris formation

Fuel failure and formation of particulate debris (PD) from the fuel is discussed in section 1.3.2. Once particulate debris is formed, the MELCOR code treats it as a porous debris bed, that excludes other PD from an effective bed volume, V_{bed}, defined by [10][11]:

$$V_{bed} = \max\left(V_{material}, \frac{V_{unmelted}}{1-\varepsilon}\right) \quad (1)$$

where, $V_{material}$ is the total volume of material in the PD, $V_{unmelted}$ is the volume of the portion of the material that has never been melted and ε is a user-defined porosity (PDPor). The unmelted PD forms a debris bed with user defined porosity (PDPor), and molten

---

9 CS7170-CS-3 and CS7170-CS-4 will be represented by a single parameter CS7170CS.

10 CS7170-CSM-3 and CS7170-CSM-4 will be represented by a single parameter CS7170CSM.

materials may fill some or all of the pores. PDPor – is defined by a user for all cells in every axial level in COR package input.

The following range was considered: PDPor = [0.3, 0.5] (-).

The modelling of control rod failure in the MELCOR model of Nordic BWR is achieved by the temperature exceeding the threshold temperature at which NS (non-supporting structure that represents control rods) collapses, independent of the remaining metal thickness [10][12]. The recommended temperature for BWR control rods collapse as PD is 1520 K [12]. If this record is not defined, the COR package will use the default melting temperature of the material specified on COR_NSM record (Steel is the default).

Based on the above, the following range is proposed: CORNSBLD = [1520, 1700] (K).

5.5.2. Debris and molten material relocation

The MELCOR code calculates the radial relocation of solid and liquid debris using [10][11]:

$$V_{rel} = V_{eq}\left(1 - \exp\left(-\frac{\Delta t}{\tau_{spr}}\right)\right) \tag{2}$$

where V_{eq} – is the volume of the material that should be moved to balance the levels between two adjacent cells, τ_{spr} – is a time constant for radial solid SC1020(1) and liquid SC1020(2) debris relocation (see [10][11] for more details).

The downward relocation of particulate debris by gravitational settling is modelled in MELCOR as a constant-velocity process, with user defined velocity VFALL. The code determines (starting from bottom to top cells) how far particulate debris from a cell can fall during one MELCOR time step. Once the lowest cell in the correspondent ring is identified, the algorithm fills the available space, until either the debris source is exhausted or there is no free volume available. The process is repeated recursively, updating conditions after every iteration, for all cells in every radial ring (see [10][11] for more details).

Furthermore, the VFALL and DHYPDLP parameters are used in the falling debris quench model, which is triggered by a failure of core support plate in one of the radial rings. It is assumed in the MELCOR code that debris would fall into the lower plenum with user-defined velocity VFALL, and the heat transfer surface area will be calculated based on the assumption that the debris particles have an equivalent spherical diameter DHYPDLP. The model is deactivated once the leading edge of the jet reaches the bottom of the vessel, which is identified as the lowermost cell with empty volume available for PD. During the time between the failure of the core support plate and the time at which the falling debris leading edge reaches the lower head, the models for candling, dissolution, and radial spreading of debris in the affected ring are deactivated [10][11].

The default values for SC1020(1) and SC1020(2) are 360 s and 60 s respectively. The default value for VFALL is 1 m/s, however the value suggested by the SOARCA study [12] is 0.01 m/s.

Based on [10][11][12] the following ranges for VFALL = [0.01, 0.1] (m/s), SC1020(1) = [180, 720] (s) and SC1020(2) = [30, 120](s) was considered.

The MELCOR candling model assumes that molten mass is generated at a constant rate over the MELCOR time step [10][11] and flows downwards due to gravity. The refreezing heat transfer coefficients for different materials (such as molten stainless steel, Zircaloy, etc.) are used to calculate the mass that refreezes on different components below. The default values are 1000 W/m^2-K in MELCOR 1.8.6, and 2500 and 7500 W/m^2-K for stainless steel and zircaloy in MELCOR 2.2, respectively. Furthermore, the MELCOR candling model allows molten materials holdup by an oxide shell until the shell is breached. The sensitivity coefficient SC1131(2) (default value 2400 K) – defines the critical temperature (breach condition) at which molten materials (Zircaloy) are released from an oxide shell (ZrO_2) or local blockage (crust). Furthermore, MELCOR uses the molten cladding drainage rate, defined by sensitivity coefficient SC1141(2) (default value 1 kg/m-s), that represents the maximum flow rate (per unit surface width) of the molten material after breakthrough. This is necessary since the assumption built into the candling model of constant generation of melt over the time step is no longer valid when molten materials have been just released after hold up by an oxide shell or by a flow blockage (crust) [10][11].

Based on [12], the following parameter ranges will be considered: HFRZSS = [1000, 2500](W/m2-K), HFRZZR = [1000, 7500](W/m2-K), SC1131(2) = [2100, 2500](K) and SC1141(2) = [0.2, 2.0](kg/m-s).

5.5.3. Material relocation in the lower plenum

MELCOR represents particulate debris beds as composed of fixed-diameter spheres. It is assumed in MELCOR that when structure failure criteria are reached, the structure is converted into particulate debris with a user defined porosity (PDPor) and particle size. Moreover, the debris porosity in every COR cell can change over time due to molten material relocation (candling) or melting of the materials in PD with lower melting points. The particulate debris equivalent diameter, together with the particulate debris porosity will define its volume and surface area, which will affect the extent of debris coolability (heat transfer surface area), oxidation (oxidation surface area), and material relocation (free volume). The diameter DHYPDLP is also used in the falling debris quench model, to calculate heat transfer area of the debris falling into water in the lower plenum, following the failure of the core support plate.

Based on [12][17] the following range for lower plenum particulate debris equivalent diameter was considered: DHYPDLP = [0.002, 0.005] (m)

In the MELCOR in-vessel falling debris quench model, it is assumed that debris falls with a user-specified velocity and heat transfer coefficient. This allows the debris to lose heat to the surrounding water in the lower plenum as it falls to the lower head, following failure of the core support plate in each radial ring [10][12][11].

The following range for the heat transfer coefficient was considered: HDBH2O = [200, 2000] (W/m^2-K).

5.6.Vessel failure modelling

It is assumed in the MELCOR code that the reactor pressure vessel (RPV) Lower Head (LH) can fail through the following mechanisms:

i. Penetration failure, when the temperature of a penetration reaches a failure temperature (TPFAIL) specified by a user, or a logical control function specified by a user [10][11].
ii. Vessel lower head wall failure due to:
    a. Creep-rupture failure of a lower head segment, which occurs in response to mechanical loading under conditions of material weakening at elevated temperatures (failure is declared when the strain fraction reaches the value

specified by SC1601(4), with default value of 0.18 – which corresponds to 18% strain);

b. Gross failure of the lower head segment is assumed when the temperature of the bottom lower head node exceeds the penetration failure temperature TPFAIL (default value 1273 K) defined by the user [10][11].

These two mechanisms are not mutually exclusive, i.e. gross vessel wall failure can follow penetration failure if respective conditions are fulfilled (see [10][11] for more details).

Based on the literature review (see ([10][11][12][21][22]) the following ranges was considered:

- TPFAIL – [1273, 1600] (K).
- HDBPN – [100, 1000] (W/m^2-K) – heat transfer coefficient between particulate debris and LH penetration (default value 1000 W/m^2-K).

The creep rupture strain limit will not be considered in the sensitivity analysis, since this parameter was identified as a parameter that has a negligible effect on the timing of the lower head failure in the analysis performed in [15].

In this work, lower head penetrations and correspondent failure modes are only modelled for instrument guide tubes (IGTs), since, according to [22], the control rod drive housing support located under the vessel limits downward displacement of control rod guide tubes to approximately 3 cm, while the thickness of the vessel lower head is around 20 cm. Therefore, the scenario with ejection of the control rod guide tubes was not considered in the analysis.

In MELCOR model of the Swedish BWR, the total of 66 IGTs are uniformly distributed between the radial rings, proportionally to the area of the horizontal cross section of the rings. Furthermore, in the analysis we assume two options for IGT failure, i.e. we assume that either 25% or 100% of IGTs would fail in every radial ring (EIGT25 and EIGT100), once the failure criterion is reached, to account for inherent randomness of the process and possible clamping of IGTs due to, for instance, vessel lower head deformation [23]. Then the initial effective area of the breach (prior to ablation) due to IGTs failure is calculated based on:

$$A_{IGT_{eff}} = N_{IGT} \pi D_{IGT}^2 / 4 \tag{3}$$

and the effective breach diameter is calculated:

$$D_{IGT_{eff}} = D_{IGT} \sqrt{N_{IGT}} \tag{4}$$

where D_{IGT} = diameter of an IGT penetration (m), and N_{IGT} = number of failed IGTs in every radial ring.

The effect of the number of failed instrumentation guide tubes N_{IGT} at every radial ring when the penetration temperature exceeds the value defined in TPFAIL can be considered in the sensitivity analysis. The study performed in [15] showed that the vessel breach size (25% vs. 100% of IGTs in respective radial ring) can have a quite significant impact on the accident progression. In the analysis of the Swedish BWR we assume that 50% of IGTs (in respective radial ring) will be ejected once the temperature of penetrations exceeds the value specified in TPFAIL.

5.7. Melt & debris ejection modelling

After the lower head has failed, the mass of each material in the bottom axial level that is available for ejection (but not necessarily ejected) is calculated. There are two options available, provided by a so-called solid debris ejection switch. In the default option (ON, IDEJ = 0), the masses of each material available for ejection are the total debris and molten pool material masses, regardless of whether or how much they are molten (see Figure 5-4). In the second option (OFF, IDEJ = 1), the masses of steel, Zircaloy, and UO2 available for ejection are simply the masses of these materials that are molten; the masses of steel oxide and control poison materials available for ejection are the masses of each of these materials multiplied by the steel melt fraction, based on an assumption of proportional mixing; the mass of ZrO_2 available for ejection is the ZrO_2 mass multiplied by the Zircaloy melt fraction. Additionally, the mass of solid UO_2 available for ejection is the Zircaloy melt fraction times the mass of UO_2 that could be relocated with the Zircaloy as calculated in the candling model using the secondary material transport model [10][11]. Furthermore, MELCOR puts additional constraints on the mass that can be ejected at vessel failure: (i) to initiate melt ejection, the mass of molten material should be greater than SC1610(2) (5000 kg – default value), or a melt fraction should be larger than SC1610(1) (0.1 – default value).

Here, the values of sensitivity coefficients SC1610(1,2) were set to zero, so any amount of melt available for ejection would be ejected. However, VTT considered it better to use the default values, in order to prevent numerical problems in the Cavity package.

We expect that limiting debris ejection to only molten materials (IDEJ 1) would lead to the vessel wall being exposed to hot oxidic debris for a longer period of time, which may result in accumulation of debris and delayed failure of the vessel LH wall.

In case of gross failure of the vessel wall, it is assumed that all debris in the bottom axial level of the corresponding ring, regardless its state, is discharged linearly over 1 s time step without taking into account the failure opening diameter. The maximum mass of all materials that can be ejected during a single COR package time step is calculated as [10][11]:

$$M_{ej} = \rho_m A_f v_{ej} \Delta t \qquad (5)$$

where ρ_m – is density of material being ejected, A_f - failure area, v_{ej} – velocity of debris being ejected, Δt – COR package time step. The fraction of the ejected material mass M_{ej} to the total mass available for ejection has a maximum value of 1.0. This fraction is applied to each material available for ejection. The velocity of material being ejected is calculated by [10][11]:

$$v_{ej} = C_d(2\Delta P/\rho_m + 2g\Delta z_d) \qquad (6)$$

where C_d is the flow discharge coefficient (C_d = 1 (default value) was used in the analysis presented in this paper), ΔP = pressure difference between LP and reactor cavity control volumes, g = gravitational acceleration constant, and Δz_d = debris and molten pool height (see references [10][11] for more details).

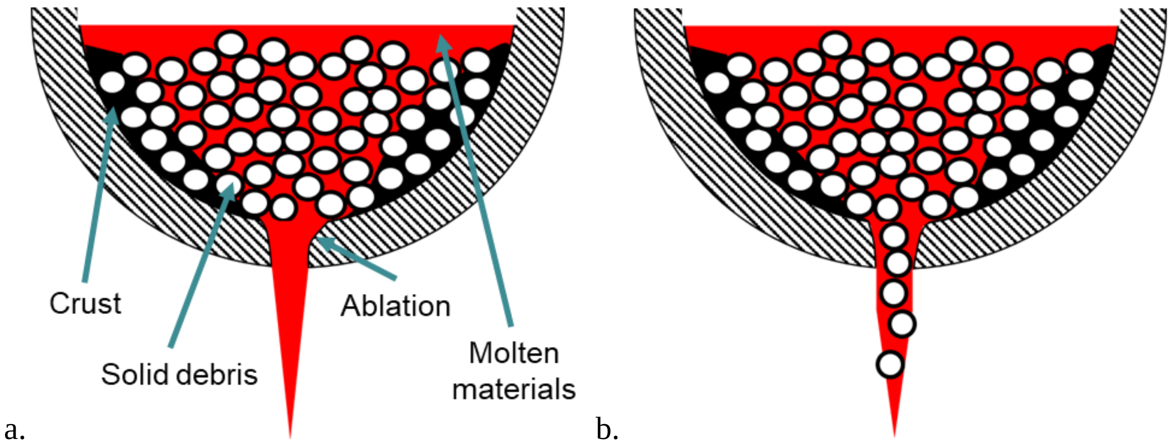

Figure 5-4. Mode of debris ejection from the vessel (a) solid debris ejection – OFF (IDEJ1); (b) solid debris ejection – ON(IDEJ0).

The effect of the mode of debris ejection from the vessel (IDEJ= 0 or 1) was considered as a phenomenological splinter [30]. The work performed in [15][31][32] and [25][33] showed that the mode of debris ejection from the vessel is the major contributor to the uncertainty in melt release conditions and conditional probability of containment failure due to ex-vessel phenomena.

5.8.Fuel Dispersal Interactions (FDI) package

Debris enters the FDI package via the Transfer Process (TP) package interface from the core (COR) package after failure of the reactor pressure vessel has been calculated.

After the introduction of debris material, the FDI package classifies the ejection event as either a low- or a high-pressure melt ejection event on the basis of the ejection velocity passed through the TP package [10][11].

Previous analysis performed in [15] showed that in high pressure scenarios the vessel lower head fails due to failure and ejection of IGTs, well before formation of significant amounts of molten materials in the lower plenum, which effectively leads to RCS depressurization through failed IGT penetrations in one of the radial rings. Furthermore, other mechanisms, such as MSL creep rupture, or SRV stucking open can lead to RCS depressurization well before the vessel LH failure. Olkiluoto 1&2 have several methods to depressurize the reactor before lower head failure. If DC power is available, the automatic depressurization system will actuate. If DC power is lost, two so-called fast opening valves will automatically open and keep the reactor pressure at a low level.

Thus, the scenario with high pressure melt ejection and associated phenomenological uncertainties are not considered as risk significant and will not be included in the present study. Low pressure RPV failure and melt ejection was considered as the dominant mode of RPV failure and debris ejection to the cavity.

No FDI modelling parameters will be considered.

5.9.Ex-vessel release

Formation of aerosols in the containment following an accident is more of an issue than formation in reactor cooling system (RCS). Time scales for the aerosol formation in the containment leads to transformations due to radiolysis, oxidation, formation of bicarbonates. There is a potential for secondary sources of aerosols in the containment due to ejection of corium, hydrogen deflagration and MCCI. Aerosols usually with low volatility produced in the containment provide a long-term aerosol and FP source [44]. The phenomena related to ex-vessel release is discussed here.

5.9.1. Fuel Coolant Interactions

FCI is complex thermohydrodynamical mixing process during a severe accident involving core melting and relocation. Premixing is the first phase in the progression of melt release to the cavity. Premixing involves fragmentation and melt dispersion. Premixing may lead to [45][44]

- Steam explosion (SE) under certain critical circumstances
- Global pressurisation of the containment from boiling or local pressurisation of pit
- Formation of debris bed based on fragmentation and solidification of melt

Phenomenologically SE occurs by the following inter-related mechanisms [46]

- Break-up of corium jet into varied size debris particles
- Interfacial heat transfer between melt and 2 phase mixture during mixing
- Fragmentation of debris submerged in water pool into finer particles
- Explosive heat transfer between finer particles and water

Jet breakup is a crucial point in premixing that results in uncertainties in generation rate and size of droplets, distribution of droplets, solidification, and void fraction [46]. Significant work has been done regarding the fragmentation and heat transfer [47][48][49]. Capillary instabilities in the case of small jets, and Rayleigh Taylor & Kelvin Helmholtz (KH) instabilities in the case of large jets are considered as the dominant mechanisms of jet breakup processes [50][51].

OECD/SERENA project was conducted to address issues of FCI and its impact on ex-vessel SE [52]. It concluded jet fragmentation model improvement is important in defining scope of SE event (premixing > voiding > explosion triggering > explosion propagation). Recent improvements in KH based models are sufficient, with further studies in jet fragmentation with local conditions, non-vertical jets and high velocity jets need focus [47].

Melt fragmentation controls void formation and melt solidification, both of which mitigate SE triggering and strength. Voiding in premixing stage is due to two phenomena – vapour (possibly with hydrogen) due to heat and mass transfer around melt drops; and two-phase flow of coolant. While physics of heat and mass transfer around drops is known sufficiently, improvements in description and experimental data can be helpful. The same can be said for two-phase flows [52]. Voiding enhances velocity difference before and after shock wave, this in turn enhances fragmentation.

FARO tests showed strong dependency of SE on void [44]. KROTOS showed presence of high voids in premixing stage, however its effect on mitigation was not analysed [53]. Melt density, coolant temperature and water sub-cooling were found to be an important parameter describing formation of voids [52]. Mitigating effect of voids was especially noted at high void fractions and at large scales [54]. Voiding is also an important effect in pressurisation stage of SE.

Melt solidification prevents fine fragmentation, thereby preventing/limiting SE. It also allows formation of coolable debris bed [55]. For melts with oxidic corium UO2/ZrO2 this phenomenon during premixing stage is responsible for strong reduction of potential explosion loads [56][57]. Solidification is dependent on the corium composition and conditions of cooling and steam removal at the surface of the droplet. Considering metallic, sub-stoichiometric or stoichiometric corium, little experimental data exist with no parametric laws [52]. Tests in KROTOS and TROI produced ambiguous results which require further understanding of the phenomena [52]. Recently crust models have been implemented in FCI codes, that need further study because the theoretical assumption of elastic behaviour of crust is unlikely [57].

Hydrogen generation by oxidation of UO2/ZrO2 melts is demonstrated with experiments (KROTOS and FARO), however its impact is not characterised because of uncertainties in kinetics of the phenomena and material properties [44]. While this is demonstrated, data is scarce, and results also show ambiguity in mitigation (in SERENA [52]) of SE and magnitude (in ZrEx). OECD report [56] concluded that this phenomenon and impact on FCI was poorly understood. Modelling is difficult firstly; it occurs in varied situations at very high melt temperatures. Secondly, strong feedback impact in 3 ways; 1) hydrogen production, 2) energy input, and 3) change melt properties.

Currently modelling of is largely parametric due to lack of analytical experimental data.

5.9.1.1.Ex-Vessel Steam Explosion

SE is a complex phenomenon involving high temperatures, supercritical pressures, oxidation and melt solidification [55]. Initial conditions of the SE depend on the premixing stage. SE process can be subdivided into 4 steps [58]

- Premixing phase
- Triggering phase
- Propagation phase
- Expansion phase

Fine fragmentation (FR) of the melt during premixing phase governs the explosivity. FR increases the contact area for rapid heat transfer between the melt and water. The thermal loads are transformed into pressure buildup leading to mechanical shockwaves. Triggering is initiated by collapse of vapour film, caused by destabilization of interface due to thermal effect or external disturbance [59]. Two type of fragmentation can be involved in a SE [65].

- Thermal fragmentation – destabilization of vapour film (cause of this is an area of study) and occurs influential at the early parts of SE
- Hydrodynamic fragmentation – involves Rayleigh-Taylor instabilities, Kevin-Helmholtz instabilities and boundary layer stripping. This fragmentation occurs in 2 integral ways: 1) drop accelerated in surrounding media; 2) shock impacts the drop and is dominant in propagation phase

Several phenomenological models regarding FR exist [60][61], models put forth by Ciccarelli & Frost [62] was consistent in early experiments performed in MISTEE [60] where the melt drops pre-fragments upon destabilisation of vapour film. The coolant was also found to be entrained in the drop as was proposed by Kim & Corradini [63]. TEXAS-V uses an adapted version of [63] to model FR.

According to Inoue [64] the destabilization of vapour film causes local contacts, this leads to strong local pressurization leading to destabilization of the drop. Further studies are based on this premise. KROTOS experiments [53] showed that SE is always possible if the triggering has enough strength. While triggering is considered stochastic event and thermal fragmentation as cause for it, Pavel et al [68] found systematic spontaneous and energetic steam explosions during spreading phase of simulants in shallow water while no SE were observed in DEFOR-S [69] and DEFOR-A. Further understanding of triggering is needed.

Following the trigger of an explosion, the initial pressure wave causes destabilization of the vapour films of surrounding melt drops leading to FR subsequently leading to high pressures. Subsequently the pressure drives hydrodynamic fragmentation owing to relative motion of melt and coolant. KROTOS experiment [66] compared SE in alumina and corium (UO_2/ZrO_2) and found SE in alumina is stronger compared to corium, leading to discussions of material effects. The velocity of the propagating front is affected by the initial peak pressure and the void.

SERENA-II [47] allowed to clarify this effect. Effect of solidification and oxidation on fragmentation and pressurization need to be addressed. There is also a need to address lateral break. FARO tests [67] have showed generation of hydrogen in the corium-water interaction. This void generation may also explain weaker explosions in corium.

Pressurization is the sudden release of energy following fragmentation. Pressurization occurs due to change in the density of the coolant. Due to low compressibility of the coolant pressurizations of upto 1000 bar have been recorded in KROTOS experiment. Two models for pressurization

- Micro-interactions approach – proposed by Chen [70] and Theofanous [71] heat from fuel melt is transferred to only a part of coolant. Heated part is transient and is determined by the entrainment of coolant into microinteraction field (melt and coolant in thermal equilibrium, called m-state). Pressurization is linked to thermal expansion of the hot liquid coolant. This model assumes that only small part of water participates in the interaction.
- Direct boiling (vapourization) or non equilibrium approach – proposed by Berthoud & Brayer [72] and used by Corradini & Tang [73] in TEXAS. Portion of the heat from melt is transferred directly to coolant, resulting in vapour boiling at the vapour liquid interface under thermal nonequilibrium. Pressure buildup is due to phase change. The remaining coolant is homogenously heated by heat not used in boiling. This coolant heatup has secondary impact.

TREPAM experiment [74] simulated heat transfers between fragments and coolant in conditions close to an explosion in reactor conditions, has shown that there exists vapour film at the surface, even in supercritical conditions, supporting the nonequilibrium approach. There is however a consensus regarding the need for further study of the phenomena involved, the use of constant value of entrainment as against constitutive law for it, integration of non-condensable gases, effect of void on the pressurization are current focus of studies.

PULIMS experiment at KTH [75][68] demonstrated that the melt might spread on the cavity floor and participate in the SE or trigger it. Certain accident scenarios with large jet and shallow pool can be susceptible to this. A premixed layer forms above the stratified melt and can spontaneously trigger SE [76].

Several phenomena were hypothesized for the existence of premixture layer [68].

- Periodic process of growth, expansion and collapse of steam bubbles, producing an impact of water on the melt, creating a splash
- Evaporation of entrapped bubbles under melt surface water
- Rapid release of non-condensable gases during melt cooling
- Melt spread interface instabilities
- Jet breakup and impingement on the melt layer

Further experiments are necessary to clarify physical phenomena for interface instability and formation of premixing layer.

5.9.2. Debris Bed Coolability

The cooling of the debris bed is provided by heat transfer to the water that ingresses into the porous bed interior. Coolability can be assessed in 2 stages

- Quenching of debris particles settled on the cavity floor
- Long-term cooling of the quenched particles

Steam generated inside debris bed is escaping upwards. Upward flow changes conditions for FCI. FCI changes particle properties (size distribution and morphology). Particle properties affect the debris bed coolability phenomena. It is essential to know how the quench front propagates, and if the bed can completely be quenched before local particles remelt.

Long-term coolability is limited by the dryout heat flux (DHF) and is associated to a steady-state where evaporated water is replaced by water ingress in the bed [77]. Fragmentation drives easy coolability, due to higher surface area for heat transfer. Fragmentation also causes uneven particle size distribution, which is unfavourable to cooling.

In boiling water reactors (BWRs) multiple control rod guide tube penetrations in the lower head may lead to early vessel failure before steel failure, leading to multiple jets of melt. The fragmentation of melt is dependent on the vessel pressure when failure occurs. High-pressure melt ejection causes melt to be in jet form with energetic gas discharge, leading to fine particles and wider spreading area. Gravity-driven melt ejection, with low vessel pressure, leads to less dispersal and dense corium collection which forms hard to cool bed.

Several experiments and theoretical programs have been performed to understand and gain knowledge regarding the coolability. General criteria accepted for a successful long-term cooling is that flow rate of coolant through the porous bed is high to prevent any local dryout. Natural circulation of coolant is expected to prevent dryout [78].

Phenomenon involved in debris bed formation and coolability is complex and involves mechanisms with own efficiency limits,

- Jet fragmentation
- Melt droplet sedimentation and interaction with coolant
- Debris agglomeration
- Particle spreading by pool flow
- Debris bed self levelling by vapour flows
- Debris bed coolability
- Post dryout behaviour with remelting

Debris bed coolability is affected by

- Debris properties
- Accident scenario parameters
- Geometrical configuration of the bed

If the pool depth is shorter than jet breakup length, then the melt will form a cake at the top of the bed. This will impede spreading of the debris and its coolability. Particle spreading due to circulation flows are effective when the coolant is [partially] vapourised. This may also affect transmissibility of fission products when there is containment failure. Previous work by Pavel [78] has shown that formation of a tall and non-coolable debris bed is very less likely and that dryout will not impede the self-levelling of the debris bed.

Dryout has received extensive focus on model development and experiment [79][80][81]. These studies assume a thermal equilibrium between debris bed and the saturated water pool. Further studies [82][83] on the propagation of quench front were performed. Recently DEBRIS facility [84] investigated quench of hot and dry debris, the boiling phenomena and validation of friction laws included in dryout models. PEARL facility performed large scale reflooding tests to study degraded core coolability with large scale debris beds [85].

With the flow of steam and coolant in a concurrent flow, and in certain regions (upper regions) it may happen that the steam flux limits coolant flux needed to replace steam and this critical steam flux determines the dryout heat flux (DHF). This is the case in a 1D homogenous particulate bed with top flooding [80] and with bottom flooding [83][86].

In further studies on multidimensional effects, mostly 2D axisymmetric conditions, natural circulation loops can be established [87], and with downcomers, DHF was found to increase [88]. With heap-like shape, complex multi-dimensional flow of coolant into the debris bed is possible [90]. DEFOR-E studies [94] showed porous beds formed is far from homogeneous. COOLOCE experiment by VTT [91][92][93] performed under SAFIR program and POMECO-HT experiment at KTH [81] investigated this multidimensionality of conical and stratified beds and found an increase in heat removal capacity.

Under SARNET program DEFOR-A [95][96] tests were performed that studied fraction of agglomeration of debris as a function of water depth, water subcooling and jet diameter. Formation of debris cake was found to be important on the coolability of the debris. Agglomeration can be avoided if the jet diameters are minimal [97][98], and with larger jets cake formation occurs.

The effect of particle diameter and porosity were studied previously, summarized in [87][89]. Larger particles have smaller surface area in comparison. Implying smaller frictional forces and flow resistance, improving coolability of porous medium. Internal voids in remelted particles (encapsulated porosity) also effect coolability and this needs to be studied in detail.

Height of debris bed is another important parameter affecting coolability. Debris is coolable if it is spread over the basemat than form a tall mound shaped bed [92][100-104]. Height is determined by phenomenon of

- melt release scenarios (rapid, gradual, multiple releases)
- pool conditions (saturated or subcooled, deep or shallow)
- melt fragmentation
- particle sedimentation and interaction with two-phase flows in the pool
- as well as avalanching of the debris heap

In a gradual melt release, natural convection can be very efficient in flattening the debris bed formed in a saturated pool, or in a subcooled pool after the onset of boiling [103][104][105]. In rapid melt release, the particle avalanching is likely to play the primary role in determining the initial debris bed shape. Shape of the bed can change by the vapor flow through the bed according to spreading/self-leveling phenomenon [106-109] which was demonstrated at KTH [110][111]. Investigations mentioned previously have demonstrated that time scale for spreading can vary significantly, depending on the initial debris bed configuration and other relevant parameters [90][103-115].

The system pressure affects coolability through steam properties. At higher pressures steam density is higher, and volume is smaller. Larger heat removal rate can be achieved with denser steam because of larger pore volume available for coolant. Squarer et al. [117] and Miyazaki et al. [116], investigated effect of pressure on dryout and noticed that the DHF increased with increasing pressure. The decrease in the latent heat of vaporization as a function of pressure counteracts the effect of the increased density but, for containment-relevant pressures, density increase is the dominant effect [118]. In reactor typical cases the system pressure to be expected depends strongly on the reactor type, as well as the accident history.

Limiting condition (DHF) for a steady state in a debris bed is given by the counter-current flooding limit (CCFL) [119], where just all evaporated coolant can be replaced. High power in bed causes dryout at the bottom, causing remelt. Enhanced coolability can be expected if coolant inflow via the bottom of the particle bed is possible.

Studies have shown that bottom flooding and multi-dimensional flooding are clearly more effective in removing heat than top flooding [81][86][120-122]. In cases with bottom flooding, the CCFL is not the limit of coolability, because not all the water necessary to maintain steady cooling has to penetrate the debris bed from above. Higher liquid saturation in lower bed causes friction of the coolant to be reduced.

Discussion in [89] showed it is generally not possible to determine the coolability of volumetric heated debris by just using bed properties like bed height, porosity, particle diameter and system pressure. A more detailed analysis with a multidimensional model to include realistic configurations is necessary.

This is similar regarding the case of inhomogeneities. Experiment by Hofmann [124] showed for a simple 1D top fed configuration, the coolability is dramatically reduced for smaller particle sizes. Reduction is due to the capillary pressure at the interface between the main particle bed and the layer of the smaller particles. This effect will be reduced if other flow paths to the main debris exist.

From the point of view of coolability, post-dryout behaviour also needs to be considered. It may happen that a new steady state is reached with stabilized temperature and without remelting [91][125]. Some form of post dryout temperature stabilization were seen in COOLOCE with truncated cone configuration.

In this case coolable refers to the limited increase of temperature, not to the loss of liquid water in the pores of the bed. It is worth considering defining the coolability limit using the solid temperature, rather than the void fraction because

- the void fraction criterion may be overly conservative
- it is the high temperature that threatens the containment integrity, not the phase fraction.

Cooling mechanisms of an ex vessel debris bed were studied in the MACE and MCCI with real corium in top flooding arrangement. These experiments defined various debris heat transfer mechanisms that could provide long-term cooling [127]. Formation of a stable crust at the interface of the coolant and debris bed that inhibits heat transfer limits the coolability. Two conditions have to be met for a stable crust [126]

- Thermal condition – interfacial temperature must be below corium freezing temperature
- Mechanical condition – mechanical loads of the agitated melt must be tolerated by the crust

This is the bulk cooling regime, where predominantly conduction and radiation heat transfers (across agitated interface) occurs, and lasts till formation of stable crust. The melt concrete interaction leads to generation of gas, and the effective heat transfer coefficient depends on gas sparging rate, bubble size, thermophysical properties of the mixture, coolant properties and containment pressure [126].

The crust is characterized by some degree of porosity, or cracks, owing to venting concrete decomposition gases. Following that the heat transfer occurs via conduction through the crust and water ingress to the melt along the thin cracks. Quenching can be completed if

- Melt depth is below the minimum depth at which decay heat can be removed via conduction alone
- Water is able to penetrate into the debris to provide sufficient augmentation to the heat transfer process

Three mechanisms can provide pathway for coolant to penetrate the debris

- Water ingression forms additional cracks due to quenching. Water ingression thins the boundary between crust and melt enhancing heat transfer and is dependent on the crack propagation process.
- Melt eruptions occurs when the pressure built up by the gases generated by corium concrete interaction is unable to vent through the cracks. The erupted melt then quenches and forms a porous particle bed in contact with the coolant. Melt is entrained in the gases, which are expedited when heat removal rate of the crust decreases, leading to higher melt temperature and more concrete interactions [126].
- It may happen that the thick crust formed is attached to the sidewalls, and with the lower melt eroding into the concrete, the suspended crust separates from the melt (volume shrinks due to decarbonisation), due to its mechanical instability from its own weight, the weight of the coolant above, accumulated dispersed material and pressure of decomposed gases. Eventually the suspended crust will fail, leading to rapid ingression of water beneath the crust [126].

The cooling mechanisms will repeat and lead to massive heat removal from the melt. For the break to happen at least one third of the melt has to be crust. The crust may also float in the melt pool, and in that case there will be no crust breach. In the experiments so far this beach has not been observed, while experts believe most probable configuration would involve crust attached to the cavity walls with a floating crust area in the middle [126][127]. The coolability of corium was demonstrated integrally in the COTELS experiments [128], whereas MACE could not clearly demonstrate coolability in top flooding condition [127]. The reasons for coolability of debris in COTELS experiments in contrast to MACE tests are speculated to be

- The sidewall concrete erosion prevented bonding of the crust on the walls
- Water was able to penetrate beneath the melt through the cracks near the sidewall and melt coolant interface
- Some inherent porosity was formed in the melt during the pouring of the melt to the concrete crucible that enhanced coolability

5.9.3. Molten Corium Concrete Interaction

When the lower drywell flooding is unavailable and the melt from the RPV collects in the cavity, or if the available coolant has all evaporated and is unable to cool the debris, there will be enhanced molten corium concrete interaction (MCCI). MCCI has the potential to cause

- Pressurization of the RCV by long-term release of non-condensable gases.
- Ablation of concrete basemat.
- Ablation of concrete side wall to degrade its capability as an RPV supporting structure.

Thermal ablation is the major process governing the interactions. MCCI have a highly complex phenomenology coupling concrete high-temperature behaviour, molten pool thermal hydraulics, thermochemistry, mechanics [129]. Without additional measures, melt-through may occur, depending on the basemat thickness.

The release of steam and gases from concrete decomposition increases the containment pressure. Moreover, the hydrogen and carbon monoxide from such concrete decomposition lead to an increase of combustible gases. A further consequence of corium concrete interaction is the release of fission products in form of vapors and aerosols.

Many experiments were conducted at Sandia National Laboratory - SWISS, SURC, HOT SOLID [130-132]. These tests mainly analyzed the behavior of concrete during the ablation process, the release of fission products, and also the ablation kinetics.

Recent experiments such as MCCI, VULCANO, COMET-L [133-138] mainly address two subjects

- The 2D aspects of the ablation
- Crust formation and melt segregation

MACE tests [137] conducted at Argonne National Laboratory (ANL) focused on quantifying fission product release during MCCI. Aerosols released in ACE tests contained mainly constituents of the concrete. In the tests with metal and limestone/sand or siliceous concrete, silicon compounds comprised 50% or more of the aerosol mass, with low releases of uranium and low-volatility fission-product elements, and high releases of tellurium and neutron absorber materials. The dry cavity test results show that core-concrete interaction during the early phase is influenced by the extent of unoxidised cladding that is initially present in the melt. During the long-term, the nature of the core-concrete interaction is found to be a strong function of concrete type.

One of the major findings of the MCCI and VULCANO tests was the observation that dry ablation tests with silica-rich concretes tend to present an anisotropic ablation, radial rate ablation to be faster than the axial ablation rate, resulting in a more efficient ablation of the sidewalls compared to downwards ablation. The tests with limestone-rich concrete showed a more isotropic ablation. CLARA [140], BALI [141] and ÉCLAIR [142] focused on anisotropic ablation behaviour. These indicated that asymmetric gas sparging alone is not responsible for the physical differences in ablation behaviour observed for different concrete types.

The oxides in corium and concrete are miscible with each other, but the metallic species are immiscible with the oxides. Because the metals are lighter than the corium oxides, a metallic layer may be formed on the surface of the oxidic pool [139]. When concrete oxides are added to the melt, its density decreases eventually below the density of the metals and the metallic layer may relocate to the bottom of the pool. On the other hand, intense stirring of the pool by the rising gas bubbles may cause the metals and the oxides to be mixed with each other. This phenomenon is a real challenge [143].

5.9.4. Effect of ex-vessel phenomena on the containment and environmental source term

In general, the major contribution to the uncertainty in energetic ex-vessel phenomena is the uncertainty in the likelihood of containment failure and unmitigated/unfiltered release of the airborne activity in the containment to the environment. The study (integrated DSA-PSA, NKS-SPARC project) performed in [144], showed that the expected value of conditional probability of unacceptable release can increase by a factor of 5, depending on the uncertainty in melt release conditions. The ex-vessel phenomena also have significant contribution to the generation and deposition of FPs and aerosols in the containment.

The major part of high-volatile FPs will be released in-vessel during the core degradation phase. Later, aerosols may be generated ex-vessel by MCCI, with pool boiling and resuspension processes also leading to FP release. Aerosols usually with low volatility produced in the containment through the MCCI provide a long-term aerosol and FP source, after the in-vessel release phase.

In case of MCCI, the melt temperature has a major influence on the quantity of aerosol and FP release. It is assumed that volatile FPs are released rapidly during the MCCI. For the less volatile components, the non-volatile release fraction depends on the molten debris structure. As the melt reacts with concrete components and as melt temperature decreases, releases decline [126]. In general, the MCCI has a negative effect on the containment pressurization rate, it has a positive effect on the rate of aerosol deposition in the containment (due to increased concentration of non-radioactive aerosols in the containment atmosphere, which promote aerosol agglomeration and gravitational settling).

For the Nordic BWR conditions, where SAM measures rely on melt-debris fragmentation and cooling in the deep pool of water in the reactor cavity, the likelihood of MCCI and its effect on the airborne activity in the containment is expected to be minimal.

Ex-vessel steam explosion can result in the release of fission products into containment as a result of interactions between molten core debris and water (FCI).

On the other hand, if the containment remains intact, the generation of fission products which may occur from the ejected melt fragments will then be accompanied by rain-out and wash-out effects. As a consequence, a large fraction of the released products will be removed from the atmosphere by serving as nuclei for the steam condensation or just by impaction of water droplets. Furthermore, significant amount of steam produced can affect deposition rates of hygroscopic FPs (such as CsOH).

5.10. In-containment and environmental source term

Engineered Safety Features models are currently available for the removal of radionuclides by pool scrubbing, filter trapping, and spray scrubbing [10][11].

5.10.1.Containment sprays scrubbing

The MELCOR SPR package, which calculates the thermal-hydraulic behaviour associated with spray systems, is coupled to the RadioNuclide (RN) package for the calculation of aerosol washout and atmosphere decontamination by the sprays. The spray model includes vapour adsorption and aerosol removal by diffusiophoresis, inertial interception and impaction, and Brownian diffusion. Aerosols and fission products removed by the sprays are deposited in the pool associated with the control volume or a user-defined sump pool.

The containment droplet diameters in MELCOR code are defined via a discrete probability distribution. In the MELCOR model of the Swedish BWR, the droplet diameter is DIAMO = 1 mm. In VTT's model of Olkiluoto 1&2, the diameter is 1.5 mm.

Note that when the SPR package is coupled to the RN package for the calculation of aerosol washout and atmosphere decontamination by sprays, there are several limitations of this interface which require some restrictions on the input to the SPR package to avoid nonphysical results associated with multiple calculations in the same control volume. When the SPR and RN packages are both active, the user should limit the spray input so that only one spray train passes through each control volume and only a single drop size is used in this spray train [10][11].

Based on [34] the following droplet size range was considered: DIAMO = [0.0001, 0.002] (m).

5.10.2.Pool scrubbing and filters trapping

The pool scrubbing models, adapted from the SPARC-90 code (A Code for Calculating Fission Product Capture in Suppression Pools, see reference [10] in MELCOR RN Package reference manual [10]), include the effects of steam condensation at the pool entrance and aerosol deposition by Brownian diffusion, gravitational setting, and inertial impaction, subject also to evaporative forces, for the rising bubble. Decontamination is calculated only for those flow paths activated on the FL_JSW input record (see the FL Package Users' Guide [11]). As further specified by the user on input record RN2_PLS, the model treats regular flow paths that vent through pools, as well as gases generated by core-concrete interactions flowing through overlying pools. Iodine vapor is also scrubbed [10][11].

Furthermore, the MELCOR RN package contains a simple filter model. When aerosols and vapours are transported through flow paths with the bulk fluid flow, a fraction of the transported RN materials may be removed by the action of filters in the flow path. A single filter can remove either aerosols or fission product vapours, but not both. However, a flow path can contain more than one filter. The efficiency of each filter is defined by decontamination factors, specified by user input. By default, a single decontamination factor is applied to all RN classes except water, for which the default DF is 1.0. Additional user input may be used to modify the DF on a class-by-class basis, including the water class. The parameters for the filter characteristics are specified on the RN2_FLT input record.

The effect of filter mass loading on the flow resistance of the associated flow path may be modelled through user input. A maximum loading may be specified for each filter; when this loading is reached, no further RN materials are removed (i.e., the DF is set to unity) [10][11].

In the Swedish MELCOR model of Nordic BWR, the SPARC-90 model is enabled for the following flow paths:

- FP203 (Blowdown pipe exit): Connecting CV230 (Blowdown pipe) and CV250 (Wetwell).
- FP207 (Overflow pipe exit): Connecting CV240 (Overflow pipe between LDW and WW) and CV250 (Wetwell).
- FP314 (ADS): Connecting CV180 (Steamlines) and CV250 (Wetwell).
- FP330 (VX105 motor operated valves in ADS): Connecting CV180 (Steamlines) and CV250 (Wetwell).

VTT's model of Olkiluoto 1&2 has the SPARC model for similar flow paths, even though the path numbers differ from the Swedish model.

Furthermore, the MELCOR model of Swedish BWR employs the Multi Venturi Scrubber System (MVSS) filter with constant decontamination factor DF=500 for aerosols implemented for the flow path connecting the upper drywell and MVSS[11]. Based on the literature review, the efficiency (DF) offered by the FILTRA-MVSS system is in the range from 100 (guaranteed DF) to 500 (design DF) [42]. MVSSDF = [100, 500] (-). VTT added the filter to the containment venting system, with a default DF of 500 for aerosols.

The following sensitivity coefficients was considered in the SPARC-90 model:

- SC7150 SPARC-90 Model Parameters. SC7150-10 vent exit condensation decontamination factor scaling factor. This factor is applied to the decontamination factor that is calculated as a result of steam condensation in the vent exit region that occurs when the bubbles are thermally equilibrated with the pool temperature. Based on [10][11] the following range was considered: SC715010 = [1, 3] (-).

- SC7151 SPARC-90 Globule Size Correlation. The SPARC-90 model employs a correlation that relates the initial size of the globule formed to the Weber number of the gas exiting the vent [10][11]. SC7151-1-1 is the Weber number multiplier used in the equation for the initial diameter of the gas globule for a sparger-type vent (see equations in RN Package user's guide [11]). The following range was considered: SC715111 = 3.45 (default value) +/- 15% = [2.9325, 3.9675] (-).

- SC7152 SPARC-90 Bubble Size/Shape Model. In the SPARC-90 Bubble size model, the mean diameter of the bubbles formed at the vent exit depends solely on the fraction of non-condensable gases, and is thus limited between 0.561 cm (with 0 fraction) and 0.681 cm (with 1 fraction), when considering default values of sensitivity coefficients [35][36]. For the purpose of sensitivity analysis, we will consider

[11] DF factor for RN Class Xe equals to 1.

SC7152-1 - initial bubble diameter correlation coefficient, with default value equal to 7.E-3 m, with the following range: SC71521 = [5.E-3, 8.E-3] (m) (see Figure 5-5).

- SC7153 SPARC-90 Bubble Rise Velocity Model. Coefficient for rise velocity correlation of small bubbles (diameter below SC7153-3 = 0.5 cm). Only the coefficient for rise velocity correlation of small bubbles SC7153-1 was considered, since it is involved in calculation of rise velocities for both, small and large bubbles (see equations in RN Package user's guide [11]). The default value of SC7153-1 is 7.876 cm/s. The following range (default +/-15%) was considered: SC71531 = [6.6946, 9.0574] (cm/s).

- SC7155 SPARC-90 Particle Impaction Model. If the gas bubbles leave the vent exit at a high velocity, the initial globules rapidly loose that velocity. The forwards globular interface, as it slows and stops, can capture particles if they have sufficient inertia. In the SPARC-90 model, inertia and drag of particles is represented by the Stokes number, which is a function of particle diameter, density, vent exit gas velocity, gas viscosity, and vent diameter (see equations in RN Package user's guide [11]). Sensitivity coefficients SC7155-1 and SC7155-5 are the multiplication constants in the DF factor correlations for small (SC7155-1) Stokes numbers, and large (SC7155-5) Stokes numbers. The transition value is defined by SC7155-4 (see [11]). The following sensitivity coefficient and ranges was considered:

    - SC7155-1, default value 1.79182 with range (default +/-15%) SC71551 = [1.5230, 2.0606] (-).

    - SC7155-5, default value 1.13893 with range (default +/-15%) SC11555 = [0.9681, 1.3098] (-).

- SC7154 – SPARC-90 Swarm Velocity Model. SPARC-90 bubble swarm rice velocity was identified as one of the most influential parameters on the pool scrubbing efficiency (DF) in [35]. Based on the analysis of SPARC-90 bubble swarm rice velocity correlation models presented in [11] and [36] with default values of sensitivity coefficients, proposed in [36] (see also red curve in Figure 5-6), the following parameter was considered: SC7154-2 = 3.011E-3 l-s/cm^2 with uncertainty range (default +/-15%) SC71542 = [2.5593E-03, 3.4626E-03] l-s/cm^2, (see the respective uncertainty range of average swarm rice velocity (cm/s) as a function of the gas injection velocity (l/s) in Figure 5-6 (blue dashed curves)). Note that the maximum velocity is limited by the sensitivity coefficient SC7154-5 = 170 cm/s (see black dashed line in Figure 5-6).

- SC7156 SPARC-90 Solute Ionization Correlations. SPARC-90 combine all particle growth mechanisms into one set of relationships, see [36]. Sensitivity coefficient array SC7156 represents additive and multiplicative factors in the van't Hoff factors, which are used in modelling hygroscopic effects that promote steam condensation on hygroscopic particles, even in subsaturated atmospheres [36][11]. Based on the analysis of the models involved (see equations 2.87 – 2.92 in [36]), all van't Hoff factors for CsI and CsOH are corrected for temperature based on equation 2.92 in [36]. For the purpose of the sensitivity analysis, we will use the multiplicative constant in a temperature correction correlation SC7156-8 with default value equal to -2.321E-3 (-) with uncertainty range (default +/-15%) SC71568 = [-2.6691e-03, -1.9728e-03] (-).

- SC7157 SPARC-90 Settling Velocity Correlation. In the SPARC-90 model a set of empirical correlations is used to determine the Reynolds number (Re) to calculate the settling velocity of particles in the rising bubbles [11]. To reduce the computational burden, for sensitivity analysis we will consider denominator factors in the settling velocity correlations (SC7157-N, N=2, 5, 8, 11, 14) = (27, 24.32, 15.71, 6.477, 1.194). The default values of sensitivity coefficients will be scaled by a scaling factor SC7157 sampled on interval [0.85, 1.15] (-), see Figure 5-7.

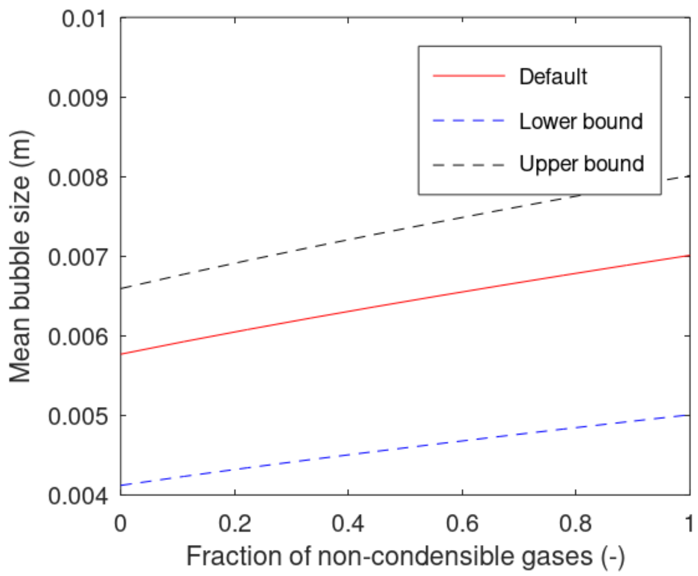

Figure 5-5. SPARC-90 Mean bubble size model.

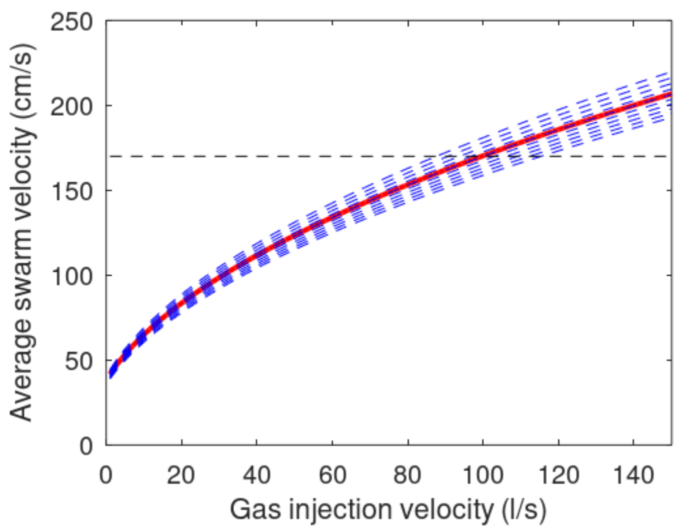

Figure 5-6. SPARC-90 average swarm velocity as a function of gas injection velocity (default model - red curve) at 9m depth.

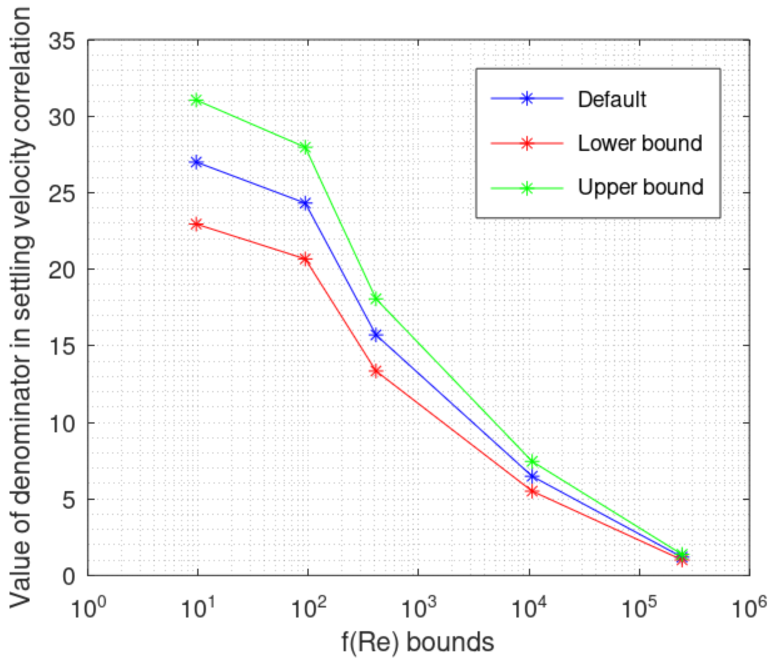

Figure 5-7. Sensitivity coefficients SC7157-Y (Y=2, 5, 8, 11, 14) vs. respective values of SC7157-X (X=1, 4, 7, 10, 13).

5.11. Summary of uncertainties of interest

Table 5-8 presents the summary of the MELCOR modeling parameters and respective ranges for the sensitivity analysis. Parameter variations not considered in the Finnish NBWR MELCOR model are highlighted.

Table 5-8. Summary of the parameters to be considered in sensitivity analysis.

N	Group	Parameter name	Default	Range	Units
1	FP Release from fuel	SC710611	1.0E-6	[5.0E-8, 1.0E-6]	m2/s
2		SC710621	1.0E-6	[2.5E-7, 1.0E-6]	m2/s
3		SC710641	3.814E5	[2.41E5, 3.814E5]	J/kg-mole
4		SC710651	6.0E-6	[6.0E-6, 1.0E-5]	m2/s
5		CORSOR-BOOTH ICRLSE	-5	-5 or -7	-
6	Core degradation and relocation	TFFAIL	1	[0.5,1.5]	-
7		TZRSSINC	1210	[1210, 1700]	K
8		TUO2ZRO2	2450	[2450, 2800]	K
9		OXM	1	[1,2,3,4]	-
10		FCELRA	0.25	[0.1, 0.25]	-
11		PDPOR	0.3	[0.3, 0.5]	-
12		CORNSBLD	1520	[1520, 1700]	K
13		VFALL	0.01	[0.01, 0.1]	m/s
14		SC10201	360	[180, 720]	s
15		SC10202	60	[30, 120]	s
16		HFRZSS	1000	[1000, 2500]	W/m2-K
17		HFRZZR	1000	[1000, 7500]	W/m2-K
18		SC11312	2400	[2100, 2500]	K
19		SC11412	0.2	[0.2, 2.0]	kg/m-s
20		DHYPDLP		[0.002, 0.005]	m
21	RPV lower head failure	HDBH2O	100	[200, 2000]	W/m2-K
22		TPFAIL	1273	[1273, 1600]	K
23		HDBPN	1000	[100, 1000]	W/m2-K
24		IDEJ	1	0 or 1	-
25	FP & Aerosol dynamics	CHI	1	[1.0, 3.0]	-
26		GAMMA	1	[1.0, 3.0]	-
27		STICK	1	[0.5, 1]	-

N	Group	Parameter name	Default	Range	Units
28		RHONOM	1000	[1000, 4900]	kg/m^3
29		NUMSEC	10	[10, 20]	
30		TURBDS	1.E-3	[7.5E-4, 1.25E-3]	m^2/s^3
31		SC7111I1	4.982	[4.2347, 5.7293]	Å
32		SC7111I2	550	[467.50, 632.50]	K
33		SC7111CS1	3.617	[3.0745,4.1595]	Å
34		SC7111CS2	97	[82.450,111.550]	K
35		SC7170CS	3.95	[3.3575, 4.5425]	kg/kg H2O
36		SC7170CSI3	0.44	[0.374, 0.5060]	kg/kg H2O
37		SC7170CSI4	2.25	[1.9125, 2.5875]	kg/kg H2O
38		SC7170CSM	0.67	[0.5695, 0.7705]	kg/kg H2O
39	Spray & pool scrubbing and filters trapping	DIAMO	0.001	[0.0001, 0.002]	m
40		SC715010	1	[1,3]	-
41		SC715111	3.45	[2.9325, 3.9675]	-
42		SC71521	0.007	[5.E-3, 8.E-3]	m
43		SC71531	7.876	[6.6946, 9.0574]	cm/s
44		SC71551	1.79182	[1.5230, 2.0606]	-
45		SC11555	1.13893	[0.9681, 1.3098]	-
46		SC71542	3.011E-3	[2.5593E-03, 3.4626E-03]	l-s/cm2
47		SC71568	-2.321E-3	[-2.6691e-03, -1.9728e-03]	-
48		SC7157	1	[0.85, 1.15]	-
49		MVSSDF	500	[100, 500]	-
50		SC3210	1	[1, 1.15]	-

Given the fact that some default values are at the end of the specified ranges, a case ID numbering of bounding analyses was defined, see Table 5-9. Cases corresponding to parameter variations not considered in the Finnish NBWR MELCOR model are highlighted.

Table 5-9. Case ID numbering for bounding parameter analyses

	Parameter	Parameter value
Case 0	Best estimate	
Case 1	SC710611	5.000E-08
Case 2	SC710621	2.500E-07
Case 3	SC710641	2.410E+05
Case 4	SC710651	1.000E-05
Case 5	TFFAIL	5.000E-01
Case 6	TFFAIL	1.500E+00
Case 7	TZRSSINC	1.700E+03
Case 8	TUO2ZRO2	2.800E+03
Case 9	FCELRA	2.500E-01
Case 10	PDPOR	3.000E-01
Case 11	PDPOR	5.000E-01
Case 12	CORNSBLD	1.700E+03
Case 13	VFALL	1.000E-01
Case 14	SC10201	1.800E+02
Case 15	SC10201	7.200E+02
Case 16	SC10202	3.000E+01
Case 17	SC10202	1.200E+02
Case 18	HFRZSS	1.000E+03
Case 19	HFRZZR	1.000E+03
Case 20	SC11312	2.100E+03
Case 21	SC11312	2.540E+03
Case 22	SC11412	1.000E+00
Case 23	DHYPDLP	5.000E-03
Case 24	HDBH2O	2.000E+02
Case 25	TPFAIL	1.600E+03
Case 26	HDBPN	1.000E+03
Case 27	CHI	3.000E+00
Case 28	GAMMA	3.000E+00
Case 29	STICK	5.000E-01
Case 30	RHONOM	4.900E+03
Case 31	NUMSEC	20
Case 32	TURBDS	7.500E-04
Case 33	TURBDS	1.250E-03
Case 34	SC7111I1	4.235E+00
Case 35	SC7111I1	5.729E+00
Case 36	SC7111I2	4.675E+02
Case 37	SC7111I2	6.325E+02
Case 38	SC7111CS1	3.075E+00
Case 39	SC7111CS1	4.160E+00
Case 40	SC7111CS2	8.245E+01
Case 41	SC7111CS2	1.116E+02
Case 42	SC7170CS	3.358E+00
Case 43	SC7170CS	4.543E+00
Case 44	SC7170CSI3	3.740E-01
Case 45	SC7170CSI3	5.060E-01
Case 46	SC7170CSI4	1.913E+00
Case 47	SC7170CSI4	2.588E+00
Case 48	SC7170CSM	5.695E-01
Case 49	SC7170CSM	7.705E-01
Case 50	DIAMO	1.000E-04
Case 51	DIAMO	2.000E-03
Case 52	SC715010	3.000E+00
Case 53	SC715111	2.933E+00
Case 54	SC715111	3.968E+00
Case 55	SC71521	5.000E-03
Case 56	SC71521	8.000E-03
Case 57	SC71531	6.695E+00
Case 58	SC71531	9.057E+00
Case 59	SC71551	1.523E+00
Case 60	SC71551	2.061E+00
Case 61	SC71555	9.681E-01
Case 62	SC71555	1.310E+00
Case 63	SC71542	2.559E-03
Case 64	SC71542	3.463E-03
Case 65	SC71568	-2.669E-03
Case 66	SC71568	-1.973E-03
Case 67	SC7157	8.500E-01
Case 68	SC7157	1.150E+00
Case 69	OXM	4
Case 70	IDEJ	1
Case 71	MVSSDF	1.000E+02
Case 72	SC3210*	1.150E+00
Case 73	CORSOR-BOOTH ICRLSE	-7

* Scaling of existing value.

6. Analysis specification

Based on the selected accident sequences from section 4.5 and the uncertainties of interest summarized in section 5.11, each of the project participant organizations responsible for MELCOR simulations in the project defined a number of bounding analysis cases. The cases were simulated using MELCOR 2.2.18019 over 24 h with reactor shutdown occurring at t = 0 h. It should be noted that the cumulative release of radionuclides for some of the studied scenarios may need a significantly longer time to stabilize. In view of this, the 24 h simulation time was chosen as a reasonable trade-off between the computation time needed to perform all analyses and the interest of presenting results as being close to the total releases.

KTH and VG performed their analyses on the same Swedish configuration NBWR model, described in section 3.2.1, while VTT performed their analyses on the Finnish configuration NBWR model, described in section 3.2.2. Release category RC7A, station blackout leading to filtered containment venting, was simulated both in the Swedish and the Finnish model, however with different assumptions regarding the mechanism for opening of MVSS.

The number of bounding cases simulated by each organization was selected based on selected accident sequences as well as on available time and computation resources.

7. Results

Note that these results cannot be interpreted statistically as no likelihoods or distributions have been associated with the identified bounding parameter ranges during the first phase of the project. Also, the results are influenced by numerical noise and time step sensitivity, whose impacts have not been quantified. Sensitivity analysis and statistical quantification is planned for the following project phases.

7.1. KTH results

KTH studied option 1 and option 2 scenarios from section 4.5.1. In option 1, scenario is initiated by a large LOCA at t = 0, without water injection/sprays. The parameter variations are shown in Table 7-1 for this scenario, and are compared to the reference case. In option 2, scenario is initiated by a SBO at t = 0. The parameter variations are shown in Table 7-2 for this scenario, and are compared to the reference case. The selected parameters that will be studied further are highlighted in the tables.

7.1.1. RC4A – Large Break LOCA leading to containment failure due to ex-vessel phenomena at RPV melt-through.

Table 7-1. RC4A bounding analysis results.

Case ID	PARAMETER	TLHF [h]	CS_ENV [-]	I2_ENV [-]	TLHF [%]	CS_ENV [%]	I2_ENV [%]
0	REFERENCE CASE	1.736	0.069	0.072	-	-	-
1	SC710611	1.783	0.055	0.082	2.736	-20.140	13.464
2	SC710621	1.767	0.051	0.066	1.824	-26.120	-8.155
3	SC710641	1.870	0.121	0.134	7.754	76.129	84.697
4	SC710651	1.852	0.044	0.052	6.689	-35.783	-28.436
5	TFFAIL	1.783	0.055	0.082	2.736	-20.140	13.464
6	TFFAIL	1.783	0.055	0.082	2.736	-20.140	13.464
7	TZRSSINC	2.003	0.052	0.066	15.416	-24.312	-8.763
8	TUO2ZRO2	2.460	0.124	0.162	41.691	80.854	123.550
9	FCELRA	2.143	0.068	0.106	23.466	-0.209	46.416
10	PDPOR	1.807	0.061	0.063	4.115	-11.481	-12.951
11	PDPOR	1.794	0.050	0.077	3.377	-26.860	6.615
12	CORNSBLD	1.732	0.071	0.073	-0.211	3.649	1.297
13	VFALL	1.319	0.065	0.064	-23.991	-5.138	-11.324
14	SC10201	1.726	0.056	0.068	-0.567	-18.614	-5.912
15	SC10201	1.779	0.057	0.073	2.472	-16.959	1.011
16	SC10202	1.985	0.059	0.066	14.363	-13.790	-8.756
17	SC10202	1.653	0.040	0.044	-4.785	-40.997	-39.583
18	HFRZSS	1.866	0.023	0.025	7.524	-66.266	-65.678
19	HFRZZR	1.910	0.063	0.099	10.026	-8.607	37.549
20	SC11312	2.241	0.073	0.111	29.129	7.151	53.501

Case ID	PARAMETER	TLHF [h]	CS_ENV [-]	I2_ENV [-]	TLHF [%]	CS_ENV [%]	I2_ENV [%]
21	SC11312	1.702	0.049	0.073	-1.966	-28.178	1.586
22	SC11412	1.924	0.034	0.037	10.851	-49.764	-48.449
23	DHYPDLP	1.594	0.058	0.061	-8.187	-14.899	-15.107
24	HDBH20	1.757	0.057	0.085	1.228	-16.750	17.447
25	TPFAIL	2.222	0.053	0.076	28.022	-23.302	5.071
26	HDBPN	1.463	0.122	0.157	-15.735	78.234	117.189
27	CHI	1.921	0.040	0.045	10.646	-41.982	-37.737
28	GAMMA	2.473	0.052	0.063	42.476	-23.925	-13.443
29	STICK	1.872	0.091	0.123	7.826	32.573	70.294
30	RHONOM	1.705	0.049	0.061	-1.763	-28.489	-14.987
31	NUMSEC	1.495	0.052	0.057	-13.852	-23.776	-20.706
32	TURBDS	1.703	0.070	0.074	-1.908	2.550	1.927
33	TURBDS	1.788	0.060	0.090	3.008	-12.646	25.003
34	SC7111I1	1.774	0.042	0.060	2.212	-38.283	-16.720
35	SC7111I1	2.351	0.142	0.183	35.415	106.815	152.978
36	SC7111I2	1.883	0.059	0.091	8.498	-14.562	26.004
37	SC7111I2	1.522	0.055	0.059	-12.333	-19.790	-18.220
38	SC7111CS1	1.918	0.067	0.103	10.474	-1.500	43.053
39	SC7111CS1	1.819	0.038	0.047	4.818	-44.673	-34.785
40	SC7111CS2	2.108	0.080	0.113	21.459	17.067	56.566
41	SC7111CS2	1.567	0.034	0.038	-9.745	-50.819	-47.864
42	SC7170CS	1.750	0.058	0.077	0.799	-14.952	6.288
43	SC7170CS	1.872	0.037	0.045	7.839	-45.943	-38.023
44	SC7170CSI3	1.737	0.073	0.103	0.095	5.876	42.974
45	SC7170CSI3	1.685	0.063	0.090	-2.954	-7.787	24.215
46	SC7170CSI4	2.424	0.098	0.130	39.658	42.766	79.604
47	SC7170CSI4	1.684	0.044	0.053	-2.960	-35.780	-26.670
48	SC7170CSM	1.797	0.061	0.102	3.536	-10.359	40.715
49	SC7170CSM	1.969	0.066	0.086	13.443	-4.070	19.214
50	DIAMO	1.783	0.055	0.082	2.736	-20.140	13.464
51	DIAMO	1.783	0.055	0.082	2.736	-20.140	13.464
52	SC715010	1.794	0.051	0.064	3.378	-25.841	-10.974
53	SC715111	1.783	0.055	0.082	2.736	-20.140	13.464
54	SC715111	1.783	0.055	0.082	2.736	-20.140	13.464
55	SC71521	1.856	0.055	0.064	6.946	-20.006	-12.077
56	SC71521	1.609	0.071	0.101	-7.294	3.420	40.002
57	SC71531	2.022	0.060	0.080	16.468	-12.937	10.810

Case ID	PARAMETER	TLHF [h]	CS_ENV [-]	I2_ENV [-]	TLHF [%]	CS_ENV [%]	I2_ENV [%]
58	SC71531	1.776	0.102	0.114	2.300	49.583	57.345
59	SC71551	1.828	0.053	0.059	5.298	-22.668	-19.039
60	SC71551	1.839	0.066	0.076	5.935	-4.123	5.138
61	SC71555	1.676	0.087	0.108	-3.438	27.187	48.817
62	SC71555	1.758	0.056	0.073	1.252	-18.026	1.036
63	SC71542	1.910	0.046	0.080	10.053	-33.490	10.654
64	SC71542	2.298	0.139	0.189	32.406	103.298	161.297
65	SC71568	1.692	0.058	0.070	-2.544	-15.284	-3.755
66	SC71568	1.732	0.064	0.075	-0.211	-6.210	3.732
67	SC7157	1.783	0.055	0.082	2.736	-20.140	13.464
68	SC7157	1.783	0.055	0.082	2.736	-20.140	13.464
69	OXM	2.042	0.056	0.071	17.620	-18.932	-1.982
70	IDEJ	1.783	0.064	0.073	2.736	-7.096	1.091
71	MVSSDF	1.783	0.055	0.082	2.736	-20.140	13.464
72	SC3210	1.680	0.049	0.057	-3.224	-28.182	-20.937
73	CORSOR-BOOTH ICRLSE	1.911	0.096	0.091	10.095	39.677	26.216

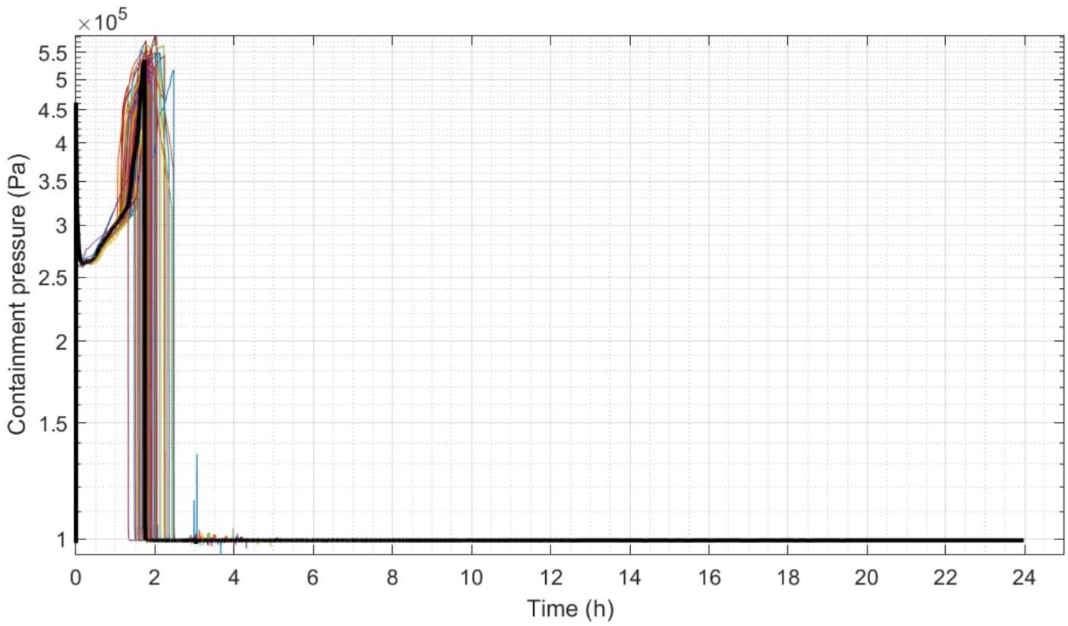

Figure 7-1. RC4A in Swedish NBWR MELCOR model - containment pressure evolution.

Since MELCOR code has limited ability to model ex-vessel steam explosion, the containment failure is postulated at the time of RPV failure. Containment failure results in a direct flow path, with 2 m^2 flow area, from the containment to the environment. This leads to rapid pressure drops, seen at around 2h.

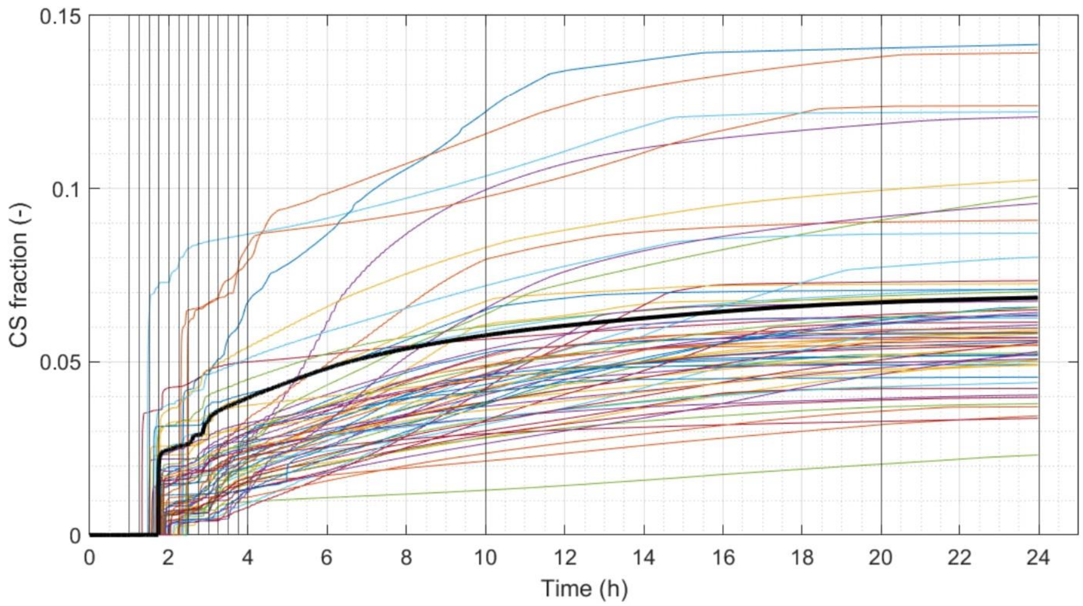

Figure 7-2. RC4A in Swedish NBWR MELCOR model – cesium release fraction to the environment.

Black line indicates the reference case. It is observed that only a few cases lead to larger release than the reference case. The results were analysed at few time slices (black vertical lines).

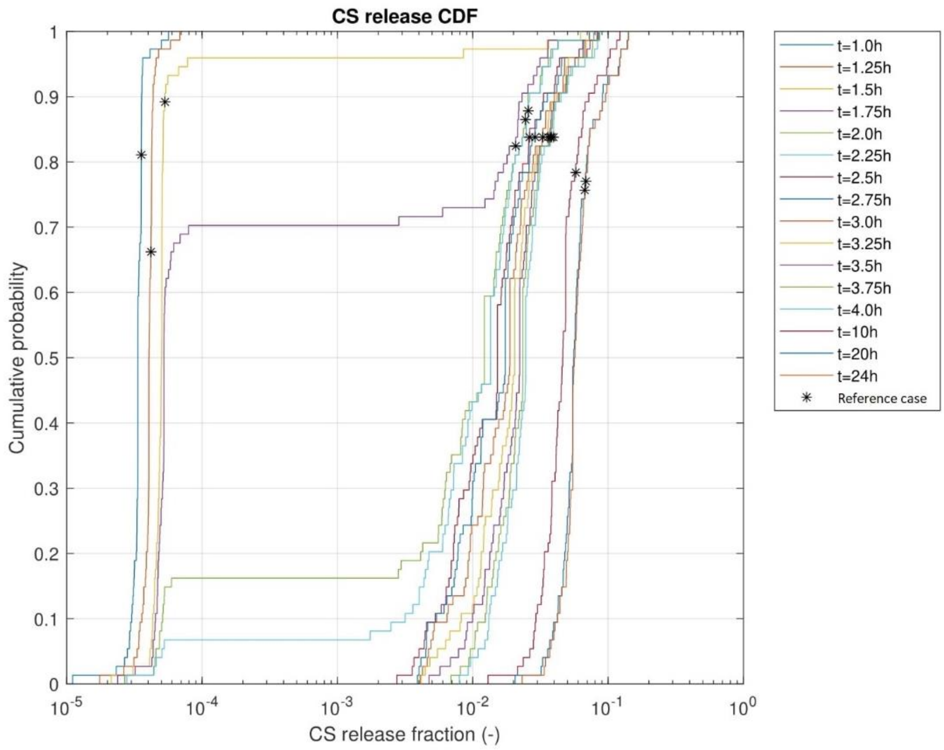

Figure 7-3. RC4A in Swedish NBWR MELCOR model – cumulative distribution for the cesium release fraction.

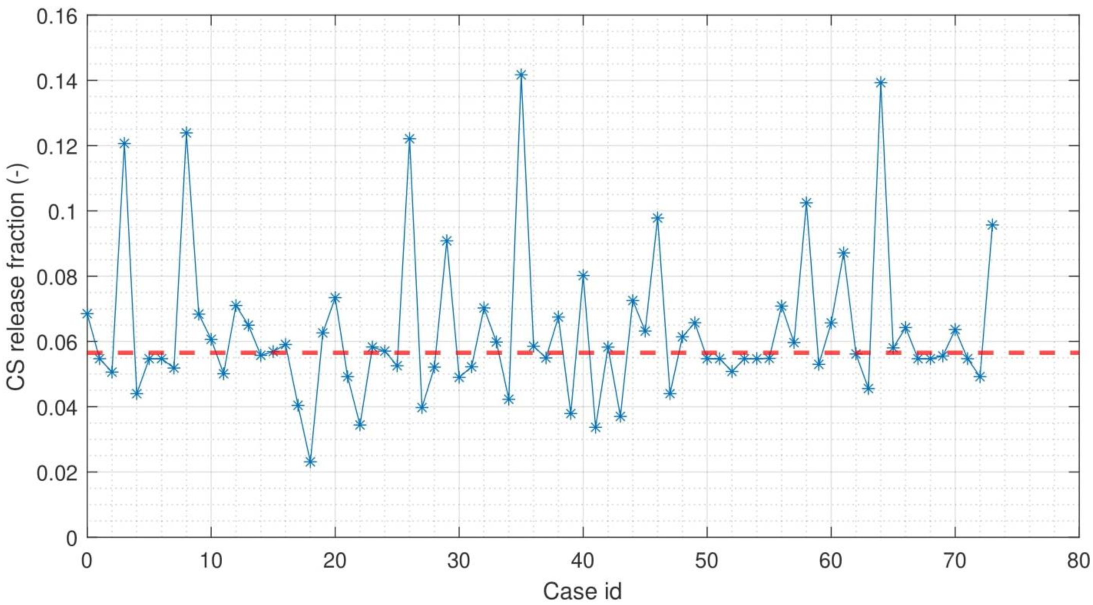

Figure 7-4. RC4A in Swedish NBWR MELCOR model - cesium release fraction to the environment.

It can be observed that the median cesium release fraction for all the cases is around 0.06.

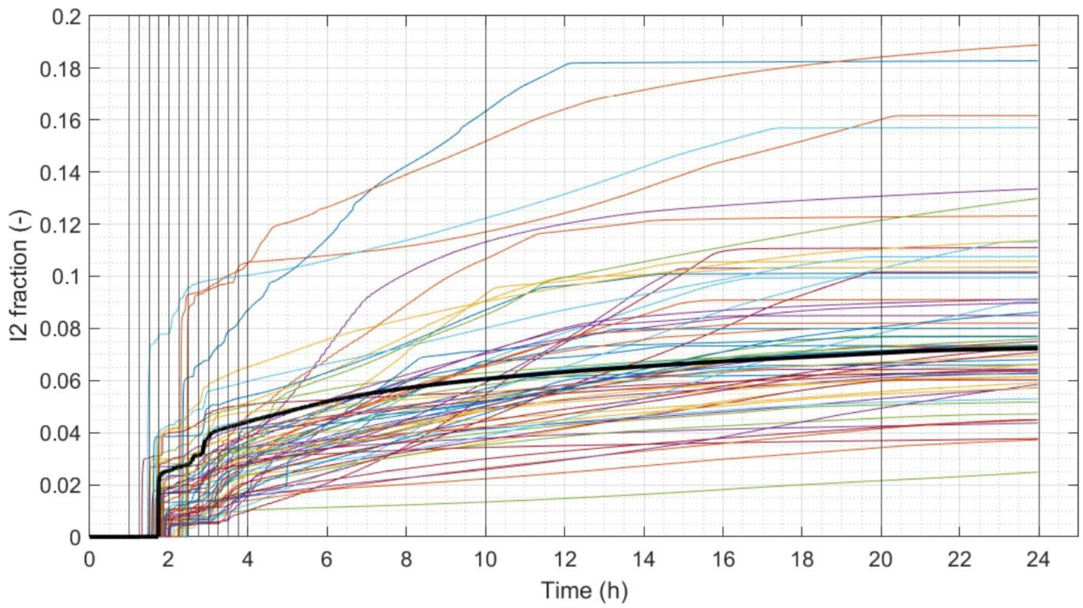

Figure 7-5. RC4A in Swedish NBWR MELCOR model - iodine release fraction to the environment.

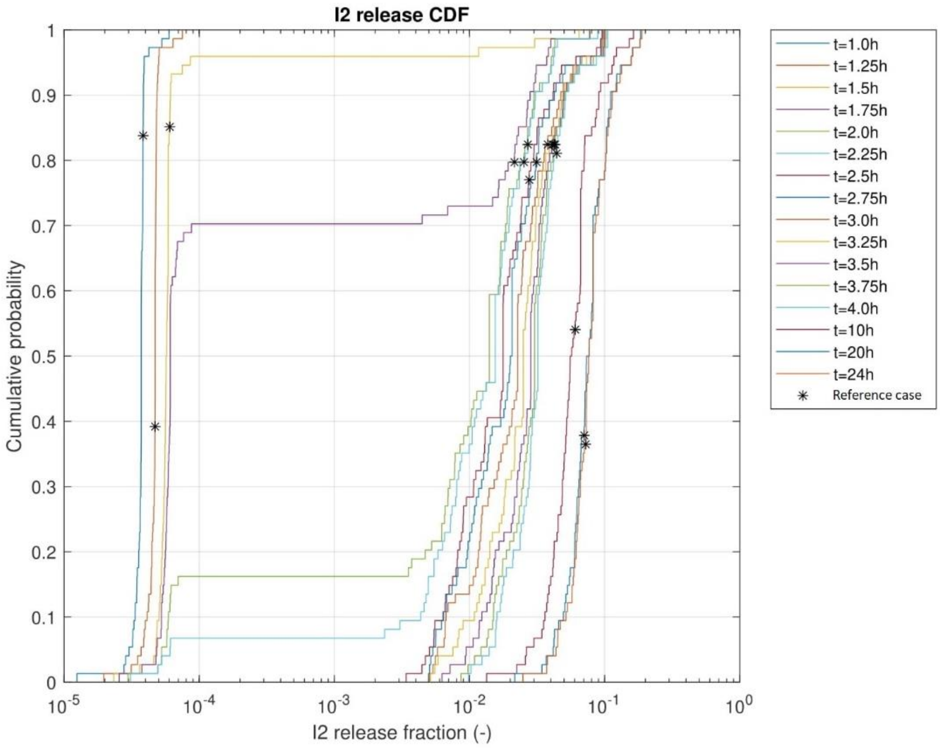

Figure 7-6. RC4A in Swedish NBWR MELCOR model – cumulative distribution for the iodine release fraction.

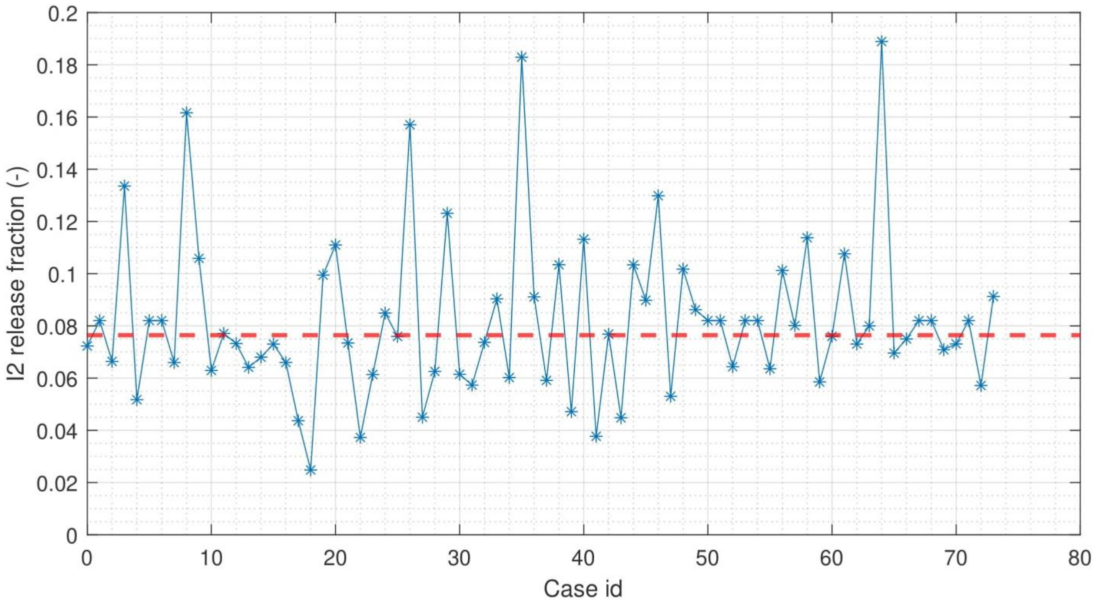

Figure 7-7. RC4A in Swedish NBWR MELCOR model - iodine release fraction to the environment.

It can be observed that the median iodine release fraction for all the cases is around 0.08.

7.1.2. RC4B – SBO leading to containment failure due to ex-vessel phenomena at RPV melt-through

Table 7-2. RC4B bounding analysis results.

Case ID	PARAMETER	TLHF [h]	CS_ENV [-]	I2_ENV [-]	TLHF [%]	CS_ENV [%]	I2_ENV [%]
0	REFERENCE CASE	2.736	0.027	0.071	-	-	-
1	SC710611	2.900	0.021	0.053	5.988	-21.475	-25.769
2	SC710621	2.592	0.033	0.122	-5.280	22.371	71.320
3	SC710641	3.886	0.013	0.019	42.028	-50.222	-72.634
4	SC710651	2.827	0.015	0.026	3.332	-45.528	-64.107
5	TFFAIL	2.900	0.021	0.053	5.988	-21.475	-25.769
6	TFFAIL	2.900	0.021	0.053	5.988	-21.475	-25.769
7	TZRSSINC	2.915	0.029	0.080	6.525	9.293	12.459
8	TUO2ZRO2	2.553	0.031	0.082	-6.701	15.450	15.463
9	FCELRA	3.044	0.024	0.101	11.267	-11.231	42.093
10	PDPOR	2.803	0.028	0.081	2.435	3.379	13.981
11	PDPOR	2.017	0.037	0.084	-26.295	38.331	18.450
12	CORNSBLD	2.844	0.032	0.102	3.958	19.252	44.123
13	VFALL	2.328	0.042	0.119	-14.923	54.793	66.743
14	SC10201	2.761	0.036	0.094	0.912	32.027	31.753
15	SC10201	2.564	0.024	0.062	-6.295	-12.371	-12.444
16	SC10202	2.864	0.028	0.081	4.669	5.073	13.724
17	SC10202	3.064	0.028	0.088	11.978	5.158	23.443
18	HFRZSS	2.436	0.035	0.120	-10.965	28.638	68.303
19	HFRZZR	2.717	0.030	0.077	-0.712	10.981	8.902
20	SC11312	3.010	0.028	0.093	10.014	4.728	30.147
21	SC11312	2.814	0.032	0.085	2.841	18.799	20.201
22	SC11412	2.153	0.033	0.092	-21.321	22.117	29.831
23	DHYPDLP	2.960	0.029	0.092	8.164	7.429	28.769
24	HDBH20	2.867	0.033	0.100	4.770	23.791	41.292
25	TPFAIL	5.153	0.033	0.124	88.323	24.401	74.593
26	HDBPN	2.472	0.037	0.154	-9.645	37.239	116.240
27	CHI	2.789	0.042	0.092	1.928	57.688	28.993
28	GAMMA	3.218	0.004	0.018	17.592	-83.678	-75.036
29	STICK	2.475	0.033	0.083	-9.544	20.892	16.168
30	RHONOM	2.767	0.021	0.032	1.116	-23.555	-54.907
31	NUMSEC	2.797	0.026	0.072	2.232	-3.995	1.005
32	TURBDS	2.847	0.045	0.163	4.061	67.758	129.735

Case ID	PARAMETER	TLHF [h]	CS_ENV [-]	I2_ENV [-]	TLHF [%]	CS_ENV [%]	I2_ENV [%]
33	TURBDS	2.322	0.034	0.105	-15.128	26.432	48.067
34	SC7111I1	2.827	0.026	0.067	3.335	-2.664	-6.161
35	SC7111I1	2.375	0.031	0.076	-13.217	15.308	6.768
36	SC7111I2	2.678	0.035	0.103	-2.134	31.365	44.306
37	SC7111I2	3.181	0.012	0.018	16.242	-56.367	-74.793
38	SC7111CS1	3.161	0.018	0.057	15.532	-31.770	-20.533
39	SC7111CS1	2.667	0.046	0.167	-2.538	71.021	134.707
40	SC7111CS2	2.736	0.034	0.127	0.000	25.652	78.947
41	SC7111CS2	2.739	0.018	0.023	0.099	-33.094	-67.328
42	SC7170CS	2.766	0.023	0.035	1.099	-14.472	-51.239
43	SC7170CS	2.650	0.035	0.121	-3.149	30.821	69.883
44	SC7170CSI3	2.625	0.032	0.132	-4.061	20.287	85.727
45	SC7170CSI3	3.097	0.026	0.089	13.197	-3.813	24.926
46	SC7170CSI4	2.814	0.034	0.086	2.842	25.144	20.322
47	SC7170CSI4	2.781	0.024	0.076	1.624	-10.187	6.203
48	SC7170CSM	3.161	0.013	0.024	15.532	-51.747	-65.569
49	SC7170CSM	2.731	0.035	0.111	-0.204	29.624	55.634
50	DIAMO	2.900	0.021	0.053	5.988	-21.475	-25.769
51	DIAMO	2.900	0.021	0.053	5.988	-21.475	-25.769
52	SC715010	2.997	0.031	0.084	9.541	13.916	17.503
53	SC715111	2.886	0.028	0.067	5.482	3.402	-5.551
54	SC715111	2.825	0.031	0.086	3.238	16.040	20.716
55	SC71521	2.253	0.035	0.096	-17.666	29.670	35.459
56	SC71521	2.633	0.039	0.095	-3.758	44.280	33.377
57	SC71531	2.919	0.035	0.108	6.700	28.852	52.259
58	SC71531	2.870	0.026	0.079	4.873	-2.551	11.180
59	SC71551	2.892	0.030	0.085	5.685	11.921	19.063
60	SC71551	3.008	0.027	0.067	9.947	-1.057	-6.191
61	SC71555	2.920	0.039	0.157	6.701	45.432	121.490
62	SC71555	3.313	0.016	0.027	21.070	-41.054	-62.541
63	SC71542	2.992	0.025	0.073	9.339	-6.979	2.757
64	SC71542	3.717	0.016	0.041	35.835	-38.958	-42.843
65	SC71568	2.670	0.029	0.078	-2.405	9.516	10.350
66	SC71568	3.092	0.025	0.068	12.992	-6.979	-3.823
67	SC7157	2.900	0.021	0.053	5.988	-21.475	-25.769
68	SC7157	2.900	0.021	0.053	5.988	-21.475	-25.769
69	OXM	2.870	0.036	0.096	4.873	34.173	34.772

Case ID	PARAMETER	TLHF [h]	CS_ENV [-]	I2_ENV [-]	TLHF [%]	CS_ENV [%]	I2_ENV [%]
70	IDEJ	2.900	0.037	0.134	5.988	36.441	88.771
71	MVSSDF	2.900	0.021	0.053	5.988	-21.475	-25.769
72	SC3210	2.789	0.031	0.081	1.928	15.947	14.586
73	CORSOR-BOOTH ICRLSE	3.561	0.016	0.055	30.151	-42.188	-22.409

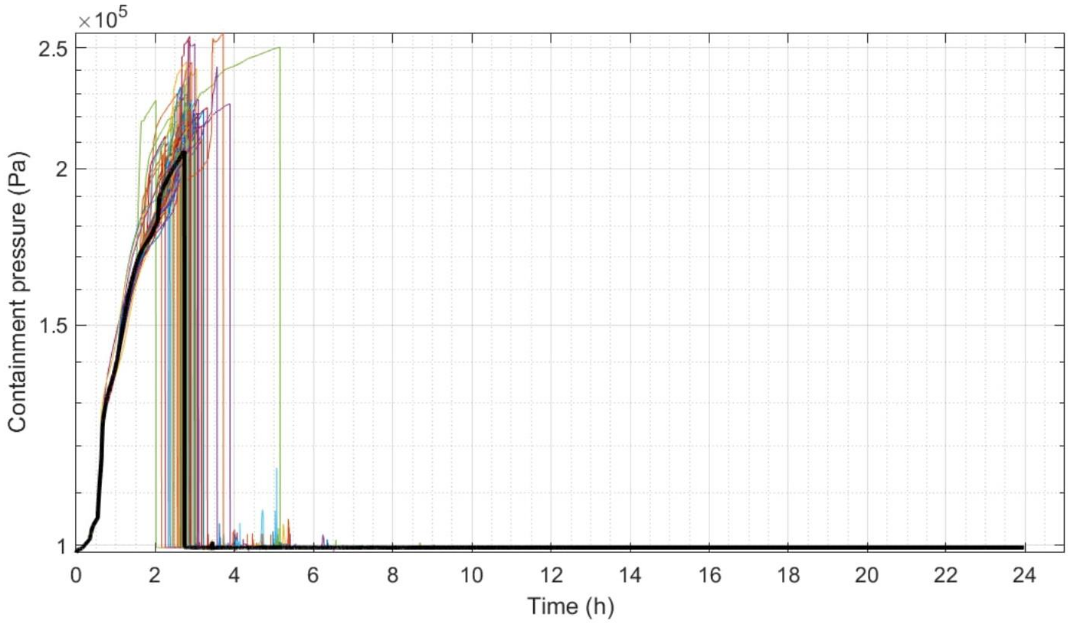

Figure 7-8. RC4B in Swedish NBWR MELCOR model - containment pressure evolution.

As mentioned before, the MELCOR code has limited ability to model ex-vessel steam explosion, the containment failure is postulated at the time of RPV failure (around 3 hours after initiating event in case of SBO). Containment failure results in a direct flow path, with 2 m^2 flow area, from the containment to the environment. The smaller peaks after RPV failure may be due to the modelling assumptions for LPME in FDI package.

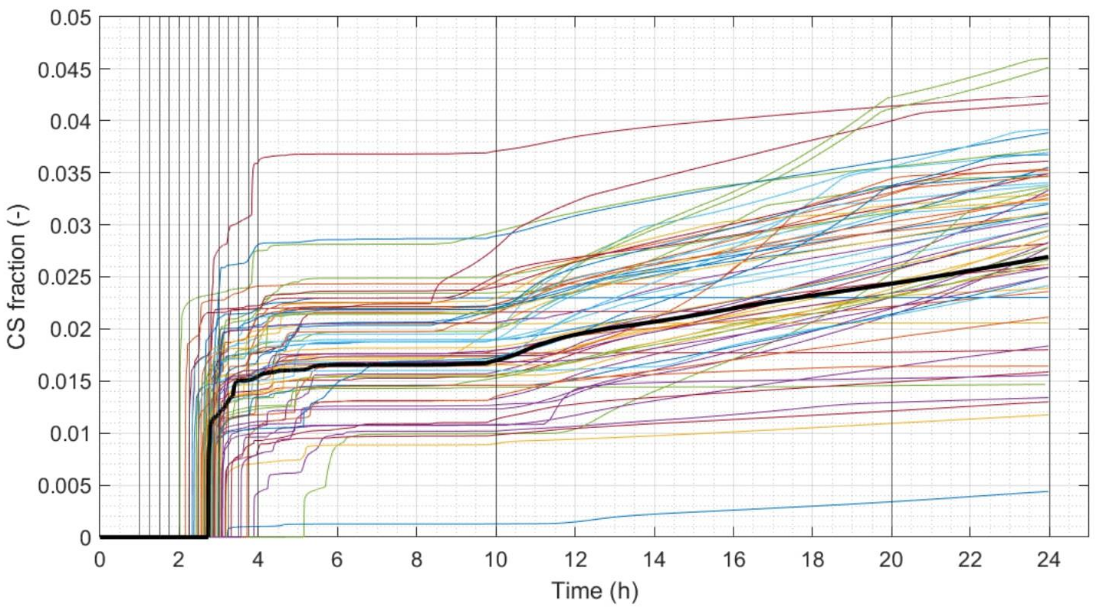

Figure 7-9. RC4B in Swedish NBWR MELCOR model - cesium release fraction to the environment.

Black line indicates the reference case. It can be observed that the release is uniformly spread on either side of the reference case. The results were analysed at few time slices (black vertical lines).

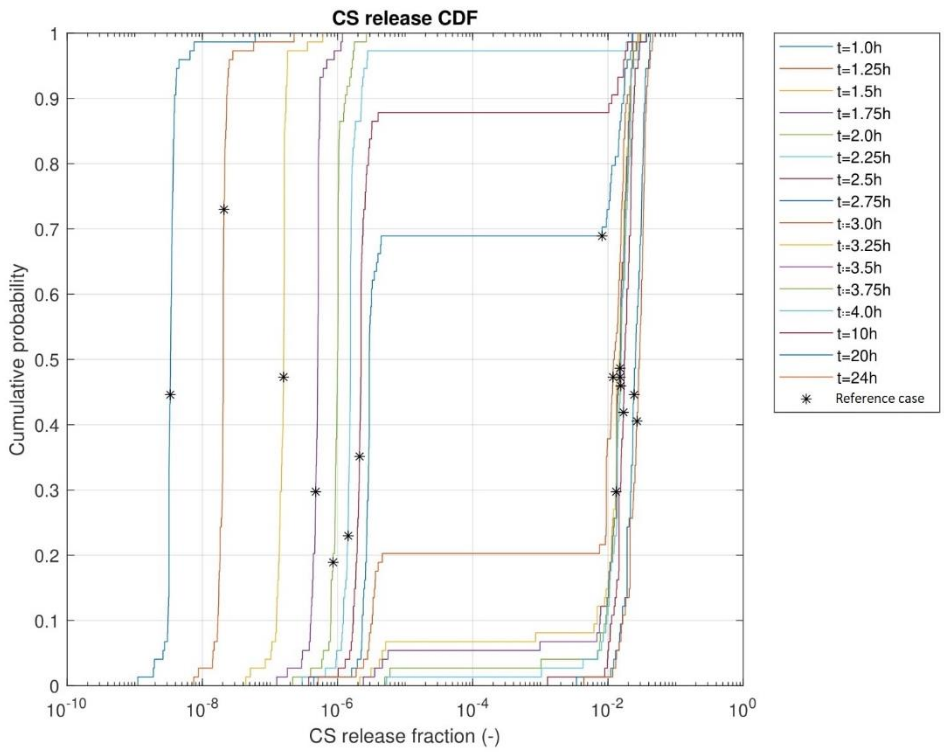

Figure 7-10. RC4B in Swedish NBWR MELCOR model – cumulative distribution for the cesium release fraction.

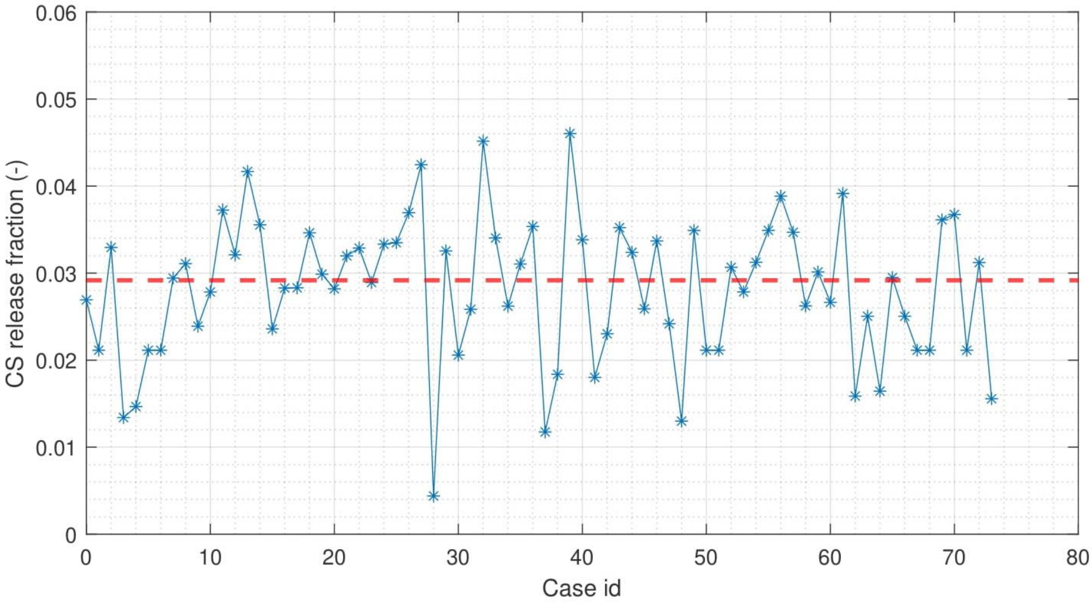

Figure 7-11. RC4B in Swedish NBWR MELCOR model - cesium release fraction to the environment.

It can be observed that the median cesium release fraction for all the cases is about 0.03.

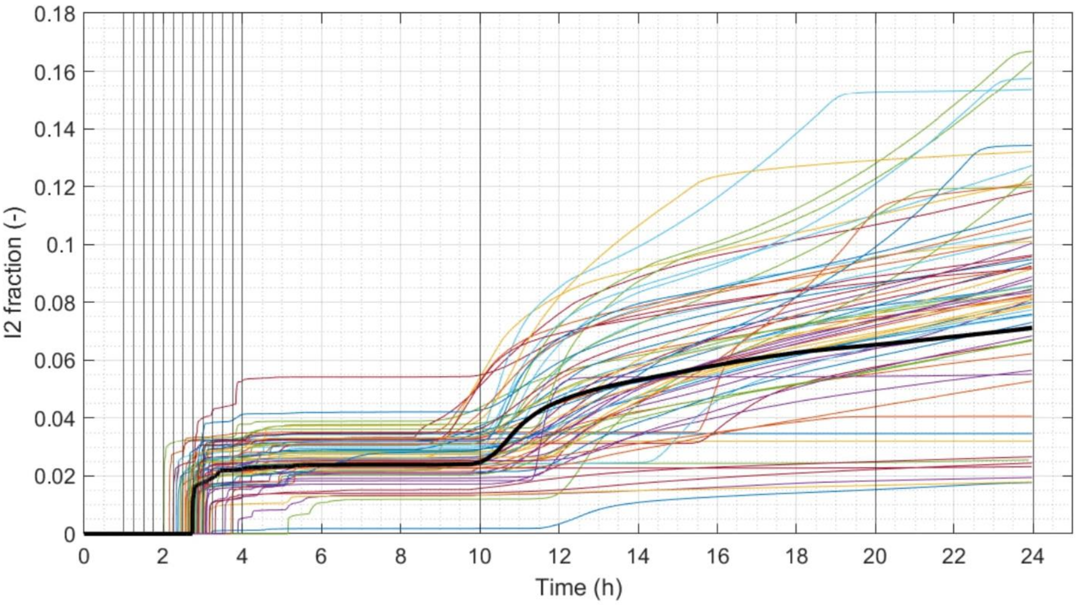

Figure 7-12. RC4B in Swedish NBWR MELCOR model - iodine release fraction to the environment.

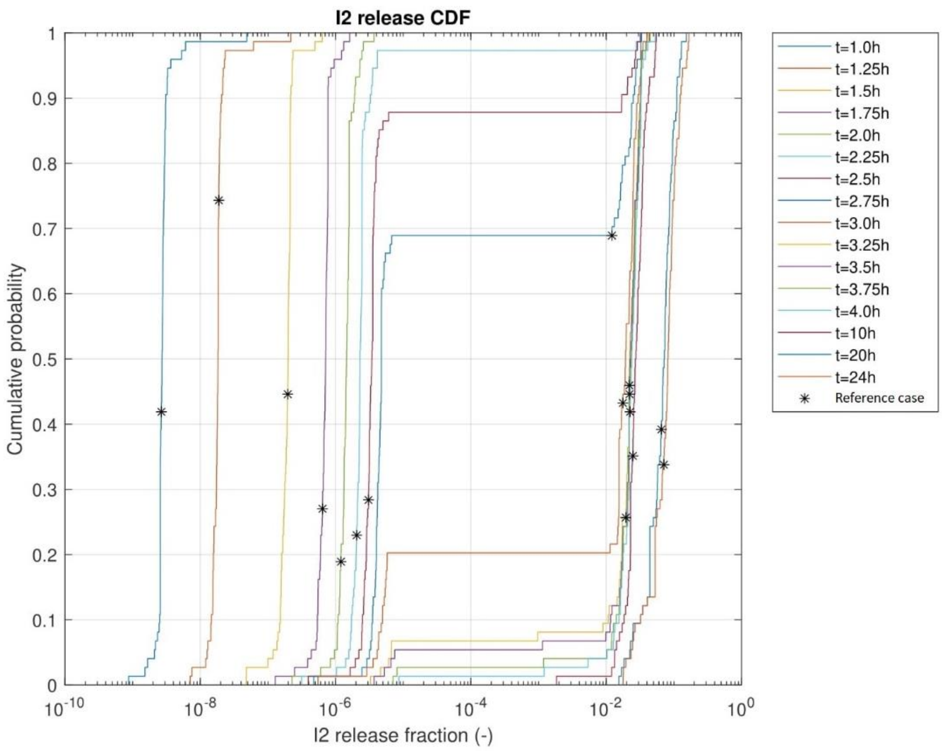

Figure 7-13. RC4B in Swedish NBWR MELCOR model – cumulative distribution for the iodine release fraction.

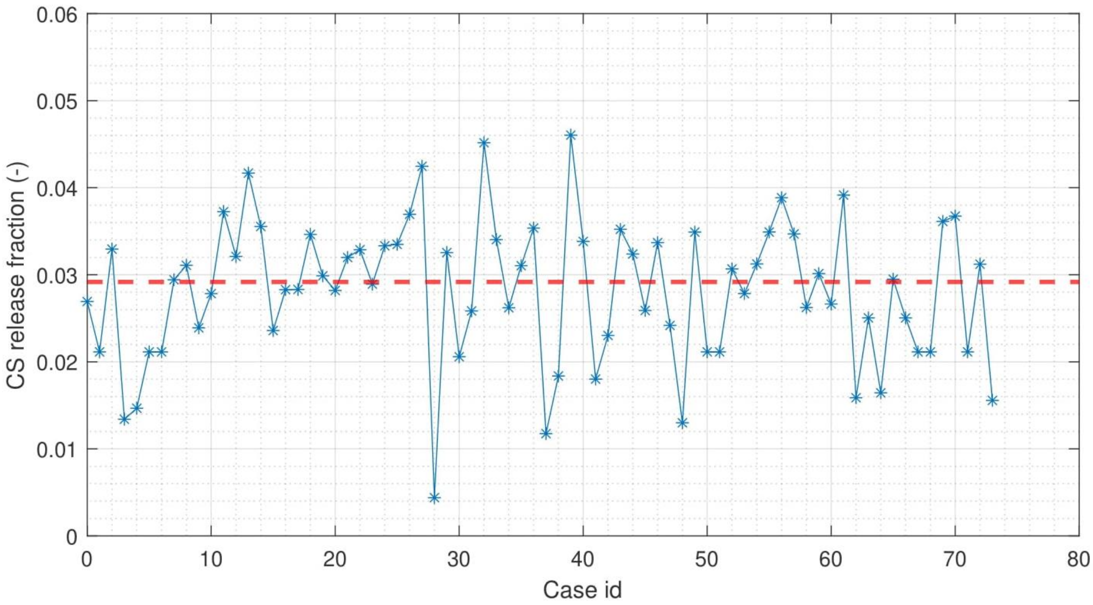

Figure 7-14. RC4B in Swedish NBWR MELCOR model - iodine release fraction to the environment.

It can be observed that the median iodine release fraction for all the cases is about 0.03.

7.2.VTT results

VTT studied the "option 2" scenario from section 4.5.2. The accident is initiated by loss of all AC power. In addition, it is assumed that the RPV failure causes a short pressure spike that breaks the rupture disk of the containment filtered venting system from the drywell. The calculations were continued until 10 h because by that time the fission product release to the environment had practically stopped. Two figures of merit were investigated: the start time of the filtered venting, and the integral cesium release to the environment during the 10 h.

Most of the parameters were varied four times including the bounding values and two values in between. The parameter variations that were observed affecting the simulation results are listed in Table 7-3 along with the calculated FCV opening times and the total cesium releases.

It was noticed that almost all the sensitivity cases caused smaller Cs release than the reference case. Therefore the relative difference between the cases was studied by comparing the calculated values to the median values of all the calculations. Parameters with major and irregular deviations in their results between their variant cases are highlighted.

Table 7-3. The results from VTT's simulations.

Case ID	Parameter	Value	T_FCV [s]	T_FCV [%]	CS_ENV [-]	CS_ENV [%]
0	Reference		6270	1.4 %	5.427E-05	50.1 %
1	SC710621	2.50E-07	6160	-0.3 %	2.132E-05	-41.0 %
2	SC710621	4.38E-07	6188	0.1 %	1.892E-05	-47.7 %
3	SC710621	6.25E-07	6182	0.0 %	2.807E-05	-22.4 %
4	SC710621	8.13E-07	5883	-4.8 %	2.560E-05	-29.2 %
5	SC710641	2.41E+05	5986	-3.2 %	2.746E-05	-24.1 %
6	SC710641	2.76E+05	6557	6.1 %	3.633E-05	0.5 %
7	SC710641	3.11E+05	6669	7.9 %	4.262E-05	17.9 %
8	SC710641	3.46E+05	6219	0.6 %	3.319E-05	-8.2 %
9	SC710651	7.00E-06	6133	-0.8 %	3.720E-05	2.9 %
10	SC710651	8.00E-06	6229	0.8 %	3.214E-05	-11.1 %
11	SC710651	9.00E-06	5986	-3.2 %	3.608E-05	-0.2 %
12	SC710651	1.00E-05	6241	1.0 %	3.800E-05	5.1 %
13	OXM	1	6221	0.6 %	3.014E-05	-16.7 %
14	OXM	2	6118	-1.0 %	3.602E-05	-0.4 %
15	OXM	3	6053	-2.1 %	4.207E-05	16.3 %
16	OXM	4	6102	-1.3 %	4.354E-05	20.4 %
17	FCELRA	0.1350	6118	-1.0 %	5.087E-05	40.7 %
18	FCELRA	0.1750	6064	-1.9 %	3.995E-05	10.5 %
19	FCELRA	0.2125	6201	0.3 %	4.631E-05	28.1 %
20	FCELRA	0.2500	6161	-0.3 %	2.463E-05	-31.9 %
21	PDPor	0.30	6221	0.6 %	2.146E-05	-40.6 %
22	PDPor	0.35	6085	-1.6 %	2.284E-05	-36.8 %
23	PDPor	0.45	6236	0.9 %	2.747E-05	-24.0 %
24	PDPor	0.50	6196	0.2 %	3.815E-05	5.5 %
25	CORNSBLD	1565	6039	-2.3 %	3.856E-05	6.6 %
26	CORNSBLD	1610	6274	1.5 %	3.178E-05	-12.1 %
27	CORNSBLD	1655	5290	-14.4 %	1.748E-05	-51.7 %

Case ID	Parameter	Value	T_FCV [s]	T_FCV [%]	CS_ENV [-]	CS_ENV [%]
28	CORNSBLD	1700	5738	-7.2 %	4.473E-05	23.7 %
29	VFALL	0.010	10504	69.9 %	5.812E-05	60.7 %
30	VFALL	0.025	5516	-10.8 %	3.269E-05	-9.6 %
31	VFALL	0.050	5742	-7.1 %	2.906E-05	-19.6 %
32	VFALL	0.075	6303	2.0 %	4.485E-05	24.0 %
33	VFALL	0.100	6249	1.1 %	4.079E-05	12.8 %
34	SC10201	180	6198	0.3 %	3.411E-05	-5.7 %
35	SC10201	315	6165	-0.3 %	2.729E-05	-24.5 %
36	SC10201	450	6156	-0.4 %	4.273E-05	18.1 %
37	SC10201	585	6202	0.3 %	4.037E-05	11.6 %
38	SC10201	720	6211	0.5 %	3.644E-05	0.8 %
39	SC10202	30.0	6260	1.3 %	3.170E-05	-12.3 %
40	SC10202	52.5	6228	0.8 %	4.448E-05	23.0 %
41	SC10202	75.0	6184	0.0 %	4.458E-05	23.3 %
42	SC10202	97.5	6170	-0.2 %	2.155E-05	-40.4 %
43	SC10202	120.0	6215	0.5 %	2.607E-05	-27.9 %
44	HFRZSS	1000	5712	-7.6 %	4.202E-05	16.2 %
45	HFRZSS	1375	6111	-1.1 %	2.729E-05	-24.6 %
46	HFRZSS	1750	6051	-2.1 %	2.424E-05	-33.0 %
47	HFRZSS	2125	6035	-2.4 %	3.511E-05	-2.9 %
48	HFRZZR	1000	5487	-11.2 %	2.414E-05	-33.2 %
49	HFRZZR	2625	6163	-0.3 %	3.844E-05	6.3 %
50	HFRZZR	4250	6110	-1.2 %	4.664E-05	29.0 %
51	HFRZZR	5875	5962	-3.6 %	2.935E-05	-18.8 %
52	SC11312	2100	6224	0.7 %	3.587E-05	-0.8 %
53	SC11312	2200	5983	-3.2 %	3.167E-05	-12.4 %
54	SC11312	2300	6100	-1.3 %	4.013E-05	11.0 %
55	SC11312	2500	5893	-4.7 %	3.928E-05	8.6 %
56	SC11412	0.20	5962	-3.6 %	3.848E-05	6.4 %
57	SC11412	0.65	6188	0.1 %	3.920E-05	8.4 %
58	SC11412	1.55	6170	-0.2 %	1.881E-05	-48.0 %
59	SC11412	2.00	5636	-8.8 %	1.499E-05	-58.5 %
60	DHYPDLP	0.00275	6270	1.4 %	5.031E-05	39.1 %
61	DHYPDLP	0.00350	6270	1.4 %	5.484E-05	51.6 %
62	DHYPDLP	0.00425	6270	1.4 %	4.862E-05	34.4 %
63	DHYPDLP	0.00500	6270	1.4 %	4.539E-05	25.5 %
64	HDBH2O	200	6270	1.4 %	5.427E-05	50.1 %

Case ID	Parameter	Value	T_FCV [s]	T_FCV [%]	CS_ENV [-]	CS_ENV [%]
65	HDBH2O	650	6270	1.4 %	5.427E-05	50.1 %
66	HDBH2O	1100	6270	1.4 %	5.411E-05	49.6 %
67	HDBH2O	1550	6270	1.4 %	5.391E-05	49.1 %
68	HDBH2O	2000	6270	1.4 %	5.065E-05	40.0 %
69	TPFAIL	1355	6274	1.5 %	5.559E-05	53.7 %
70	TPFAIL	1437	6277	1.6 %	5.520E-05	52.6 %
71	TPFAIL	1518	6281	1.6 %	5.404E-05	49.4 %
72	TPFAIL	1600	6286	1.7 %	5.234E-05	44.7 %
73	HDBPN	100	6475	4.7 %	4.882E-05	35.0 %
74	HDBPN	325	6316	2.2 %	5.285E-05	46.1 %
75	HDBPN	550	6288	1.7 %	4.334E-05	19.8 %
76	HDBPN	775	6277	1.5 %	5.414E-05	49.7 %
77	CHI	1.5	6086	-1.5 %	4.630E-05	28.0 %
78	CHI	2.0	6225	0.7 %	5.458E-05	50.9 %
79	CHI	2.5	6092	-1.4 %	5.675E-05	56.9 %
80	CHI	3.0	6179	0.0 %	5.399E-05	49.3 %
81	GAMMA	1.5	6150	-0.5 %	2.055E-05	-43.2 %
82	GAMMA	2.0	6367	3.0 %	2.069E-05	-42.8 %
83	GAMMA	2.5	6267	1.4 %	3.281E-05	-9.3 %
84	GAMMA	3.0	6060	-2.0 %	1.715E-05	-52.6 %
85	STICK	0.500	6228	0.8 %	2.268E-05	-37.3 %
86	STICK	0.625	6181	0.0 %	6.113E-05	69.0 %
87	STICK	0.750	6251	1.1 %	4.434E-05	22.6 %
88	STICK	0.875	6268	1.4 %	2.941E-05	-18.7 %
89	RHONOM	1975	5932	-4.0 %	5.112E-05	41.4 %
90	RHONOM	2950	5890	-4.7 %	5.072E-05	40.2 %
91	RHONOM	3925	6182	0.0 %	3.530E-05	-2.4 %
92	RHONOM	4900	6197	0.3 %	2.582E-05	-28.6 %
93	NUMSEC	13	6417	3.8 %	2.201E-05	-39.1 %
94	NUMSEC	15	6229	0.8 %	2.604E-05	-28.0 %
95	NUMSEC	18	6276	1.5 %	2.005E-05	-44.5 %
96	NUMSEC	20	6172	-0.2 %	2.417E-05	-33.2 %
97	SC7111I1	4.2347	6185	0.1 %	3.901E-05	7.9 %
98	SC7111I1	4.6084	6222	0.7 %	3.093E-05	-14.5 %
99	SC7111I1	5.3557	6289	1.7 %	5.524E-05	52.8 %
100	SC7111I1	5.7293	5994	-3.0 %	3.289E-05	-9.1 %
101	SC7111I2	467.50	6314	2.1 %	2.620E-05	-27.6 %

Case ID	Parameter	Value	T_FCV [s]	T_FCV [%]	CS_ENV [-]	CS_ENV [%]
102	SC7111I2	508.75	6165	-0.3 %	2.815E-05	-22.1 %
103	SC7111I2	591.25	6175	-0.1 %	4.789E-05	32.4 %
104	SC7111I2	632.50	6276	1.5 %	4.132E-05	14.3 %
105	SC7111CS1	3.0745	6257	1.2 %	3.261E-05	-9.8 %
106	SC7111CS1	3.3458	6255	1.2 %	2.719E-05	-24.8 %
107	SC7111CS1	3.8883	6449	4.3 %	3.652E-05	1.0 %
108	SC7111CS1	4.1595	6061	-2.0 %	4.478E-05	23.8 %
109	SC7111CS2	82.450	6151	-0.5 %	2.465E-05	-31.8 %
110	SC7111CS2	89.773	6041	-2.3 %	2.347E-05	-35.1 %
111	SC7111CS2	104.275	5855	-5.3 %	5.241E-05	44.9 %
112	SC7111CS2	111.550	6165	-0.3 %	3.783E-05	4.6 %
113	SC7170CS	3.3575	6055	-2.0 %	4.400E-05	21.7 %
114	SC7170CS	3.6538	6311	2.1 %	2.923E-05	-19.2 %
115	SC7170CS	4.2463	6267	1.4 %	3.151E-05	-12.9 %
116	SC7170CS	4.5425	5941	-3.9 %	3.615E-05	0.0 %
117	SC7170CSI3	0.374	6248	1.1 %	3.111E-05	-14.0 %
118	SC7170CSI3	0.407	6207	0.4 %	3.229E-05	-10.7 %
119	SC7170CSI3	0.473	6197	0.3 %	4.063E-05	12.4 %
120	SC7170CSI3	0.506	6196	0.2 %	5.231E-05	44.6 %
121	SC7170CSI4	1.9125	6167	-0.2 %	2.598E-05	-28.2 %
122	SC7170CSI4	2.0813	6020	-2.6 %	3.862E-05	6.8 %
123	SC7170CSI4	2.4188	6392	3.4 %	3.325E-05	-8.1 %
124	SC7170CSI4	2.5875	6331	2.4 %	3.462E-05	-4.3 %
125	SC715010	1.50	5984	-3.2 %	3.972E-05	9.8 %
126	SC715010	2.00	6087	-1.5 %	3.438E-05	-4.9 %
127	SC715010	2.50	6180	0.0 %	2.243E-05	-38.0 %
128	SC715010	3.00	6061	-2.0 %	3.636E-05	0.5 %
129	SC715111	2.9325	6119	-1.0 %	2.160E-05	-40.3 %
130	SC715111	3.1913	6271	1.5 %	3.480E-05	-3.8 %
131	SC715111	3.7088	6320	2.2 %	3.704E-05	2.4 %
132	SC715111	3.9675	6279	1.6 %	2.664E-05	-26.3 %
133	SC71521	5.00E-03	6137	-0.7 %	3.235E-05	-10.5 %
134	SC71521	5.75E-03	6179	0.0 %	2.772E-05	-23.3 %
135	SC71521	6.50E-03	6146	-0.6 %	3.618E-05	0.0 %
136	SC71521	7.25E-03	6068	-1.8 %	3.004E-05	-16.9 %
137	SC71521	8.00E-03	6259	1.3 %	3.048E-05	-15.7 %
138	SC71531	6.6900	6160	-0.4 %	3.524E-05	-2.6 %

Case ID	Parameter	Value	T_FCV [s]	T_FCV [%]	CS_ENV [-]	CS_ENV [%]
139	SC71531	7.2853	6161	-0.3 %	4.577E-05	26.6 %
140	SC71531	8.4667	6132	-0.8 %	2.473E-05	-31.6 %
141	SC71531	9.0574	6153	-0.5 %	2.723E-05	-24.7 %
142	SC71551	1.5230	5892	-4.7 %	3.908E-05	8.1 %
143	SC71551	1.6574	6120	-1.0 %	2.730E-05	-24.5 %
144	SC71551	1.9262	6003	-2.9 %	5.274E-05	45.8 %
145	SC71551	2.0606	5884	-4.8 %	4.870E-05	34.7 %
146	SC71555	0.9968	6035	-2.4 %	5.128E-05	41.8 %
147	SC71555	1.0535	6170	-0.2 %	2.275E-05	-37.1 %
148	SC71555	1.2244	6158	-0.4 %	2.635E-05	-27.2 %
149	SC71555	1.3098	6236	0.9 %	2.965E-05	-18.0 %
150	SC71542	2.5593E-03	6164	-0.3 %	2.281E-05	-36.9 %
151	SC71542	2.7851E-03	5870	-5.0 %	2.494E-05	-31.0 %
152	SC71542	3.2368E-03	6042	-2.2 %	3.358E-05	-7.2 %
153	SC71542	3.4626E-03	6097	-1.4 %	3.751E-05	3.7 %
154	SC71568	-1.9728E-03	6120	-1.0 %	4.542E-05	25.6 %
155	SC71568	-2.1469E-03	6319	2.2 %	2.665E-05	-26.3 %
156	SC71568	-2.4950E-03	6173	-0.1 %	3.160E-05	-12.6 %
157	SC71568	-2.6691E-03	6375	3.1 %	4.865E-05	34.5 %
158	MVSSDF	100	6270	1.4 %	2.666E-04	637.2 %
159	MVSSDF	200	6270	1.4 %	1.360E-04	276.1 %
160	MVSSDF	300	6270	1.4 %	8.945E-05	147.3 %
161	MVSSDF	400	6270	1.4 %	6.560E-05	81.4 %
162	DECAYH	0.94	6542	5.8 %	3.526E-05	-2.5 %
163	DECAYH	0.97	6350	2.7 %	2.455E-05	-32.1 %
164	DECAYH	1.03	5692	-7.9 %	3.874E-05	7.1 %
165	DECAYH	1.06	5711	-7.6 %	4.098E-05	13.3 %
	Median		6181		3.616E-05	

The FCV starting times are plotted in Figure 7-15 along with the median of all cases.

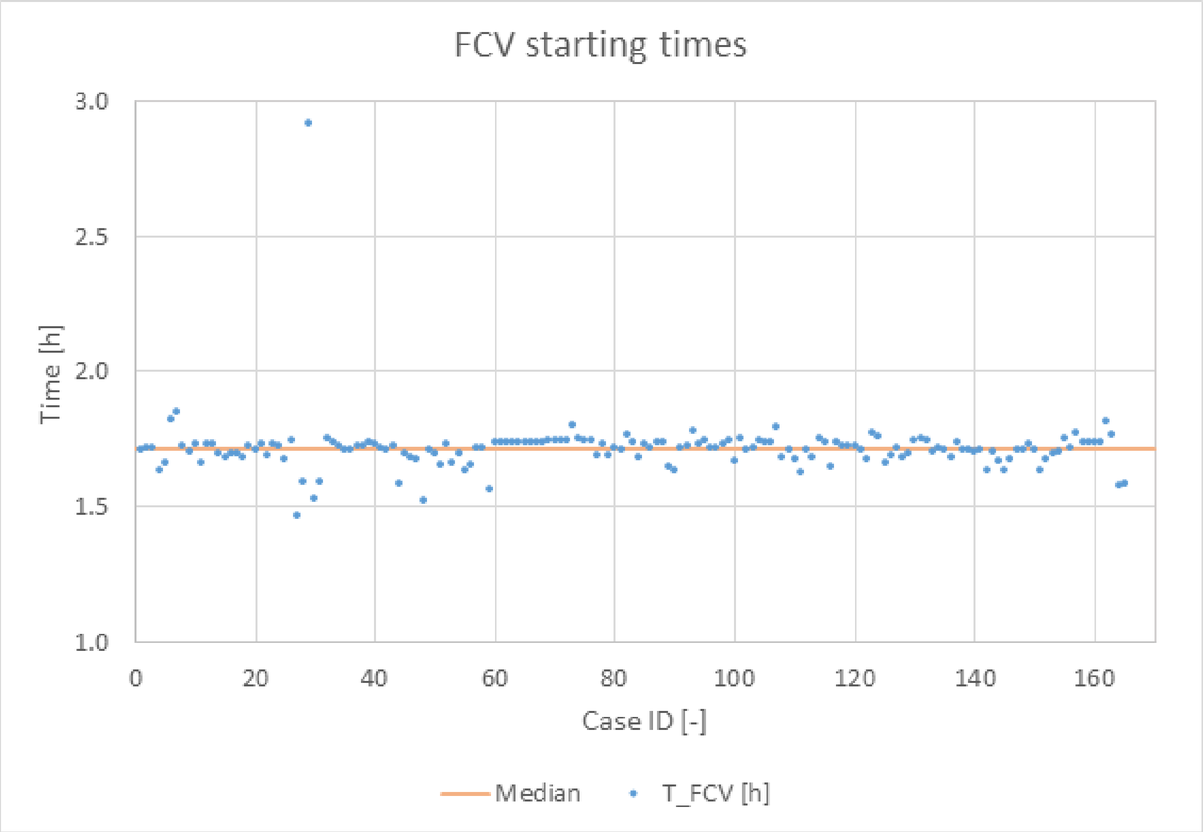

Figure 7-15. The opening times of filtered containment venting by case ID, and the median of all cases.

In most cases, the effect of the parameter variations on the FCV opening times appears to be small. Some larger deviations can be observed in the variations of parameters SC710641, CORNSBLD, VFALL, HFRZSS, HFRZZR, SC11412 and DECAYH. The most notable deviation occurs when VFALL = 0.01. However, a closer look reveals that the LHF occurs around the same time as in the other cases (t = 5980 s) and that the delay in the start of FCV is caused by the slow accumulation of melt in the lower head. The melt ejection does not begin before there is at least 5000 kg of melt in the lower plenum, or at least 10 % of the materials in the lower plenum are molten.

The release of cesium during the simulation period is presented in Figure 7-16.

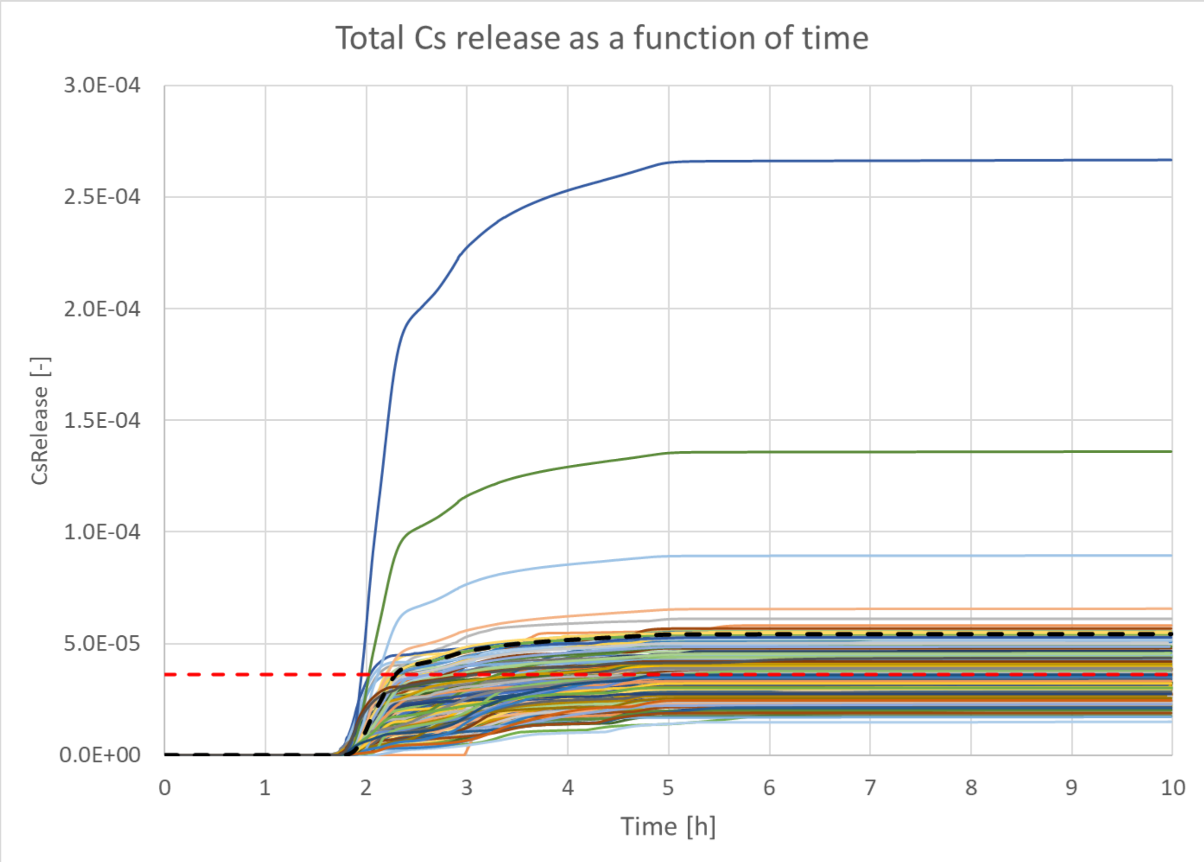

Figure 7-16. The total release of cesium as a function of time in simulated cases. The dashed black curve represents the cesium release during the reference case, and the dashed red line represents the median of the total cesium releases.

By far the largest releases were obtained by reducing the DF of the filtered venting system (the MVSSDF parameter). This is an obvious result, since almost all of the Cs is released through the venting system, and the role of the containment leakage is very small in this scenario.

In almost all cases, changing the parameter values unexpectedly resulted into lower cesium releases than in the reference case. As shown in Table 7-3 and Figure 7-16 , the median of the release is 33% lower than the release in the reference case. At least a partial reason is that in the reference case, a significant amount of MCCI occurred in the pedestal, generating hydrogen and thereby increasing the flow rate through the filtered venting system. In many variant cases, little or no MCCI occurred. The severe accident management strategy of Olkiluoto 1&2 aims at preventing MCCI by flooding the pedestal before the melt ejection, but MELCOR does not have models for particle bed formation and coolability. The irregular variation of the MCCI obscures the effect of the varied parameters on the Cs release. In next year's studies, the concrete erosion will be switched off in the Cavity package, in order to obtain comparable results.

The cesium release can also be observed changing rather irregularly between the variants of almost all the parameters. Due to this behavior and the lower Cs releases, it is difficult to point out which parameter variations have the highest impact on the simulation results. Therefore, only the large and irregular deviations are highlighted in Table 7-3. This result highlights that investigating the effect of certain parameters on the results would require a large number of calculations, which would allow a statistical analysis of the results to see if there is a correlation or not. Choosing any single calculation as a reference case may not be justified because all calculations involve some random variation ("numerical noise").

7.3. VG results

Results of MELCOR simulations performed by VG during the project are described in the following sections. The following accident sequences have been studied:

- RC7A – Station blackout leading to filtered venting
- RC8 – Recovered station blackout leading to diffuse leakage
- RC7B – Feedwater line LOCA and station blackout, leading to filtered venting
- RC5 – LOCA with failing PS function and failure to close unfiltered venting line

Based on typical PSA results after introduction of independent core cooling systems, it should be noted that the two latter sequences for internal events represent release categories with very low frequencies; numbers lower than 10^{-8} and 10^{-11} per reactor year respectively are not unreasonable. They have been included to study sequences that from a deterministic analysis perspective represent reasonable worst-case limits for release paths that are fully represented in the models.

7.3.1. RC7A – Station blackout leading to filtered venting

The accident sequence was defined by the following system availabilities:

- Reactor shutdown is successful at t=0.
- AFW, ECCS, RHR and CSS are all assumed unavailable from t=0.
- ADS is initiated according to standard control logic.
- LDW flooding system is initiated according to standard control logic.
- FCV opens when the containment pressure exceeds 5.5 bar (absolute).

Selected results for all bounding analysis cases are shown in Figure 7-17 - Figure 7-23. It can be noted that FCV opening times range from 4 to 7 h from initiating event, however with most cases within 5 to 6 h, see Figure 7-19. The time from lower head failure to FCV opening, for the base case amounting to almost 3 h, is in this respect substantial, as a typical assumption in PSA is that FCV opening occurs at the time of lower head failure, see Figure 7-23.

An overview of parameter significance in terms of relative differences compared to the best estimate case in selected figures of merit is given in

Table 7-4. These results will be used for screening of parameters for sensitivity analysis in the next project phase. The parameters whose bounding cases lead to the 9 largest absolute variations in total Cs release are highlighted in the table.

Table 7-4. RC7A bounding analyses parameter significance

Parameter	Value	Case ID	T_FCV [h]	T_LHF [h]	T_FCV -T_LHF [h]	H2 COR [kg]	CS_ENV [-]	I_ENV [-]
Best estimate		0	5.61	2.90	2.71	527.0	5.58E-06	3.32E-04
SC710611	5.00E-08	1	0%	0%	0%	0%	0%	0%
SC710621	2.50E-07	2	-6%	-21%	10%	-16%	40%	91%
SC710641	2.41E+05	3	19%	26%	12%	-1%	52%	-70%
SC710651	1.00E-05	4	-6%	-2%	-11%	1%	11%	18%
TFFAIL	5.00E-01	5	0%	0%	0%	0%	0%	0%
TFFAIL	1.50E+00	6	0%	0%	0%	0%	0%	0%
TZRSSINC	1.70E+03	7	5%	1%	9%	8%	18%	-18%
TUO2ZRO2	2.80E+03	8	3%	3%	4%	-2%	33%	10%
FCELRA	2.50E-01	9	-8%	6%	-23%	18%	36%	12%
PDPOR	3.00E-01	10	8%	-3%	21%	-19%	36%	57%
PDPOR	5.00E-01	11	1%	-22%	25%	-1%	51%	4%
CORNSBLD	1.70E+03	12	-3%	-3%	-3%	14%	34%	100%
VFALL	1.00E-01	13	-13%	-21%	-5%	-22%	28%	100%
SC10201	1.80E+02	14	1%	-4%	6%	23%	56%	47%
SC10201	7.20E+02	15	1%	-16%	21%	-12%	41%	111%
SC10202	3.00E+01	16	-3%	-1%	-5%	5%	35%	5%
SC10202	1.20E+02	17	0%	6%	-5%	15%	22%	-27%
HFRZSS	1.00E+03	18	-8%	-9%	-7%	5%	5%	-1%
HFRZZR	1.00E+03	19	2%	-3%	9%	-3%	28%	87%
SC11312	2.10E+03	20	6%	5%	7%	-8%	21%	91%
SC11312	2.54E+03	21	5%	28%	-21%	-2%	23%	-63%
SC11412	1.00E+00	22	-14%	-11%	-17%	-19%	26%	144%
DHYPDLP	5.00E-03	23	-1%	-2%	1%	9%	58%	56%
HDBH2O	2.00E+02	24	-3%	-1%	-5%	7%	74%	67%
TPFAIL	1.60E+03	25	32%	78%	-18%	12%	88%	110%
HDBPN	1.00E+03	26	7%	-15%	31%	-6%	57%	196%
CHI	3.00E+00	27	-7%	1%	-16%	4%	202%	35%
GAMMA	3.00E+00	28	-6%	-11%	-2%	5%	-71%	-25%
STICK	5.00E-01	29	3%	-15%	23%	-6%	124%	155%
RHONOM	4.90E+03	30	-11%	-5%	-19%	5%	11%	130%
NUMSEC	20	31	-5%	-6%	-5%	17%	-2%	12%
TURBDS	7.50E-04	32	-10%	1%	-22%	8%	76%	75%
TURBDS	1.25E-03	33	8%	-21%	38%	1%	47%	168%
SC7111I1	4.24E+00	34	0%	-5%	5%	-10%	32%	34%
SC7111I1	5.73E+00	35	-5%	-13%	4%	-14%	59%	97%
SC7111I2	4.68E+02	36	6%	-16%	29%	25%	45%	119%
SC7111I2	6.33E+02	37	2%	-8%	12%	15%	47%	109%
SC7111CS1	3.08E+00	38	-2%	-9%	6%	-17%	40%	132%
SC7111CS1	4.16E+00	39	4%	-5%	13%	-7%	33%	87%
SC7111CS2	8.25E+01	40	-2%	-13%	10%	-1%	70%	115%

Parameter	Value	Case ID	T_FCV [h]	T_LHF [h]	T_FCV -T_LHF [h]	H2 COR [kg]	CS_ENV [-]	I_ENV [-]
SC7111CS2	1.12E+02	41	-1%	-8%	6%	-11%	52%	99%
SC7170CS	3.36E+00	42	6%	-5%	17%	12%	78%	160%
SC7170CS	4.54E+00	43	10%	6%	14%	0%	19%	5%
SC7170CSI3	3.74E-01	44	-4%	-6%	-2%	-10%	27%	137%
SC7170CSI3	5.06E-01	45	-25%	7%	-59%	6%	74%	14%
SC7170CSI4	1.91E+00	46	22%	31%	13%	-1%	127%	58%
SC7170CSI4	2.59E+00	47	-3%	-7%	1%	2%	22%	58%
SC7170CSM	5.70E-01	48	8%	-2%	18%	-2%	51%	67%
SC7170CSM	7.71E-01	49	-11%	-8%	-14%	2%	16%	127%
DIAMO	1.00E-04	50	0%	0%	0%	0%	0%	0%
DIAMO	2.00E-03	51	0%	0%	0%	0%	0%	0%
SC715010	3.00E+00	52	3%	-4%	9%	-10%	11%	108%
SC715111	2.93E+00	53	4%	-18%	27%	-15%	52%	147%
SC715111	3.97E+00	54	25%	40%	9%	-17%	-2%	-82%
SC71521	5.00E-03	55	6%	2%	10%	12%	28%	2%
SC71521	8.00E-03	56	-3%	-7%	1%	5%	15%	88%
SC71531	6.70E+00	57	-4%	-3%	-5%	11%	23%	67%
SC71531	9.06E+00	58	1%	-7%	10%	-14%	64%	218%
SC71551	1.52E+00	59	-1%	6%	-9%	-4%	10%	10%
SC71551	2.06E+00	60	10%	-17%	39%	-3%	79%	127%
SC71555	9.68E-01	61	6%	-2%	16%	1%	18%	100%
SC71555	1.31E+00	62	-4%	-11%	2%	4%	57%	92%
SC71542	2.56E-03	63	5%	3%	8%	4%	33%	6%
SC71542	3.46E-03	64	-6%	-10%	-2%	2%	52%	40%
SC71568	-2.67E-03	65	-7%	-7%	-6%	-3%	2%	30%
SC71568	-1.97E-03	66	2%	-5%	10%	7%	25%	109%
SC7157	8.50E-01	67	0%	0%	0%	0%	0%	0%
SC7157	1.15E+00	68	0%	0%	0%	0%	0%	0%
OXM	4	69	-3%	-8%	1%	-14%	62%	90%
IDEJ	1	70	10%	0%	20%	15%	93%	108%
MVSSDF	1.00E+02	71	0%	0%	0%	0%	79%	4%
SC3210*	1.15E+00	72	-12%	-9%	-15%	12%	46%	119%
CORSOR-BOOTH ICRLSE	-7	73	20%	8%	32%	-1%	-18%	62%

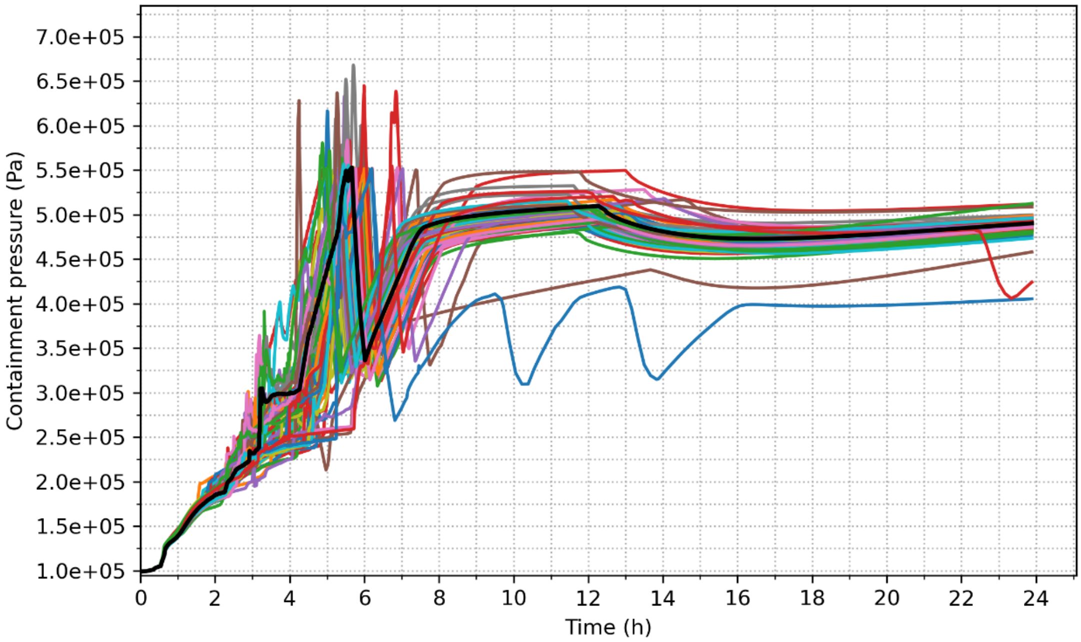

Figure 7-17. RC7A in Swedish NBWR MELCOR model - containment pressure.

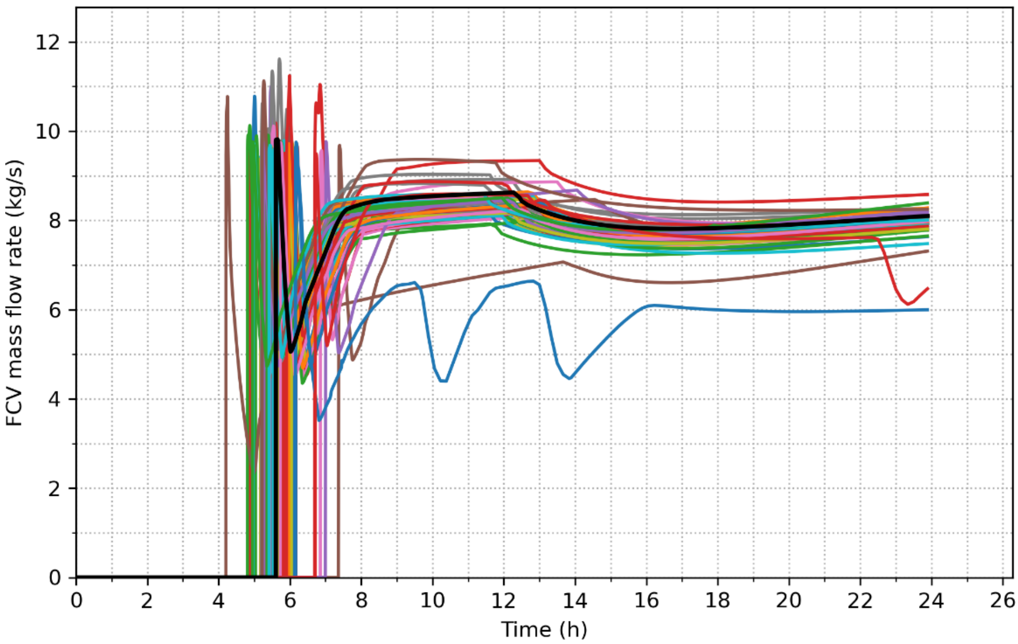

Figure 7-18. RC7A in Swedish NBWR MELCOR model – filtered containment venting flow rate.

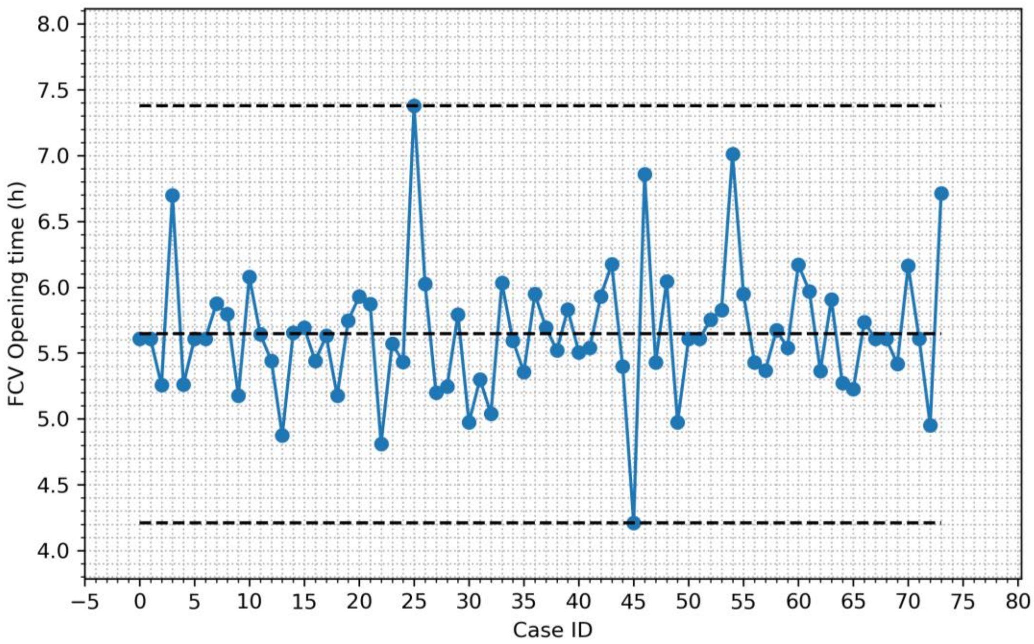

Figure 7-19. RC7A in Swedish NBWR MELCOR model –filtered containment venting opening times.

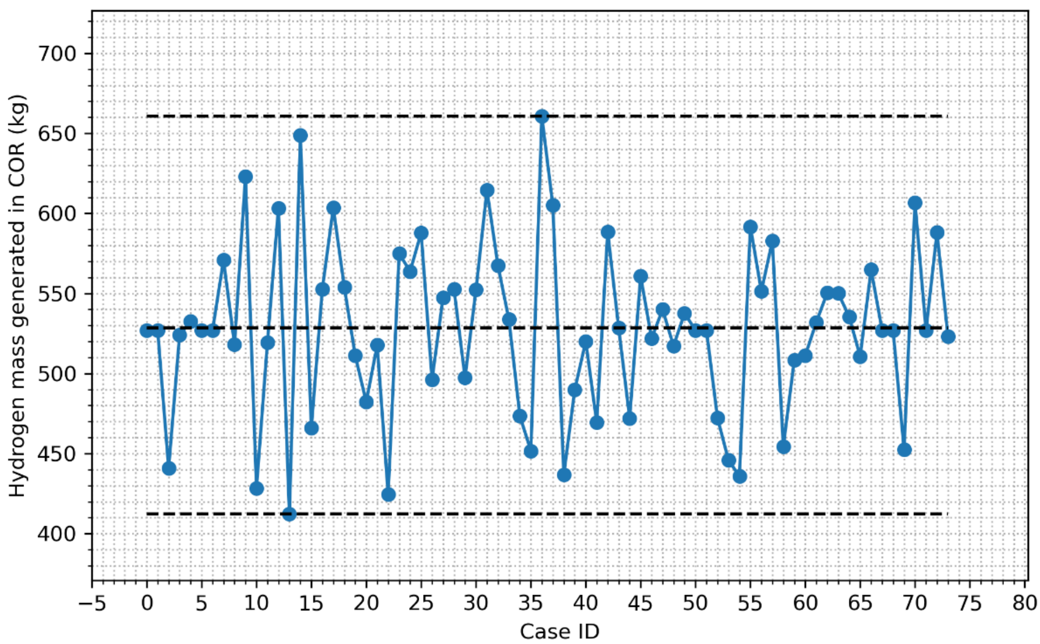

Figure 7-20. RC7A in Swedish NBWR MELCOR model – total hydrogen masses from COR package.

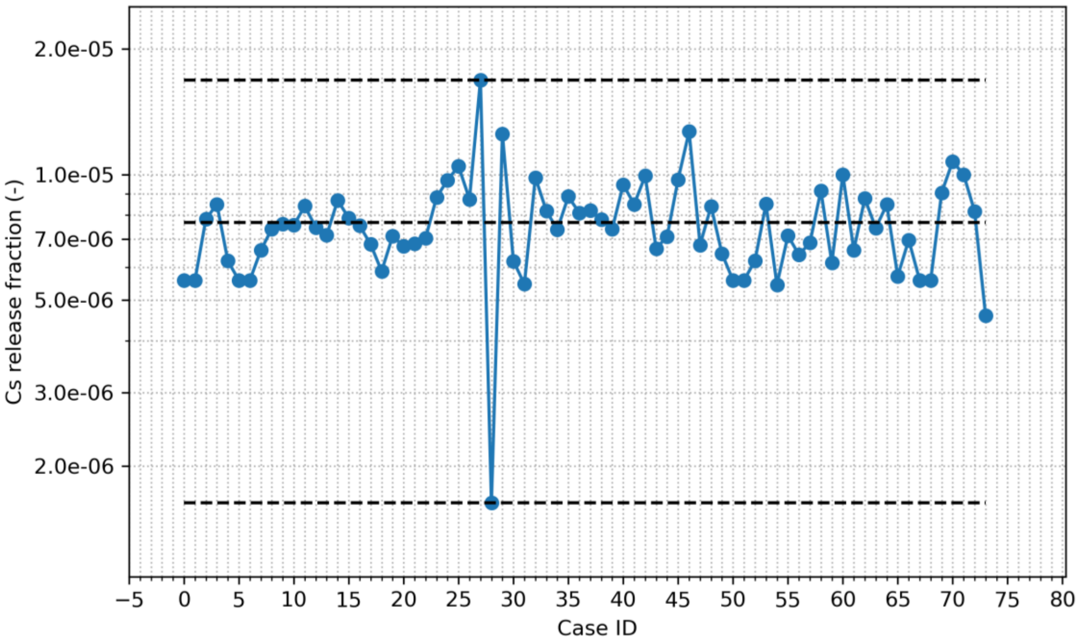

Figure 7-21. RC7A in Swedish NBWR MELCOR model – total Caesium release fractions to environment.

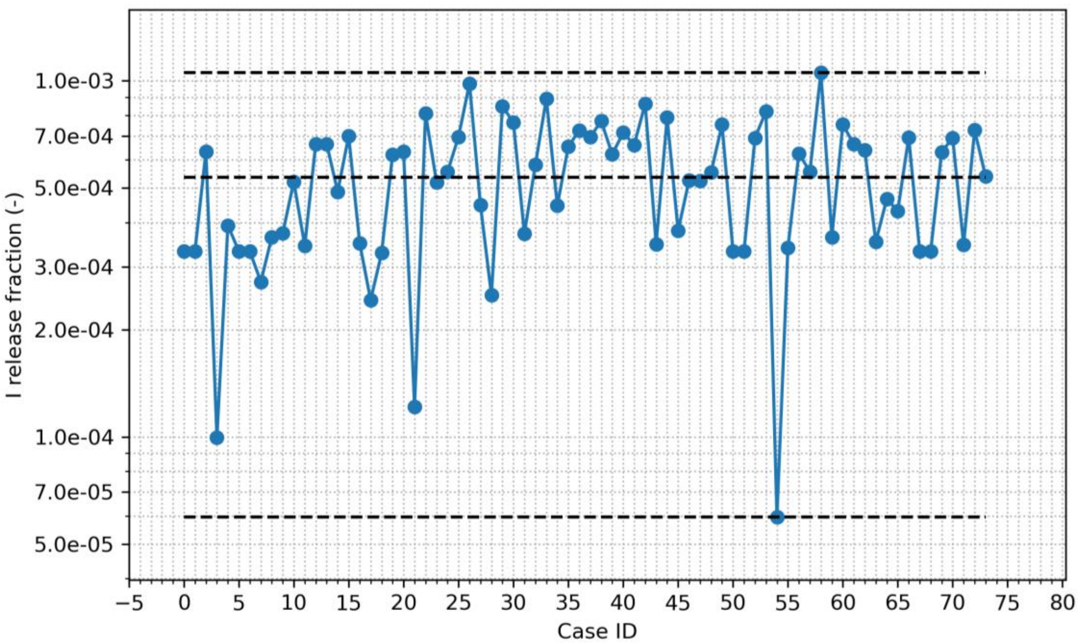

Figure 7-22. RC7A in Swedish NBWR MELCOR model – total Iodine release fractions to environment.

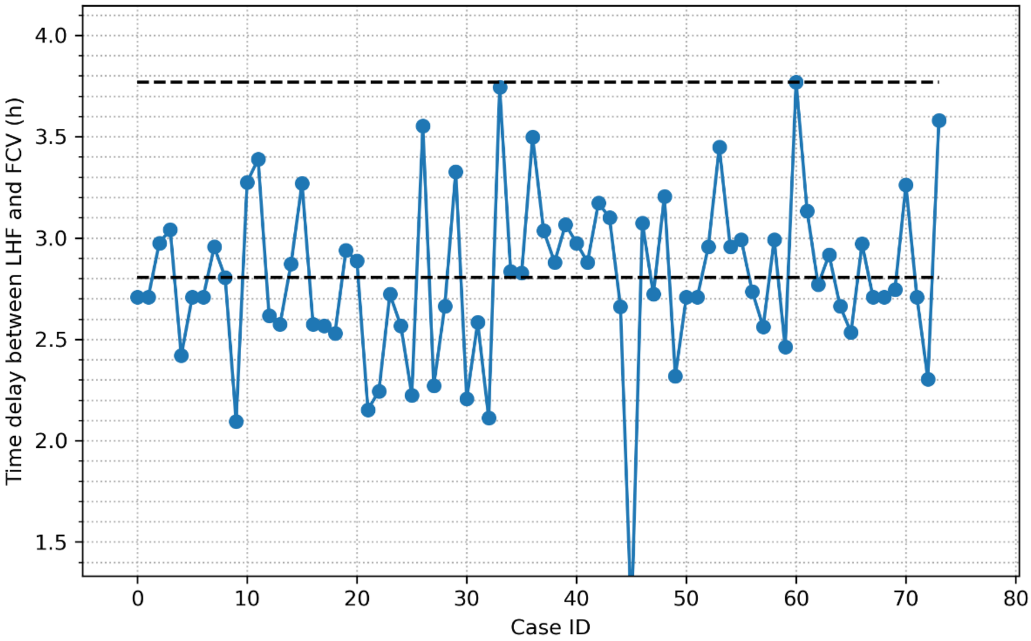

Figure 7-23. RC7A in Swedish NBWR MELCOR model – time delays from lower head failure to opening of filtered containment venting.

7.3.2. RC8 – Recovered station blackout leading to diffuse leakage

The accident sequence was defined by the following system availabilities:

- Reactor shutdown is successful at t=0.
- AFW, ECCS, RHR and CSS are all assumed unavailable from t = 0 h.
- ECCS, RHR and CSS are assumed recovered at t = 2 h.
- ADS is initiated according to standard control logic.
- LDW flooding system is initiated according to standard control logic.
- FCV opens if the containment pressure exceeds 5.5 bar (absolute).

Selected results for all bounding analysis cases are shown in Figure 7-24 - Figure 7-27.

An overview of parameter significance in terms of relative differences compared to the best estimate case in selected figures of merit is given in Table 7-5. These results will be used for screening of parameters for sensitivity analysis in the next project phase. The parameters whose bounding cases lead to the 9 largest absolute variations in total Cs release are highlighted in the table.

Table 7-5. RC8 bounding analyses parameter significance

Parameter	Value	CaseID	H2 COR [kg]	CS_ENV[-]	I_ENV[-]	T_LHF [h]
Best estimate		0	419.0	9.5E-07	2.0E-06	3.03
SC710611	5.00E-08	1	-30%	7%	-25%	N/A
SC710621	2.50E-07	2	-37%	-46%	-62%	N/A
SC710641	2.41E+05	3	-37%	86%	0%	N/A
SC710651	1.00E-05	4	-34%	-36%	-56%	N/A
TFFAIL	5.00E-01	5	-30%	7%	-25%	N/A
TFFAIL	1.50E+00	6	-30%	7%	-25%	N/A
TZRSSINC	1.70E+03	7	-32%	0%	-33%	N/A
TUO2ZRO2	2.80E+03	8	20%	36%	176%	2.86
FCELRA	2.50E-01	9	-16%	8%	-22%	N/A
PDPOR	3.00E-01	10	-26%	13%	-20%	N/A
PDPOR	5.00E-01	11	18%	78%	159%	2.25
CORNSBLD	1.70E+03	12	-26%	17%	-15%	N/A
VFALL	1.00E-01	13	-34%	-11%	-41%	N/A
SC10201	1.80E+02	14	-29%	9%	-24%	N/A
SC10201	7.20E+02	15	-4%	16%	-13%	3.17
SC10202	3.00E+01	16	-26%	13%	-19%	N/A
SC10202	1.20E+02	17	-27%	16%	-17%	N/A
HFRZSS	1.00E+03	18	-37%	-14%	-45%	N/A
HFRZZR	1.00E+03	19	-30%	12%	-21%	N/A
SC11312	2.10E+03	20	-22%	18%	-15%	N/A
SC11312	2.54E+03	21	-28%	17%	-17%	N/A
SC11412	1.00E+00	22	-33%	15%	-21%	N/A
DHYPDLP	5.00E-03	23	-29%	8%	-25%	N/A
HDBH2O	2.00E+02	24	-30%	7%	-25%	N/A
TPFAIL	1.60E+03	25	-30%	7%	-25%	N/A
HDBPN	1.00E+03	26	-30%	7%	-25%	N/A
CHI	3.00E+00	27	-31%	18%	-24%	N/A
GAMMA	3.00E+00	28	-22%	-77%	-88%	N/A
STICK	5.00E-01	29	-35%	4%	-31%	N/A
RHONOM	4.90E+03	30	-35%	6%	-26%	N/A
NUMSEC	20	31	-22%	0%	-28%	N/A
TURBDS	7.50E-04	32	-34%	-7%	-37%	N/A
TURBDS	1.25E-03	33	16%	55%	130%	2.29
SC7111I1	4.24E+00	34	36%	13%	18%	2.57
SC7111I1	5.73E+00	35	-31%	9%	-23%	N/A
SC7111I2	4.68E+02	36	-24%	21%	-9%	N/A
SC7111I2	6.33E+02	37	-28%	11%	-22%	N/A
SC7111CS1	3.08E+00	38	-29%	8%	-24%	N/A
SC7111CS1	4.16E+00	39	-29%	14%	-20%	N/A
SC7111CS2	8.25E+01	40	-29%	16%	-14%	N/A
SC7111CS2	1.12E+02	41	-29%	5%	-27%	N/A

Parameter	Value	CaseID	H2 COR [kg]	CS_ENV[-]	I_ENV[-]	T_LHF [h]
SC7170CS	3.36E+00	42	-28%	13%	-21%	N/A
SC7170CS	4.54E+00	43	-28%	8%	-20%	N/A
SC7170CSI3	3.74E-01	44	-29%	15%	-16%	N/A
SC7170CSI3	5.06E-01	45	-29%	2%	-32%	N/A
SC7170CSI4	1.91E+00	46	-31%	8%	-28%	N/A
SC7170CSI4	2.59E+00	47	-29%	14%	-20%	N/A
SC7170CSM	5.70E-01	48	16%	104%	204%	2.05
SC7170CSM	7.71E-01	49	-29%	14%	-21%	N/A
DIAMO	1.00E-04	50	-28%	10%	-17%	N/A
DIAMO	2.00E-03	51	-28%	33%	1%	N/A
SC715010	3.00E+00	52	-30%	-7%	-33%	N/A
SC715111	2.93E+00	53	22%	7%	27%	2.43
SC715111	3.97E+00	54	-32%	-23%	-50%	N/A
SC71521	5.00E-03	55	-33%	-15%	-44%	N/A
SC71521	8.00E-03	56	-32%	1%	-32%	N/A
SC71531	6.70E+00	57	-31%	24%	-14%	N/A
SC71531	9.06E+00	58	-34%	-26%	-51%	N/A
SC71551	1.52E+00	59	-28%	17%	-17%	N/A
SC71551	2.06E+00	60	23%	69%	71%	2.31
SC71555	9.68E-01	61	-33%	11%	-20%	N/A
SC71555	1.31E+00	62	-29%	23%	-15%	N/A
SC71542	2.56E-03	63	-27%	15%	-20%	N/A
SC71542	3.46E-03	64	9%	2%	52%	2.72
SC71568	-2.67E-03	65	-25%	13%	-17%	N/A
SC71568	-1.97E-03	66	-35%	-25%	-52%	N/A
SC7157	8.50E-01	67	-28%	15%	-13%	N/A
SC7157	1.15E+00	68	-28%	15%	-13%	N/A
OXM	4	69	-31%	11%	-20%	N/A
IDEJ	1	70	-28%	15%	-13%	N/A
MVSSDF	1.00E+02	71	-28%	15%	-13%	N/A
SC3210*	1.15E+00	72	-22%	68%	24%	N/A
CORSOR-BOOTH ICRLSE	-7	73	-15%	-33%	-53%	N/A

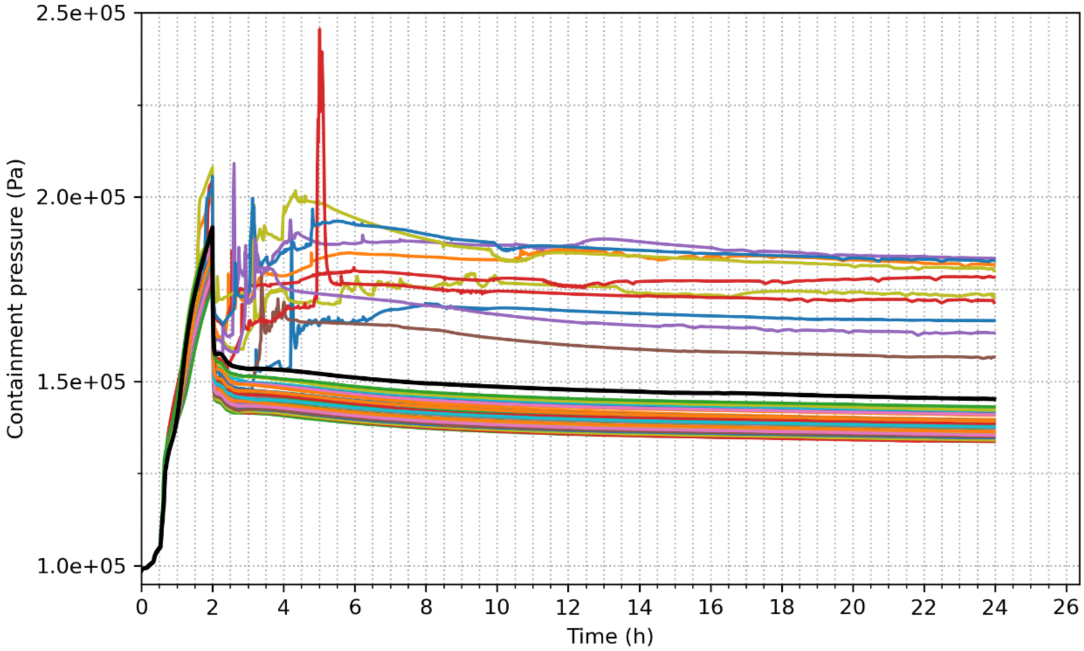

Figure 7-24. RC8 in Swedish NBWR MELCOR model - containment pressure.

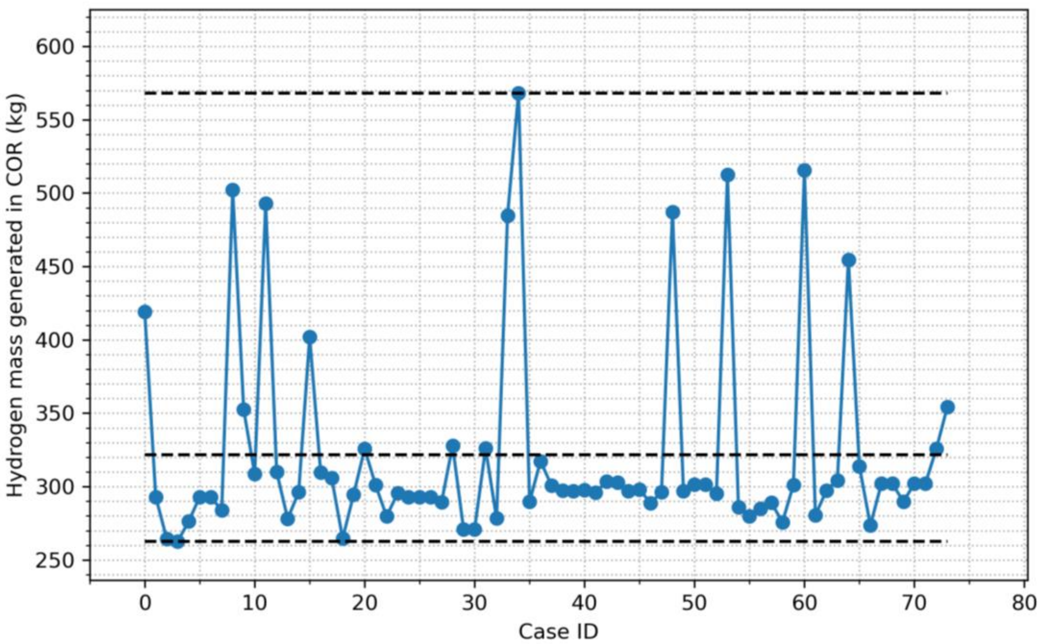

Figure 7-25. RC8 in Swedish NBWR MELCOR model – total hydrogen masses from COR package.

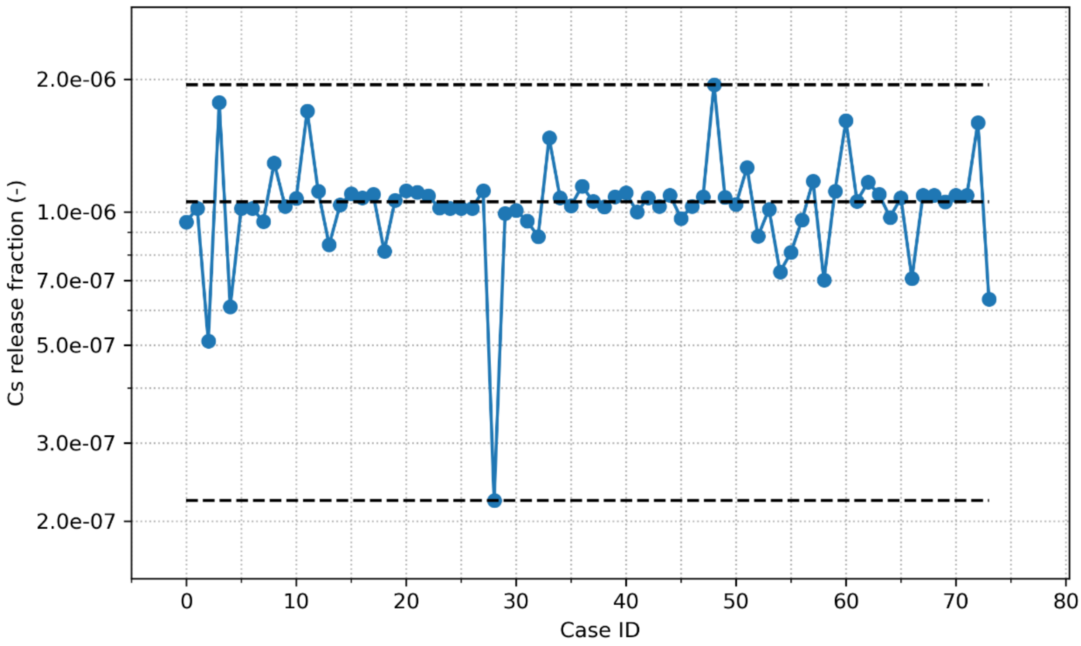

Figure 7-26. RC8 in Swedish NBWR MELCOR model – total Caesium release fractions to environment.

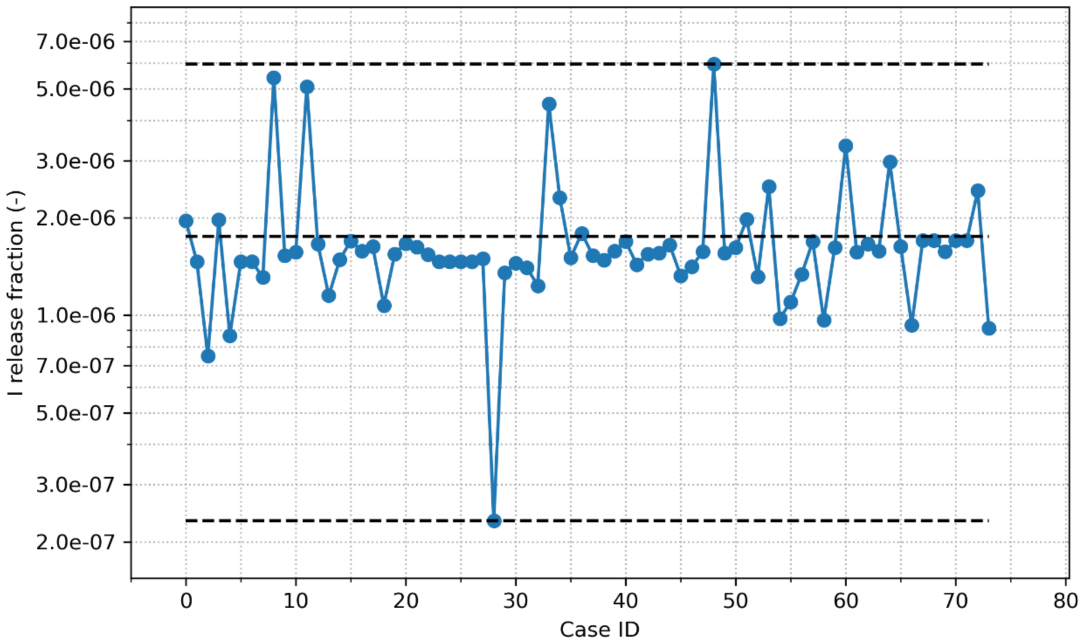

Figure 7-27. RC8 in Swedish NBWR MELCOR model – total Iodine release fractions to environment.

7.3.3. RC7B – Feedwater line LOCA and station blackout, leading to filtered venting

The accident sequence was defined by the following system availabilities:

- Feedwater line LOCA with successful reactor shutdown at t=0.
  (Subsequent feedwater isolation valve closure assumed successful.)
- AFW, ECCS, RHR and CSS are all assumed unavailable from t=0.
- ADS is initiated according to standard control logic.
- LDW flooding system is initiated according to standard control logic.
- FCV opens when the containment pressure exceeds 5.5 bar (absolute).

Selected results for all bounding analysis cases are shown in Figure 7-28 - Figure 7-34. It can be noted that FCV opening times range approximately from 1,5 to 5 h from initiating event, see Figure 7-30. The time from lower head failure to FCV opening, is generally not as large as for the SBO case, however with some cases still resulting in a delay of about 3 h, see Figure 7-34.

An overview of parameter significance in terms of relative differences compared to the best estimate case in selected figures of merit is given in Table 7-6. These results will be used for screening of parameters for sensitivity analysis in the next project phase. The parameters whose bounding cases lead to the 9 largest absolute variations in total Cs release are highlighted in the table.

Table 7-6. RC7B bounding analyses parameter significance

Parameter	Value	Case ID	T_FCV [h]	T_LHF [h]	T_FCV -T_LHF [h]	H2 COR [kg]	CS_ENV [-]	I_ENV [-]
Best estimate		0	3.64	1.76	1.88	508.1	6.21E-04	4.38E-04
SC710611	5.00E-08	1	0%	0%	0%	0%	0%	0%
SC710621	2.50E-07	2	6%	-23%	33%	17%	-70%	-56%
SC710641	2.41E+05	3	-43%	27%	-108%	-16%	-65%	-39%
SC710651	1.00E-05	4	-54%	-8%	-97%	26%	-87%	-73%
TFFAIL	5.00E-01	5	0%	0%	0%	0%	0%	0%
TFFAIL	1.50E+00	6	0%	0%	0%	0%	0%	0%
TZRSSINC	1.70E+03	7	-45%	14%	-100%	23%	-60%	-52%
TUO2ZRO2	2.80E+03	8	21%	-1%	42%	44%	-78%	-60%
FCELRA	2.50E-01	9	30%	22%	37%	-13%	-14%	-7%
PDPOR	3.00E-01	10	30%	-17%	74%	12%	49%	36%
PDPOR	5.00E-01	11	-52%	7%	-108%	28%	-77%	-66%
CORNSBLD	1.70E+03	12	-47%	6%	-97%	34%	-49%	-25%
VFALL	1.00E-01	13	18%	-3%	38%	-18%	-53%	-51%
SC10201	1.80E+02	14	-7%	2%	-16%	-25%	-57%	-48%
SC10201	7.20E+02	15	4%	-2%	9%	-5%	-68%	-68%
SC10202	3.00E+01	16	12%	4%	20%	-3%	-75%	-66%
SC10202	1.20E+02	17	0%	69%	-64%	11%	72%	54%
HFRZSS	1.00E+03	18	27%	-15%	67%	-9%	-62%	-61%
HFRZZR	1.00E+03	19	25%	-2%	50%	-3%	-78%	-73%
SC11312	2.10E+03	20	-50%	9%	-105%	30%	-42%	-21%
SC11312	2.54E+03	21	-48%	17%	-108%	-14%	-77%	-70%
SC11412	1.00E+00	22	1%	-15%	17%	-5%	-84%	-80%
DHYPDLP	5.00E-03	23	3%	-5%	12%	-1%	41%	31%
HDBH2O	2.00E+02	24	8%	1%	16%	4%	26%	20%
TPFAIL	1.60E+03	25	-41%	30%	-107%	4%	209%	159%
HDBPN	1.00E+03	26	-45%	-15%	-73%	2%	-78%	-54%
CHI	3.00E+00	27	-55%	0%	-107%	6%	-79%	-70%
GAMMA	3.00E+00	28	-36%	29%	-97%	19%	-61%	-44%
STICK	5.00E-01	29	-20%	-3%	-37%	12%	-83%	-67%
RHONOM	4.90E+03	30	8%	-21%	36%	36%	-78%	-65%
NUMSEC	20	31	-46%	9%	-98%	23%	-79%	-63%
TURBDS	7.50E-04	32	18%	0%	35%	-18%	-73%	-69%
TURBDS	1.25E-03	33	-49%	10%	-105%	31%	-84%	-72%
SC7111I1	4.24E+00	34	-53%	0%	-102%	3%	-69%	-53%
SC7111I1	5.73E+00	35	-10%	12%	-31%	7%	-58%	-48%
SC7111I2	4.68E+02	36	-26%	0%	-51%	-29%	-85%	-62%
SC7111I2	6.33E+02	37	24%	-15%	62%	-2%	-60%	-57%
SC7111CS1	3.08E+00	38	-42%	35%	-115%	-5%	-71%	-41%
SC7111CS1	4.16E+00	39	-52%	-1%	-100%	22%	-78%	-63%
SC7111CS2	8.25E+01	40	19%	1%	36%	2%	-68%	-42%

SC7111CS2	1.12E+02	41	-23%	-1%	-44%	-6%	-81%	-67%
SC7170CS	3.36E+00	42	-54%	1%	-105%	36%	-68%	-54%
SC7170CS	4.54E+00	43	-2%	13%	-15%	8%	-73%	-69%
SC7170CSI3	3.74E-01	44	-12%	-6%	-17%	-11%	-85%	-61%
SC7170CSI3	5.06E-01	45	43%	-8%	90%	-7%	-42%	-45%
SC7170CSI4	1.91E+00	46	15%	5%	24%	8%	-67%	-37%
SC7170CSI4	2.59E+00	47	-55%	-2%	-105%	55%	-80%	-67%
SC7170CS M	5.70E-01	48	-57%	-12%	-98%	25%	-85%	-72%
SC7170CS M	7.71E-01	49	20%	11%	29%	4%	-73%	-64%
DIAMO	1.00E-04	50	0%	0%	0%	0%	0%	0%
DIAMO	2.00E-03	51	0%	0%	0%	0%	0%	0%
SC715010	3.00E+00	52	21%	10%	32%	13%	-40%	-34%
SC715111	2.93E+00	53	0%	0%	0%	0%	0%	0%
SC715111	3.97E+00	54	0%	0%	0%	0%	0%	0%
SC71521	5.00E-03	55	-53%	15%	-118%	-26%	-89%	-82%
SC71521	8.00E-03	56	15%	-9%	38%	7%	11%	8%
SC71531	6.70E+00	57	11%	15%	7%	30%	-56%	-41%
SC71531	9.06E+00	58	2%	6%	-1%	12%	200%	177%
SC71551	1.52E+00	59	6%	4%	8%	6%	-78%	-72%
SC71551	2.06E+00	60	-4%	4%	-12%	12%	-77%	-52%
SC71555	9.68E-01	61	-29%	-14%	-44%	-37%	-89%	-78%
SC71555	1.31E+00	62	-49%	9%	-103%	25%	-82%	-72%
SC71542	2.56E-03	63	-19%	-5%	-31%	36%	-56%	-41%
SC71542	3.46E-03	64	38%	4%	69%	7%	168%	134%
SC71568	-2.67E-03	65	-50%	1%	-98%	38%	-62%	-35%
SC71568	-1.97E-03	66	13%	2%	24%	0%	-62%	-61%
SC7157	8.50E-01	67	0%	0%	0%	0%	0%	0%
SC7157	1.15E+00	68	0%	0%	0%	0%	0%	0%
OXM	4	69	1%	11%	-9%	8%	-12%	-5%
IDEJ	1	70	113%	-22%	240%	17%	4903%	6205%
MVSSDF	1.00E+02	71	0%	0%	0%	0%	31%	75%
SC3210*	1.15E+00	72	6%	-10%	20%	-21%	-44%	-39%
CORSOR-BOOTH ICRLSE	-7	73	18%	-5%	40%	-12%	148%	103%

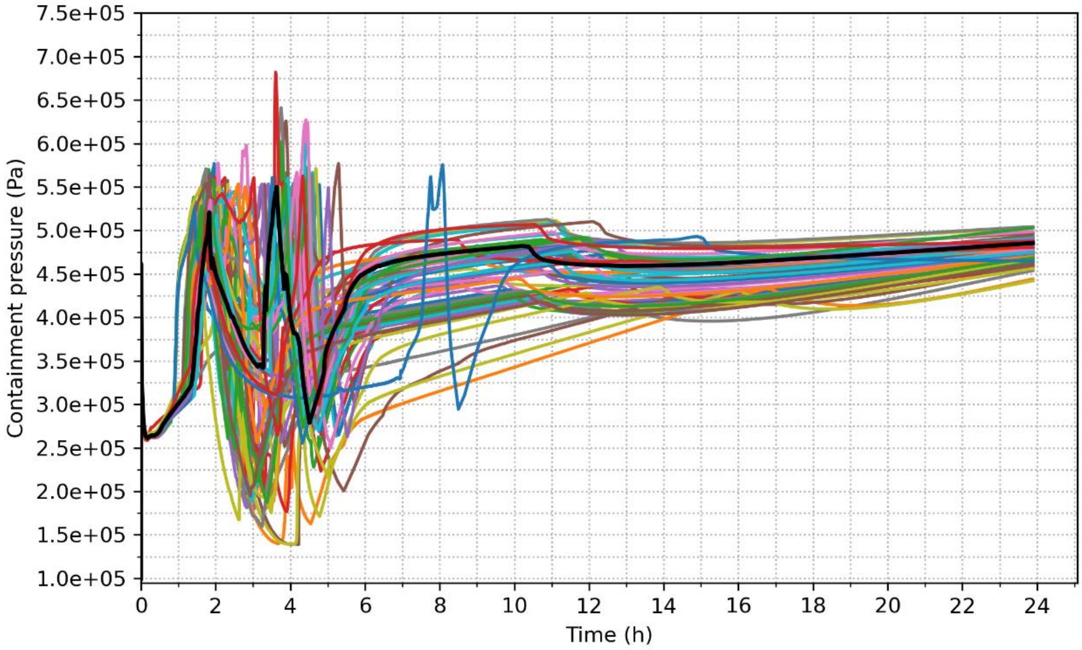

Figure 7-28. RC7B in Swedish NBWR MELCOR model - containment pressure.

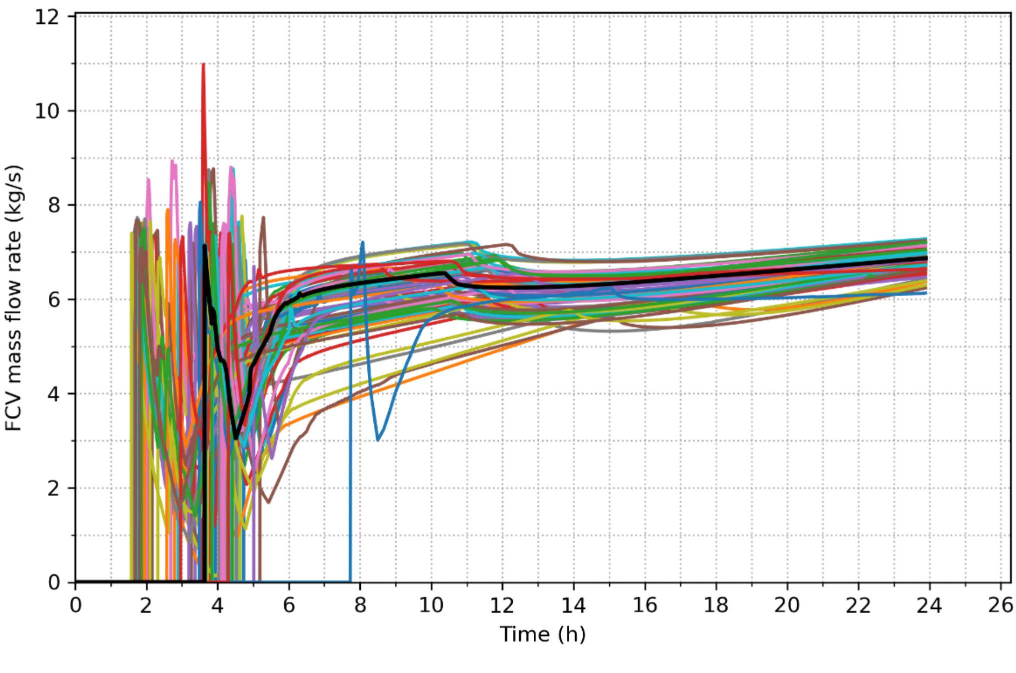

Figure 7-29. RC7B in Swedish NBWR MELCOR model – filtered containment venting flow rate.

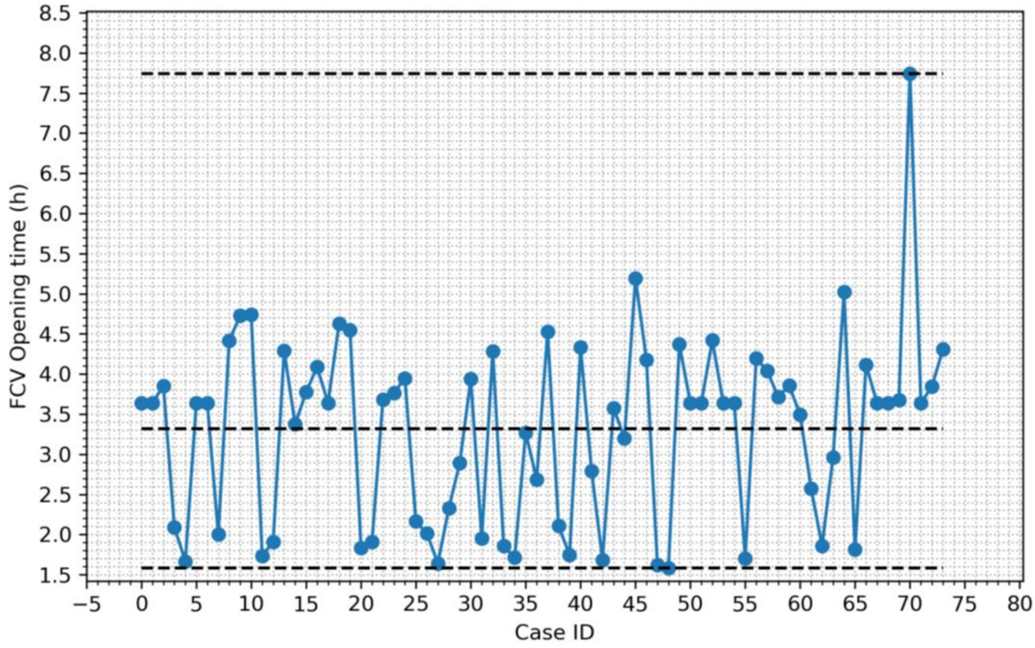

Figure 7-30. RC7B in Swedish NBWR MELCOR model –filtered containment venting opening times.

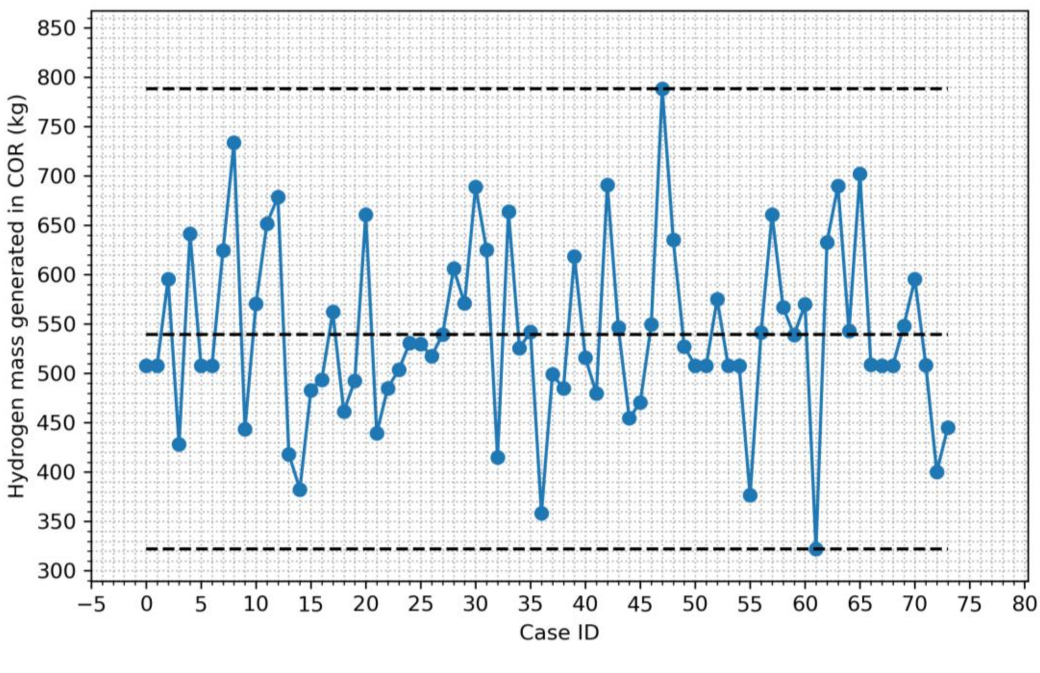

Figure 7-31. RC7B in Swedish NBWR MELCOR model – total hydrogen masses from COR package.

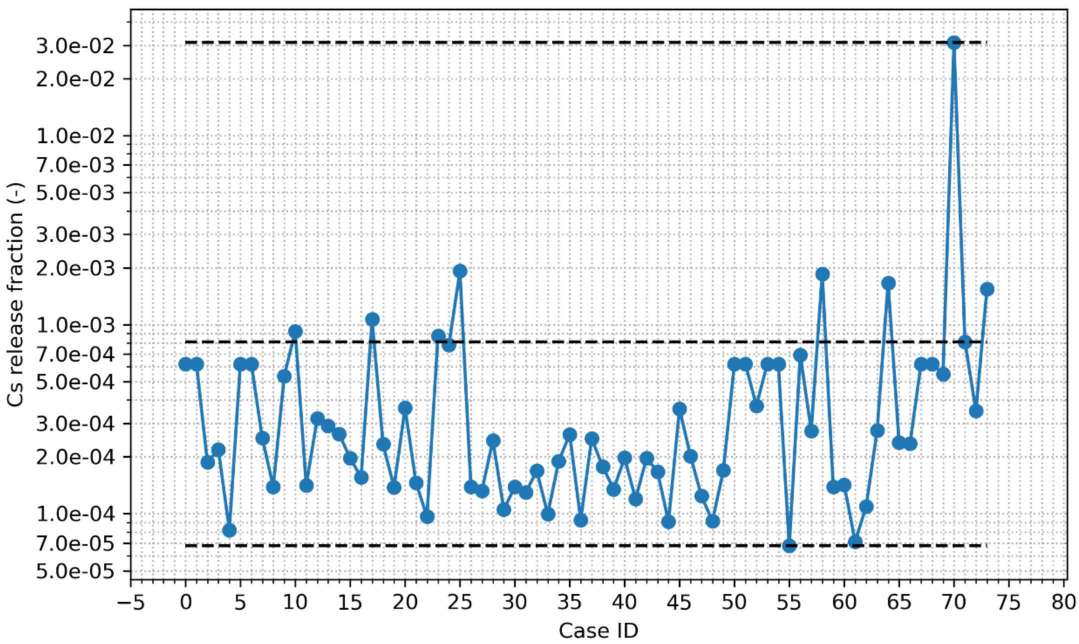

Figure 7-32. RC7B in Swedish NBWR MELCOR model – total Caesium release fractions to environment.

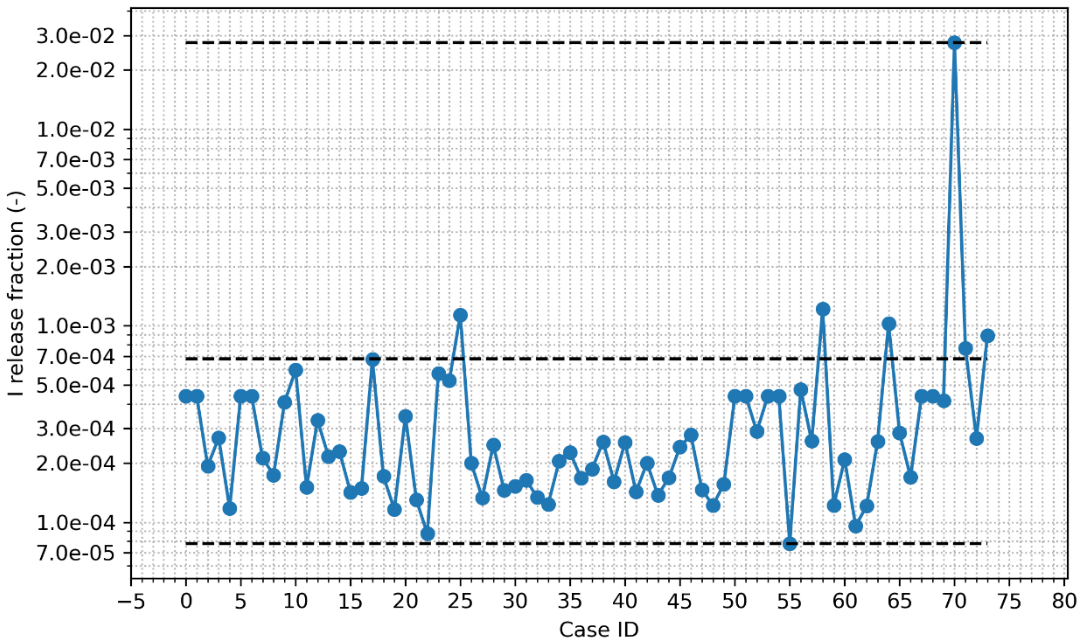

Figure 7-33. RC7B in Swedish NBWR MELCOR model – total Iodine release fractions to environment.

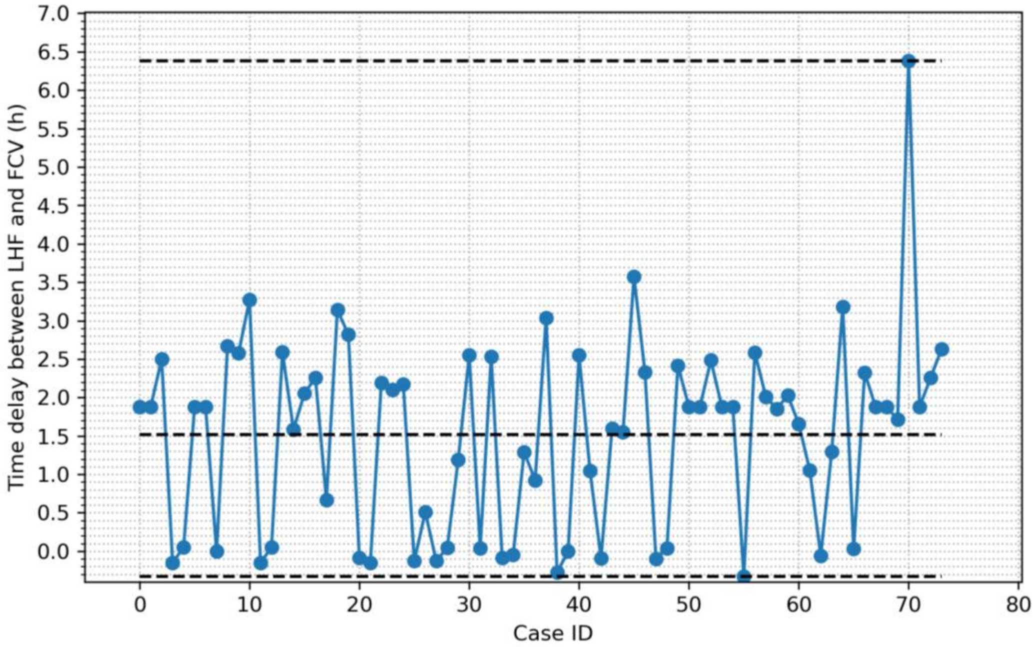

Figure 7-34. RC7B in Swedish NBWR MELCOR model – time delays from lower head failure to opening of filtered containment venting.

The results presented in Figure 7-32 show quite significant difference in the fraction of Cs released to the environment in Case 70 (IDEJ = 1) compared to the rest of the results. IDEJ is the modelling switch that limits the mode of debris ejection from the vessel (see section 5.7 for more details) to (i) in case of IDEJ = 1- only molten materials; (ii) in case of IDEJ = 0 (default) – both molten and solid materials. Effectively it means that in case of IDEJ =1 the UO2/ZrO2 debris will remain in vessel until either complete remelting or vessel lower head failure due to creep-rupture.

The exposed debris in the vessel will heat-up the atmosphere inside the vessel and the containment (Figure 7-35) which can lead to revaporization of the aerosols suspended in the vessel/containment atmosphere.

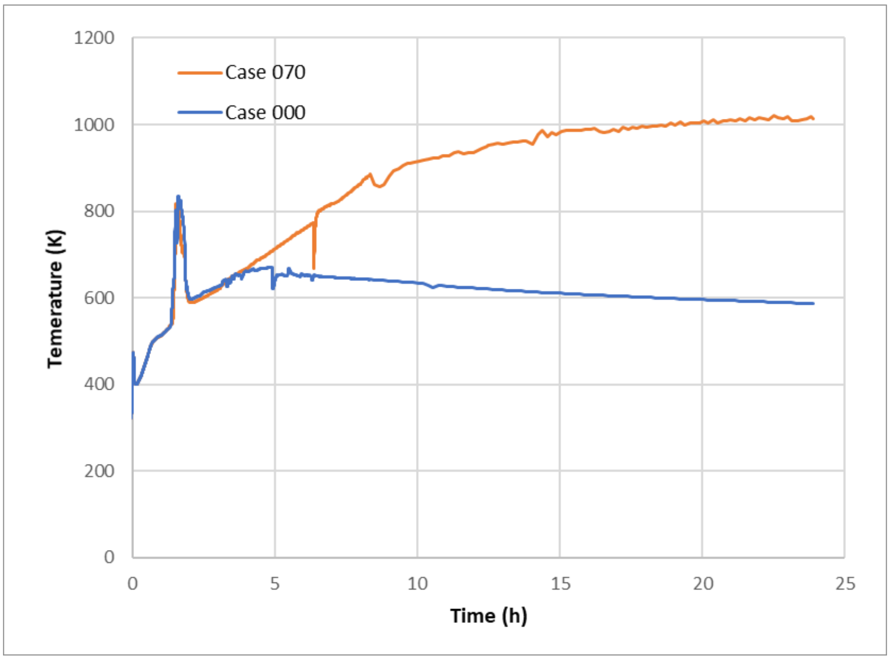

Figure 7-35. RC7B in Swedish NBWR MELCOR model – atmosphere temperature in the containment.

The MELCOR model of Swedish BWR employs the Multi Venturi Scrubber System (MVSS) implemented as a simple filter with constant decontamination factor DF=500 for aerosols (see section 5.10.2 for more details). It means that the radioactive vapours will be released to the environment without any filtering/decontamination.

An additional sensitivity calculation was performed for the Case 70 with DF = 500 for both aerosols and vapours (excluding noble gases, i.e. DF=1 for RN class 1 (Xe) – always released as vapour). Figure 7-36 shows the comparison of the fraction of Cs released to the environment with (i) only aerosols filtering (Orange – NVF) and (ii) both aerosols and vapours filtering (Blue – WVF). The release of Cs to the environment is almost two orders of magnitude smaller in case of both aerosols and vapours filtering than in case of aerosols filtering only, which is also reflected in the fraction of Cs deposited in the MVSS filter illustrated in Figure 7-37.

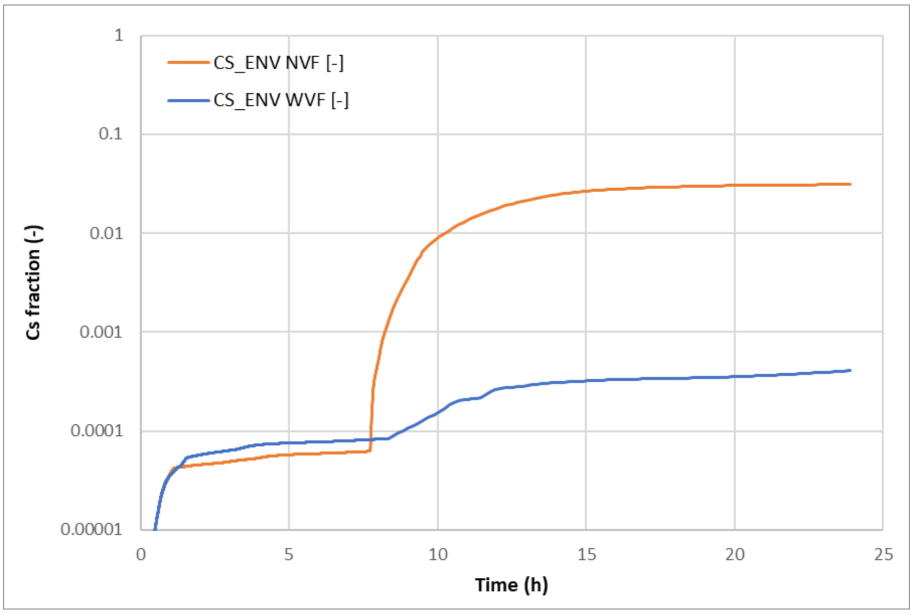

Figure 7-36. RC7B in Swedish NBWR MELCOR model – Case 70 (IDEJ = 1) – fraction of Cs released to the environment.

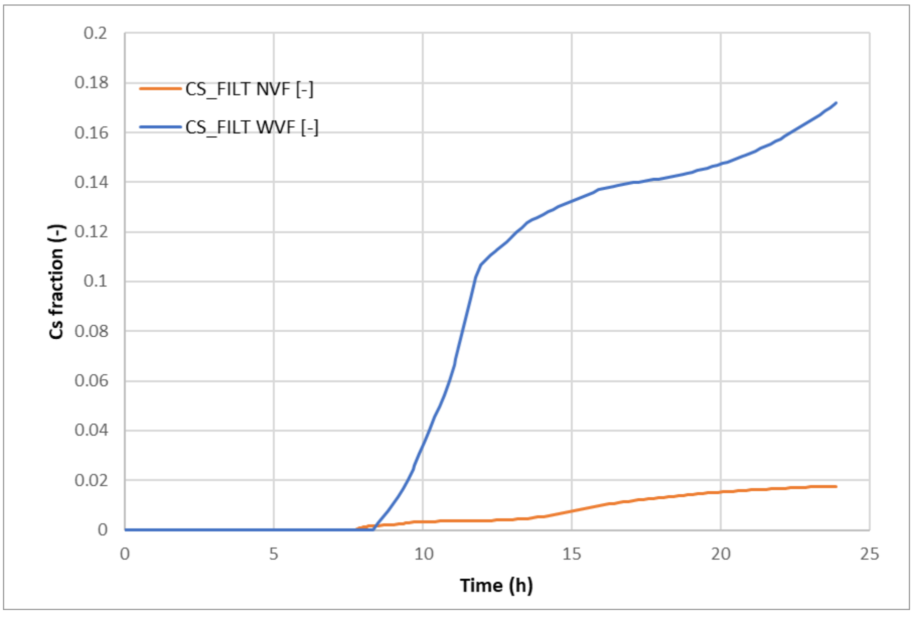

Figure 7-37. RC7B in Swedish NBWR MELCOR model – Case 70 (IDEJ = 1) – fraction of Cs deposited in the MVSS system.

The results presented above indicate quite significant effect of the modelling of MVSS system, modelling of the mode of debris ejection from the vessel on the containment and environmental source terms.

7.3.4. RC5A – LOCA with failing PS function and failure to close unfiltered containment venting line

The accident sequence was defined by the following system availabilities:

- Feedwater line LOCA with successful reactor shutdown at t=0. (Subsequent feedwater isolation valve closure assumed successful.)
- 75% of the blowdown pipes cross-section area is assumed unavailable, thereby deteriorating the PS function.
- AFW, ECCS, RHR and CSS are all assumed unavailable from t=0.
- ADS is initiated according to standard control logic.
- LDW flooding system is initiated according to standard control logic.
- FCV and unfiltered containment venting opens when the containment pressure exceeds 5.5 bar and 6.5 bar (absolute) respectively.
- Automatic valve closure in the unfiltered containment venting line fails.

To evaluate the effect of containment pressure response in case of LB-LOCA with partially degraded PS-function, a set of simulations was performed with (a) 25%, (b) 50% and (c) 75% of the total flow area in the blowdown pipes. The results, presented in Figure 7-38, show that a LB-LOCA would lead to the opening of the rupture disk in the containment venting line in case of 75% reduction of the blowdown pipes flow area (PS function 25%). In case of 50% reduction of the blowdown pipes flow area, the maximum pressure is very close to the pressure setpoint of the containment venting line, thus a reduction of >50% is very likely to lead to the venting line opening.

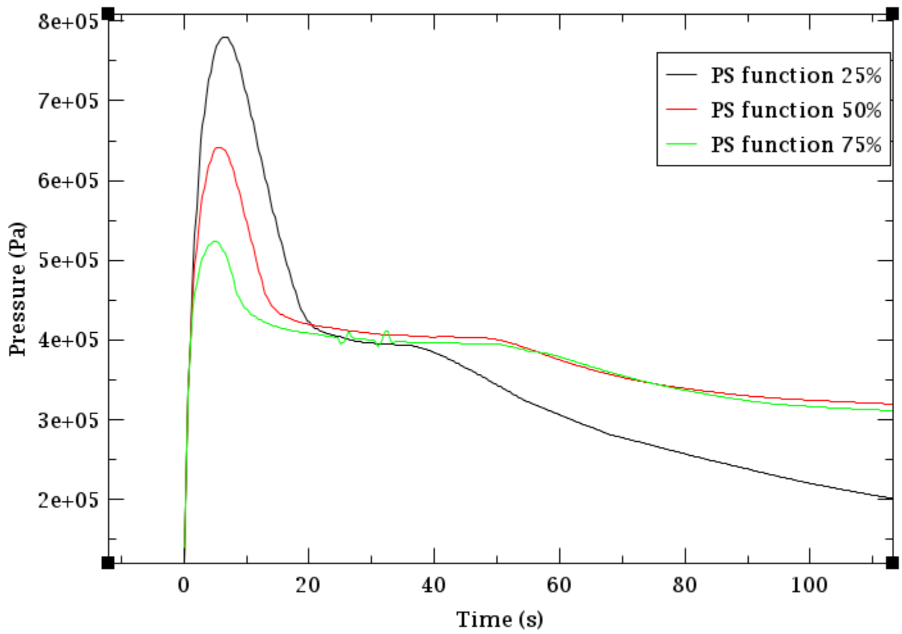

Figure 7-38. Containment pressure response at LB-LOCA with (black curve) 25%, (red curve) 50%, (green curve) 75% of the blowdown pipes flow area.

Selected results for all bounding analysis cases are shown in Figure 7-39 - Figure 7-42.

An overview of parameter significance in terms of relative differences compared to the best estimate case in selected figures of merit is given in Table 7-7. These results will be used for screening of parameters for sensitivity analysis in the next project phase. The parameters whose bounding cases lead to the 9 largest absolute variations in total Cs release are highlighted in the table.

Table 7-7. RC5A bounding analyses parameter significance

Parameter	Value	CaseID	T_LHF [h]	H2 COR [kg]	CS_ENV[-]	I_ENV[-]
Best estimate		0	1.8	477.8	3.4E-01	3.6E-01
SC710611	5.00E-08	1	-2%	-16%	2%	1%
SC710621	2.50E-07	2	15%	1%	12%	17%
SC710641	2.41E+05	3	12%	88%	-6%	-13%
SC710651	1.00E-05	4	-19%	0%	10%	15%
TFFAIL	5.00E-01	5	-2%	-16%	2%	1%
TFFAIL	1.50E+00	6	-2%	-16%	2%	1%
TZRSSINC	1.70E+03	7	1%	52%	2%	0%
TUO2ZRO2	2.80E+03	8	-5%	-6%	-1%	-4%
FCELRA	2.50E-01	9	15%	32%	3%	5%
PDPOR	3.00E-01	10	12%	15%	-2%	-5%
PDPOR	5.00E-01	11	-32%	43%	42%	46%
CORNSBLD	1.70E+03	12	21%	41%	2%	2%
VFALL	1.00E-01	13	7%	-2%	-3%	6%
SC10201	1.80E+02	14	7%	37%	3%	2%
SC10201	7.20E+02	15	12%	29%	-2%	-3%
SC10202	3.00E+01	16	-11%	6%	9%	8%
SC10202	1.20E+02	17	9%	7%	3%	-1%
HFRZSS	1.00E+03	18	-5%	10%	-2%	-3%
HFRZZR	1.00E+03	19	14%	35%	-5%	-4%
SC11312	2.10E+03	20	1%	-2%	-6%	-5%
SC11312	2.54E+03	21	9%	15%	-3%	-3%
SC11412	1.00E+00	22	21%	-5%	4%	1%
DHYPDLP	5.00E-03	23	10%	-15%	-5%	-6%
HDBH2O	2.00E+02	24	-2%	-20%	-3%	-6%
TPFAIL	1.60E+03	25	10%	-20%	-1%	-4%
HDBPN	1.00E+03	26	-14%	27%	-2%	-3%
CHI	3.00E+00	27	3%	32%	22%	14%
GAMMA	3.00E+00	28	17%	0%	-27%	-24%
STICK	5.00E-01	29	-14%	-5%	6%	2%
RHONOM	4.90E+03	30	10%	15%	3%	4%
NUMSEC	20	31	-2%	22%	1%	-2%
TURBDS	7.50E-04	32	2%	10%	-1%	1%
TURBDS	1.25E-03	33	0%	5%	5%	3%
SC7111I1	4.24E+00	34	51%	8%	10%	3%
SC7111I1	5.73E+00	35	16%	12%	0%	-2%
SC7111I2	4.68E+02	36	0%	75%	-1%	-3%
SC7111I2	6.33E+02	37	11%	37%	-2%	-3%
SC7111CS1	3.08E+00	38	45%	26%	9%	7%
SC7111CS1	4.16E+00	39	22%	0%	3%	4%
SC7111CS2	8.25E+01	40	9%	15%	3%	1%
SC7111CS2	1.12E+02	41	-4%	16%	6%	7%
SC7170CS	3.36E+00	42	5%	28%	0%	-1%

Parameter	Value	CaseID	T_LHF [h]	H2 COR [kg]	CS_ENV[-]	I_ENV[-]
SC7170CS	4.54E+00	43	15%	39%	-3%	-5%
SC7170CSI3	3.74E-01	44	-11%	-19%	2%	1%
SC7170CSI3	5.06E-01	45	12%	7%	5%	4%
SC7170CSI4	1.91E+00	46	-1%	19%	6%	4%
SC7170CSI4	2.59E+00	47	25%	21%	3%	4%
SC7170CSM	5.70E-01	48	10%	41%	-3%	-6%
SC7170CSM	7.71E-01	49	12%	29%	-2%	-5%
DIAMO	1.00E-04	50	-2%	-16%	2%	1%
DIAMO	2.00E-03	51	-2%	-16%	2%	1%
SC715010	3.00E+00	52	-1%	5%	-3%	-4%
SC715111	2.93E+00	53	-2%	-16%	2%	1%
SC715111	3.97E+00	54	-2%	-16%	2%	1%
SC71521	5.00E-03	55	8%	40%	-2%	-2%
SC71521	8.00E-03	56	18%	10%	3%	-3%
SC71531	6.70E+00	57	16%	40%	2%	-2%
SC71531	9.06E+00	58	1%	7%	9%	7%
SC71551	1.52E+00	59	16%	29%	-6%	-1%
SC71551	2.06E+00	60	5%	32%	2%	0%
SC71555	9.68E-01	61	6%	55%	0%	0%
SC71555	1.31E+00	62	13%	30%	1%	0%
SC71542	2.56E-03	63	3%	9%	0%	-2%
SC71542	3.46E-03	64	7%	-1%	-4%	-4%
SC71568	-2.67E-03	65	-2%	-16%	2%	1%
SC71568	-1.97E-03	66	-2%	-16%	2%	1%
SC7157	8.50E-01	67	-2%	-16%	2%	1%
SC7157	1.15E+00	68	-2%	-16%	2%	1%
OXM	4	69	21%	2%	2%	0%
IDEJ	1	70	-2%	-12%	8%	6%
MVSSDF	1.00E+02	71	-2%	-16%	2%	1%
SC3210*	1.15E+00	72	12%	-2%	4%	4%
CORSOR-BOOTH ICRLSE	-7	73	12%	-2%	4%	4%

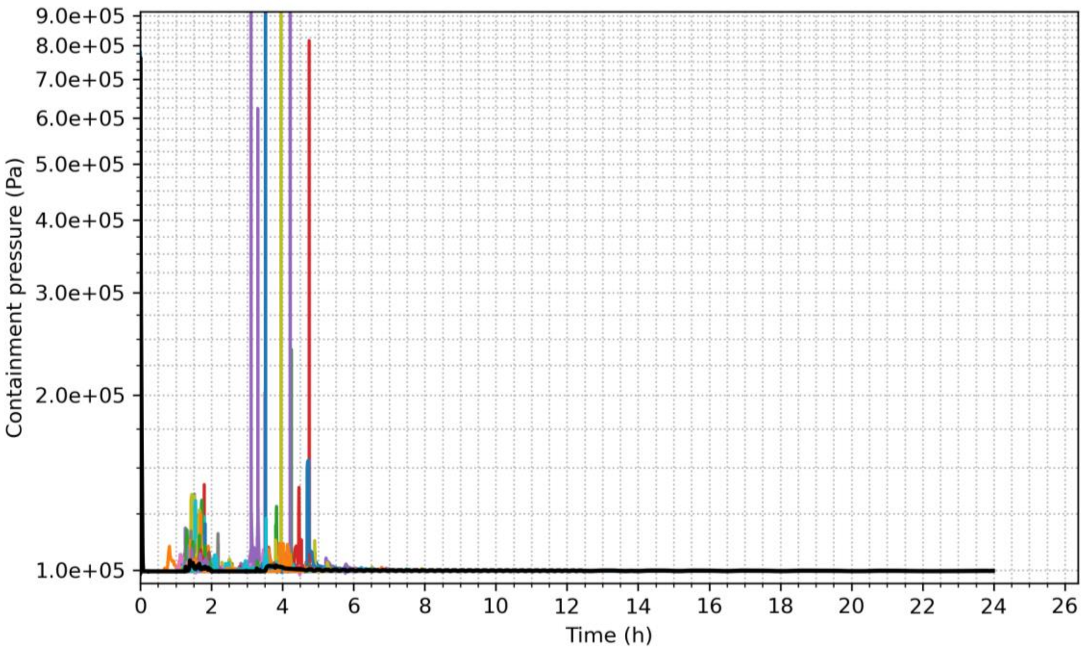

Figure 7-39. RC5A in Swedish NBWR MELCOR model - containment pressure.

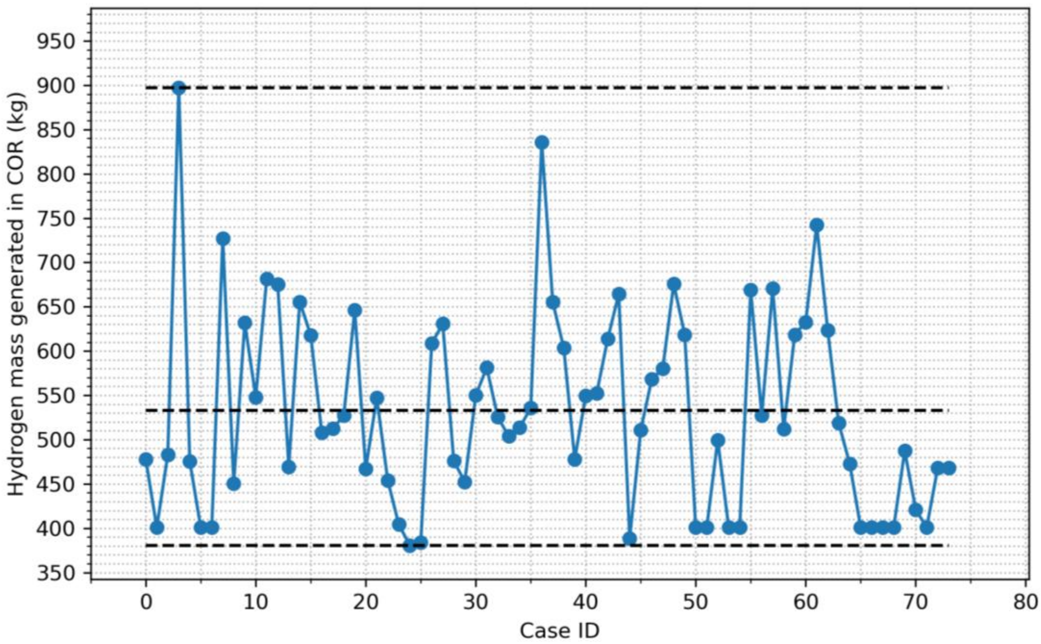

Figure 7-40. RC5A in Swedish NBWR MELCOR model – total hydrogen masses from COR package.

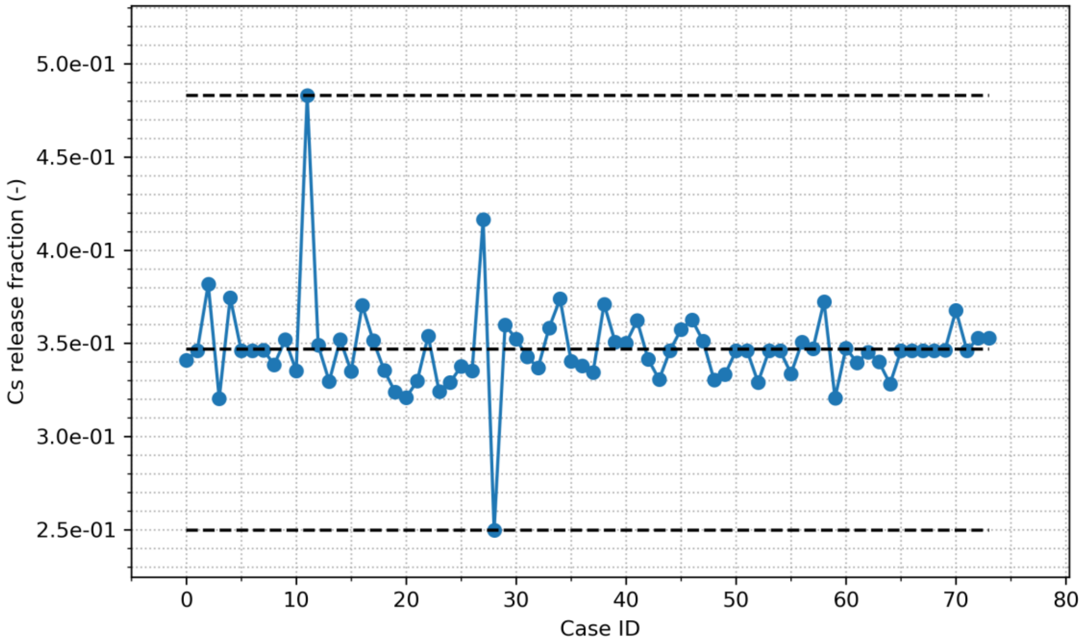

Figure 7-41. RC5A in Swedish NBWR MELCOR model – total Caesium release fractions to environment.

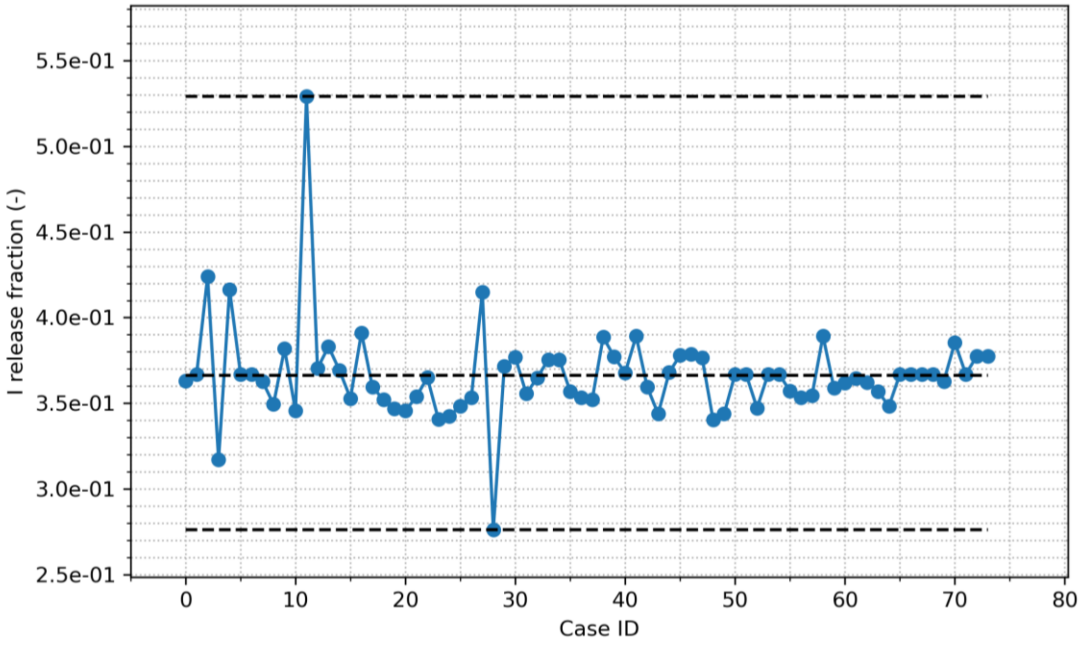

Figure 7-42. RC5A in Swedish NBWR MELCOR model – total Iodine release fractions to environment.

7.3.5. Summary

Figure 7-43 illustrate, based on typical L2 PSA results and the simulations performed in this work, a normalized frequency uncertainty distribution of RC7A (SBO), RC8, RC7B (LOCA) and RC5 release categories, together with their respective spread of the fraction of Cs core inventory released to the environment, as presented in figures 7-21, 7-26, 7-32 and 7-41. Note that the spread and distribution along the frequency axis is subject to limitations and assumptions in L1 & L2 PSA parametric uncertainty analysis while the Cs release axis uncertainty so far is only a parameter range scoping study. Absolute frequency results of operational plants are usually not cited in open sources while typical target values of 10^{-5} per year for core damage frequency and 10^{-7} per year for large release frequency are instructive, see e.g. [6] for an open overview of targets in use in Sweden and Finland.

The results show that all simulations performed for RC7A (SBO), RC8 and RC5 are within prescribed limits for respective release categories, i.e. RC7A (SBO) and RC8 belong to acceptable release category according to the SSM MVSS design criterion, and RC5 belongs to large early release. Simulations performed for RC7B (LOCA) show that in some MELCOR calculations the fraction of Cs core inventory released to the environment exceed the design criterion.

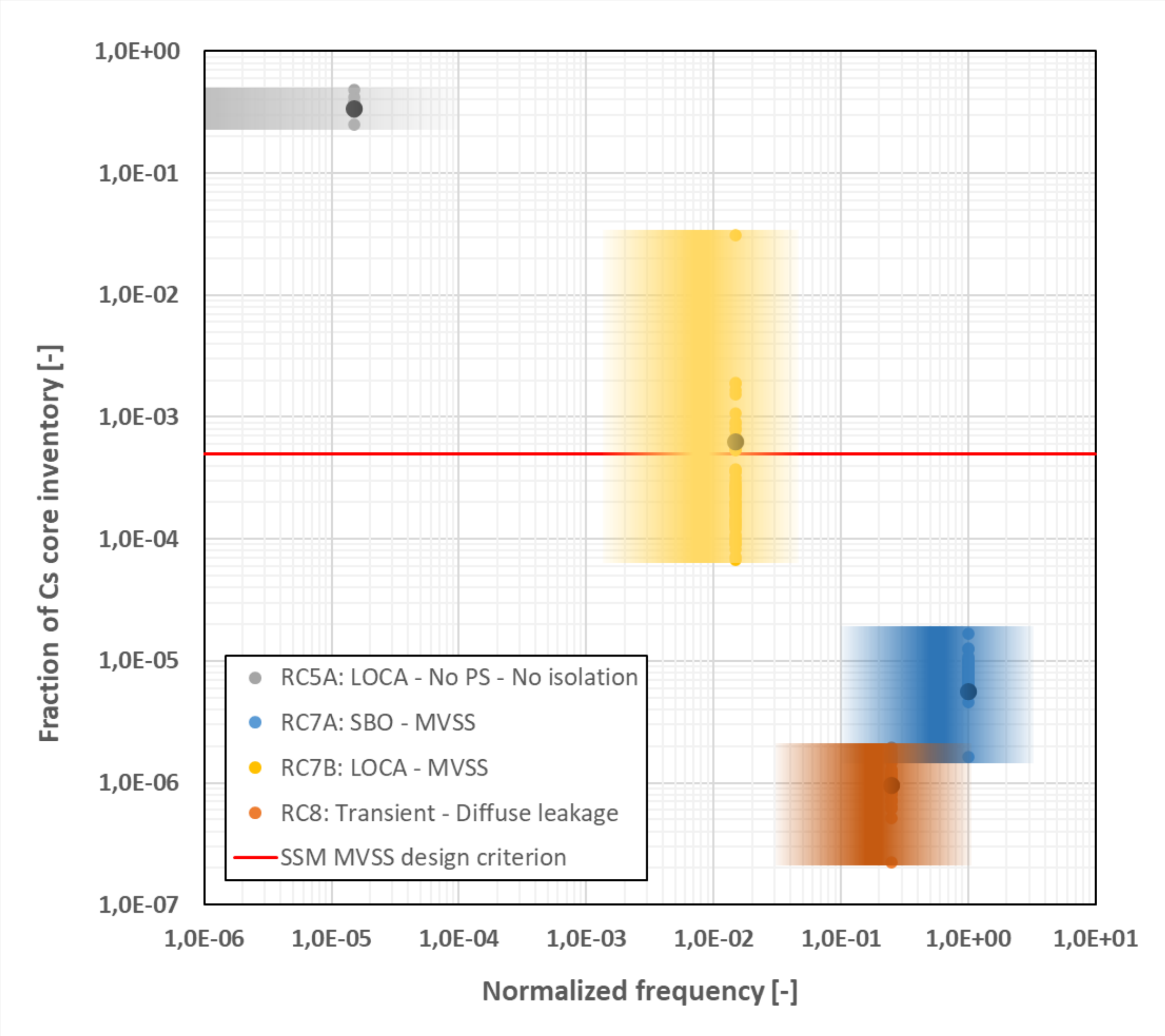

Figure 7-43. Distribution of Fraction of Cs inventory released to the environment as a function of Distribution of normalized RC frequency.

It should be noted that the MELCOR code is quite sensitive to the maximum time step used in analysis, thus, without proper sensitivity and uncertainty analysis the results should be considered as indicative. Sensitivity and uncertainty analysis is planned for the second phase of the project.

8. Discussion and conclusions.

The main goal of the first phase of the project was to identify a set of representative accident scenarios and relevant deterministic modelling parameters that can affect accident progression and the magnitude of the source term released to the environment. To achieve these goals, a set of activities has been performed that include the review of the safety design of the Swedish and Finnish BWRs; review of the PSA L2 for a typical Nordic BWR and identification of risk significant accident sequences; review of severe accident phenomena and respective modelling in the MELCOR code as well as identification of epistemic modelling parameters that can affect severe accident progression and the source term. Furthermore, the work includes the best-estimate and bounding assessments of the magnitude of fission products released to the environment.

Review of the Swedish and Finnish Nordic BWR designs and respective MELCOR modelling has been performed, to identify similarities and differences in the designs. The main differences are the reactor thermal power (larger mass of fuel/larger decay heat in Swedish BWR), gas volume in the containment and capacity of active safety systems. Another important difference in the design is the possibility of filtered containment venting from both the drywell and the wetwell in the Finnish BWR design. The filter design in itself is also different in Sweden and Finland.

Based on the review of PSA L2 for a typical Nordic BWR design, as well as insights from the emergency preparedness and response and national regulators, a set of risk significant accident sequences was selected for the analysis. The selected accident sequences include accident scenarios that lead to acceptable release (diffuse leakage from the intact containment, filtered containment venting in case of transient or LOCA), as well as scenarios that lead to unacceptable release (either due to containment rupture due to ex-vessel phenomena or unfiltered containment venting in case of failed containment isolation, or containment bypass sequences). Note that the detailed deterministic modelling of the sequences that lead to containment rupture (failure of the hatch door in the lower drywell) or containment bypass (IS-LOCA, un-isolated break in MSLs or transient with failed isolation of MSLs) require detailed modelling of the systems and structures located outside the containment to obtain more realistic/less conservative results. Current results, e.g., for RC4A or RC4B release categories, can be considered as conservative, and can be refined in the latter phases of the project.

In total, 50 MELCOR code parameters were selected for further analysis based on the review of the MELCOR modelling of severe accident phenomena and uncertain epistemic (phenomenological) modelling parameters that can affect severe accident progression and the source term released to the environment. These parameters involved in the modelling of core degradation and relocation, fission products release from fuel, debris behaviour in the core region and vessel lower head, vessel lower head failure, fission products behaviour in the RCS and the containment, as well as modelling of the filter trapping, containment sprays and pool scrubbing.

Preliminary screening of the MELCOR code modelling parameters and accident scenarios was performed using best-estimate + bounding assessment, where modelling parameters were varied one-at-a-time from the default (or best-estimate) value to the minimum/maximum values on the specified ranges, which results in 74 MELCOR code evaluations per accident scenario for VG/KTH. MELCOR code calculations performed by VTT include intermediate values of some parameters, which resulted in 166 code evaluations per accident scenario.

The results of VG MELCOR calculations are summarized in Figure 7-43, which illustrate, based on typical L2 PSA results and the simulations performed in this work, a normalized frequency uncertainty distribution of RC7A (SBO), RC8, RC7B (LOCA) and RC5 release categories, together with their respective spread of the fraction of Cs core inventory released to the environment. The spread and distribution along the frequency axis is subject to limitations and assumptions in L1 & L2 PSA parametric uncertainty analysis while the Cs release axis uncertainty the result of the best-estimate + bounding analysis. The results show that all simulations performed for RC7A (SBO), RC8 and RC5 are within prescribed limits for respective release categories, i.e. RC7A (SBO) and RC8 belong to acceptable release category according to the SSM MVSS design criterion, and RC5 belongs to large early release. Simulations performed for RC7B (LOCA) show that in some MELCOR calculations the fraction of Cs core inventory released to the environment exceed the design criterion.

Furthermore, the results indicate that the importance of different modelling parameters depend on the accident scenario, for instance, the most influential parameter for RC7B is IDEJ (the mode of debris ejection from the vessel), while for RC7A other parameters, such as CHI (Aerosol dynamic shape factor), GAMMA (Aerosol agglomeration shape factor), STICK (aerosol particles sticking probability) have significant influence on the fraction of Cs released to the environment. MELCOR simulations performed for RC8 (recovered SBO) scenario show that the Cs release is larger in scenarios where ECCS recovery does not prevent vessel lower head failure and debris ejection from the vessel (10 out 74 cases predict vessel lower head failure if ECCS and containment sprays recover after 2 hours after initiating event). Simulation results for RC5A (LOCA with deteriorated PS function and failed containment isolation) show that the uncertainty in the Cs release is relatively small, and mostly limited to PDPor (particulate debris porosity).

VTT simulations of RC7A scenario (unmitigated SBO) showed that almost all the sensitivity cases caused smaller Cs release than the reference case. Therefore, the relative difference between the cases was studied by comparing the calculated values to the median values of all the calculations. In most cases, the effect of the parameter variations on the FCV opening times appears to be small. Some larger deviations can be observed in the variations of parameters SC710641, CORNSBLD, VFALL, HFRZSS, HFRZZR, SC11412 and DECAYH. The most notable deviation occurs when VFALL = 0.01. However, a closer look reveals that the LHF occurs around the same time as in the other cases (t = 5980 s) and that the delay in the start of FCV is caused by the slow accumulation of melt in the lower head. The melt ejection does not begin before there is at least 5000 kg of melt in the lower plenum, or at least 10 % of the materials in the lower plenum are molten. The largest releases were obtained by reducing the DF of the filtered venting system (the MVSSDF parameter). This is an obvious result, since almost all of the Cs is released through the venting system, and the role of the containment leakage is very small in this scenario. In almost all cases, changing the parameter values unexpectedly resulted into lower cesium releases than in the reference case, at least a partial reason is that in the reference case, a significant amount of MCCI occurred in the pedestal, generating hydrogen and thereby increasing the flow rate through the filtered venting system. In many variant cases, little or no MCCI occurred. The severe accident management strategy of Olkiluoto 1&2 aims at preventing MCCI by flooding the pedestal before the melt ejection, but MELCOR does not have models for particle bed formation and coolability. The irregular variation of the MCCI obscures the effect of the varied parameters on the Cs release. In next year's studies, the concrete erosion will be switched off in the Cavity package in order to obtain comparable results.

The cesium release can also be observed changing rather irregularly between the variants of almost all the parameters. Due to this behavior and the lower Cs releases, it is difficult to point out which parameter variations have the highest impact on the simulation results. This result highlights that investigating the effect of certain parameters on the results would require a large number of calculations, which would allow a statistical analysis of the results to see if there is a correlation or not. Choosing any single calculation as a reference case may not be justified because all calculations involve some random variation ("numerical noise").

KTH calculations were performed for RC4B (unmitigated SBO with containment failure due to ex-vessel phenomena at RPV melt-through) and RC4A (unmitigated LOCA with containment failure due to ex-vessel phenomena at RPV melt-through). In case of LOCA, the postulated containment failure due to ex-vessel steam explosion occurs at around 2h after initiating event (the time of vessel lower head failure). The fraction of Cs released to the environment is withing ~4-15% in most of the cases. Furthermore, in case of LOCA, only a few cases lead to a larger release than the reference case. In case of SBO, the postulated containment failure due to ex-vessel steam explosion occurs at around 3h after initiating event (the time of vessel lower head failure). The difference between the timing of vessel lower head failure between LOCA and SBO scenarios is relatively small, since in case of LOCA the coolant inventory is lost through the break in the RCS, while in case of SBO, the coolant is lost due to RCS depressurization at approximately 30 min after initiating event. In case of SBO, the fraction of Cs released to the environment is within ~1-4% of the core inventory. This difference can be explained by the greater effect of suppression pool scrubbing in case of SBO.

9. Outlook

The present study showed that the MELCOR code is quite sensitive to the parameter and time step variations and results are subject to numerical noise, which makes direct interpretation of the results quite challenging, without proper statistical treatment. Such statistical treatment can be achieved by application of methods and tools for sensitivity and uncertainty analysis.

Thus, the goal of the second phase of the project will be evaluation of the sensitivity of the magnitude of the fission products release in different accident scenarios (aleatory uncertainty) to the variability in deterministic modelling parameters (epistemic uncertainty), identification of the major contributors to the uncertainty, as well as quantification of the uncertainty in the results.

The work will include a review of available literature, development and implementation of the algorithms for sensitivity analysis and uncertainty quantification with MELCOR.

The sensitivity and uncertainty calculations with MELCOR will be performed for the accident scenarios identified in the first phase of the project for both the Swedish and Finnish plant configurations. Additional dedicated codes and tools may be used to address uncertainty in specific severe accident phenomena, which are either not modelled or over-simplified in MELCOR, such as ex-vessel steam explosion and debris coolability (e.g. the ROAAM+ tool developed by KTH). Insights regarding the impact of the results on the analysis of off-site consequences and emergency preparedness and response will be provided. Furthermore, this work may include assessment of available literature as well as relevant new methods concerning source term estimation for containment bypass sequences.

Acknowledgements

NKS conveys its gratitude to all organizations and persons who by means of financial support or contributions in kind have made the work presented in this report possible.

The work performed by VG was performed with additional support from the Swedish Radiation Protection Authority (SSM).

Disclaimer

The views expressed in this document remain the responsibility of the author(s) and do not necessarily reflect those of NKS. In particular, neither NKS nor any other organisation or body supporting NKS activities can be held responsible for the material presented in this report.

References

[1] Preparedness and Response for a Nuclear or Radiological Emergency, INTERNATIONAL ATOMIC ENERGY AGENCY, 2015

[2] Actions to Protect the Public in an Emergency due to Severe Conditions at a Light Water Reactor, INTERNATIONAL ATOMIC ENERGY AGENCY, 2013

[3] Störningshandboken – BWR, SKI Rapport 03:02, 2003

[4] Nilsson L., Development of an Input Model to MELCOR 1.8.5 for Oskarshamn 3 BWR, SKI Report 2007:05, May 2006.

[5] Strandberg, M., Hydrogen Fire Risk in BWR Simulations with MELCOR. Research Report VTT-R-00669-17, 2017.

[6] Holmberg J-E., Knochenhauer M., Probabilistic Safety Goals Phase 1 – Status and Experiences in Sweden and Finland, SKI Report 2007:06.

[7] Regulatory Guide 1.174 U.S. Nuclear Regulatory Commission, Regulatory Guide 1.174, Revision 1, An Approach for using Probabilistic Risk Assessment in Risk-Informed Decisions on Plant-Specific Changes to the Licensing Basis.

[8] H. Bateman, The solution of a system of differential equations occurring in the theory of radioactive transformations, Proc. Cambridge Philos. Soc. 15 (1910) 423–427.

[9] REGULATORY GUIDE 1.183, ALTERNATIVE RADIOLOGICAL SOURCE TERMS FOR EVALUATING DESIGN BASIS ACCIDENTS AT NUCLEAR POWER REACTORS, U.S. NRC., 2000.

[10] L.L. Humphries, B.A. Beeny, F. Gelbard, T. Haskin, D.L. Louie, J. Phillips, R.C. Schmidt, MELCOR Computer Code Manuals Vol. 2: Reference Manual Version 2.2.18019, SAND2021-0241 O, 2021.

[11] L.L. Humphries, B.A. Beeny, F. Gelbard, D.L. Louie, J. Phillips, MELCOR Computer Code Manuals Vol. 1: Primer and Users' Guide Version 2.2.19018, SAND2021-0252 O, 2021.

[12] Kyle Ross, Jesse Phillips, Randall O. Gauntt, Kenneth C. Wagner, MELCOR Best Practices as Applied in the State-of-the-Art Reactor Consequence Analyses (SOARCA) Project, NUREG/CR-7008, 2014.

[13] Larry Humphries, Jesse Phillips, Rod Schmidt, Brad Beeny, David Louie, and Nate Bixler, MELCOR Code Change History: Revision 14959 to 18019, SAND2020-14302. 2020.

[14] Sergey Galushin, Pavel Kudinov, Analysis of the effect of MELCOR modelling parameters on in-vessel accident progression in Nordic BWR, Nuclear Engineering and Design, Volume 350, 2019, Pages 243-258, ISSN 0029-5493, https://doi.org/10.1016/j.nucengdes.2019.04.040.

[15] Sergey Galushin, Pavel Kudinov, Sensitivity and uncertainty analysis of the vessel lower head failure mode and melt release conditions in Nordic BWR using MELCOR code, Annals of Nuclear Energy, Volume 135, 2020, 106976, ISSN 0306-4549, https://doi.org/10.1016/j.anucene.2019.106976.

[16] SARNET Technical Report, In-Vessel Core Degradation in Water-Cooled Reactor Severe Accidents, State-of-the-Art Report Update, (CoreSOAR), 1996-2018, SARNET Report No. SARNET-CoreSOAR-D3, 2018.

[17] Magallon, D., Characteristics of corium debris bed generated in large-scale fuel-coolant interaction experiments. Nuclear Engineering and Design 236 (2006)

[18] V. F. Urbanic and T. R. Heidrich, "High-Temperature Oxidation of Zircaloy-2 and Zircaloy-4 in Steam," J. Nuc. Matls., 75, pp. 251-261 (1978).

[19] P. Darnowski, P. Mazgaj, M. Włostowski, Uncertainty and Sensitivity Analysis of the In-Vessel Hydrogen Generation for Gen-III PWR and Phebus FPT-1 with MELCOR 2.2. Energies 2021, 14, 4884. https://doi.org/10.3390/en14164884.

[20] R. O. Gauntt, N. E. Bixler, and K. C. Wagner, An Uncertainty Analysis of the Hydrogen Source Term for a Station Blackout Accident in Sequoyah Using MELCOR 1.8.5, SAND2014-2210.

[21] Sandia National Laboratories (SNL), NUREG/CR-5582: Lower Head Failure Experiments and Analyses, 1998.

[22] Rempe, J.L., Chavez, S.A., Thinnes, G.L., Allison, C.M., Korth, G.E., Witt, R.J., Sienicki, J.J., Wang, S.K., Stickler, L.A., Heath, C.H., Snow, S.D., 1993. Light Water Reactor Lower Head Failure Analysis, NUREG/CR-5642, EGG-2618. Idaho National Engineering Laboratory, USA.

[23] Martin, C.T., 2013. Coupled 3D Thermomechanical Analysis of Nordic BWR Lower Head Failure Master Thesis. Royal Institute of Technology, Stockholm.

[24] Villanueva, W., Tran, C.-T., Kudinov, P., 2012. Coupled thermo-mechanical creep analysis for boiling water reactor pressure vessel wall lower head. Nucl. Eng. Design 249, 146–153.

[25] NKS-R Report, "Scenarios and Phenomena Affecting Risk of Containment Failure and Release Characteristics", NKS-428, ISBN 978-87-7893-518-2.

[26] NEA, State-of-the-Art Report on Nuclear Aerosols, NEA/CSNI/R(2009)5.

[27] P. Mattie, R. Gauntt, K. Ross, N. Bixler, D. Osborn, C. Sallaberry, and J. Jones, State-of-the-Art Reactor Consequence Analyses Project Uncertainty Analysis of the Unmitigated Long-Term Station Blackout of the Peach Bottom Atomic Power Station, NUREG/CR-7155, SAND2012-10702P.

[28] Bruno Gonfiotti and Sandro Paci, Stand-Alone Containment Analysis of the Phébus FPT Tests with the ASTEC and the MELCOR Codes: The FPT-0 Test, Science and Technology of Nuclear Installations Volume 2017, Article ID 1450648, 25 pages https://doi.org/10.1155/2017/1450648.

[29] Randall O. Gauntt, Tracy Radel, Michael A. Salay, and Donald A. Kalinich, Analysis of Main Steam Isolation Valve Leakage in Design Basis Accidents Using MELCOR 1.8.6 and RADTRAD, SAND2008-6601.

[30] T. G. Theofanous, "On Proper Formulation of Safety Goals and Assessment of Safety Margins for Rare and High-Consequence Hazards," Reliability Engineering and System Safety, 54, pp.243-257, (1996).

[31] S. Galushin, P. Kudinov, "Comparison of Vessel Failure Mode and Melt Release Conditions in Unmitigated and Mitigated Station Blackout Scenarios in Nordic BWR using MELCOR code", ICONE-27, 27th International Conference on Nuclear Engineering, Tsukuba, Ibaraki, Japan, May 19-24, 2019.

[32] S. Galushin, P Kudinov "Uncertainty Analysis of Vessel Failure Mode and Melt Release in Station Blackout Scenario in Nordic BWR Using MELCOR Code." 18th International Topical Meeting on Nuclear Reactor Thermal Hydraulics (NURETH-18), Portland, OR, USA, August 18-22, (2019).

[33] P. Kudinov, S. Galushin, D. Grishchenko, S. Yakush, "Development of Risk Oriented Accident Analysis Methodology (ROAAM+) for Assessment of Ex-Vessel Severe Accident Management Effectiveness", 18th International Topical Meeting on Nuclear Reactor Thermal Hydraulics (NURETH-18), Portland, OR, USA, August 18-22, (2019).

[34] D. A. Powers, S. B. Burson, "A Simplified Model of Aerosol Removal by Containment Sprays", NUREG/CR-5966, 1993.

[35] L.E. Herranz, M.J. Escudero, V. Peyrés, J. Polo, J.López-Jiménez, Review and assessment of pool scrubbing models, Informes Técnicos Ciemat 784, Enero 1996

[36] P. C. Owczarski, K. W. Burk, SPARC-90: A Code for Calculating Fission Product Capture in Suppression Pools, NUREG/CR5765. 1991.

[37] A. Saltelli, S. Tarantola, F. Campolongo and M. Ratto, "Sensitivity Analysis in Practice. A Guide to assessing scientific models". John Wiley & Sons Ltd, The Atrium, Southern Gate, Chichester, West Sussex PO19 8SQ, England. 2004.

[38] F. Campolongo, J. Cariboni, A. Saltelli, An effective screening design for sensitivity analysis of large models, Environmental Modelling & Software, Volume 22, Issue 10, 2007, Pages 1509-1518, ISSN 1364-8152. 2007.

[39] Adams, B.M., et al., Dakota, A Multilevel Parallel Object-Oriented Framework for Design Optimization, Parameter Estimation, Uncertainty Quantification, and Sensitivity Analysis: Version 6.0 Reference Manual. 2014, Sandia National Laboratories. (2014).

[40] Troy C. Haskin, The MELCOR Plot File Format, SAND2018-9566, 2018.

[41] L. Soffer, S. B. Burson, CM. Ferrell, R. Y. Lee, J. N. Ridgely, Accident Source Terms for Light-Water Nuclear Power Plants, NUREG-1465, 1995.

[42] Per Olof Nilsson, FILTRA-MVSS (Multi MVSS (Multi Venturi Venturi Scrubber System), Presentation to U.S. NRC, Washington DC, October 11, 2012.

[43] K. Ross, N. Bixler, S. Weber, C. Sallaberry, and J. Jones, State-of-the-Art Reactor Consequence Analyses Project. Uncertainty Analysis of the Unmitigated Short-Term Station Blackout of the Surry Power Station, draft report.

[44] Renaud Meignen, Stephane Picchi, Julien Lamome, Bruno Raverdy, Sebastian Castrillon Escobar, Gregory Nicaise, 2014, The challenge of modeling fuel–coolant interaction: Part I – Premixing, Nuclear Engineering and Design, Volume 280, pp. 511-527.

[45] Kwang-Il Ahn, Sun-Hee Park, Hee-Dong Kim, Hyun Sun Park, 2012, The plant-specific uncertainty analysis for an ex-vessel steam explosion-induced pressure load using a TEXAS–SAUNA coupled system, Nuclear Engineering and Design, Volume 249, pp. 400-412.

[46] Matjaž Leskovar, Mitja Uršič, 2016, Ex-vessel Steam Explosion Analysis for Pressurized Water Reactor and Boiling Water Reactor, Nuclear Engineering and Technology, Volume 48, Issue 1, pp. 72-86.

[47] Renaud Meignen, Bruno Raverdy, Michael Buck, Georg Pohlner, Pavel Kudinov, Weimin Ma, Claude Brayer, Pascal Piluso, Seong-Wan Hong, Matjaž Leskovar, Mitja Uršič, Giancarlo Albrecht, Ilona Lindholm, Ivan Ivanov, 2014, Status of steam explosion understanding and modelling, Annals of Nuclear Energy, Volume 74, pp. 125-133.

[48] Longkun He, Pengfei Liu, Bo Kuang, 2021, Jet Fragmentation Characteristics During Molten Fuel and Coolant Interactions, Nuclear Science and Engineering, Volume 195, Issue 4, pp. 367-390.

[49] T.N. Dinh, V.A. Bui, R.R. Nourgaliev, J.A. Green, B.R. Sehgal, 1999, Experimental and analytical studies of melt jet-coolant interactions: a synthesis, Nuclear Engineering and Design, Volume 189, Issues 1–3, pp. 299-327.

[50] M. Bürger, S.H. Cho, E.v. Berg, A. Schatz, 1995, Breakup of melt jets as pre-condition for premixing: Modeling and experimental verification, Nuclear Engineering and Design, Volume 155, Issues 1–2, pp. 215-251.

[51] E.v. Berg, M. Bürger, S.H. Cho, A. Schatz, 1994, Modeling of the breakup of melt jets in liquids for LWR safety analysis, Nuclear Engineering and Design, Volume 149, Issues 1–3, pp. 419-429.

[52] Nuclear Energy Agency, 2015, OECD/SERENA Project Report – Summary and Conclusions, NEA/CSNI/R(2014)15.

[53] I. Huhtiniemi, D. Magallon, 2001, Insight into steam explosions with corium melts in KROTOS, Nuclear Engineering and Design, Volume 204, Issues 1–3, pp. 391-400.

[54] Renaud Meignen, Bruno Raverdy, Michael Buck, Manfred Burger, Georg Pohlner, 2012, On The Role Of Void On Steam Explosion Loads, ERMSAR, Cologne, March 21-23.

[55] Renaud Meignen, Bruno Raverdy, Stephane Picchi, Julien Lamome, 2014, The challenge of modeling fuel–coolant interaction: Part II – Steam explosion, Nuclear Engineering and Design, Volume 280, pp. 528-541.

[56] J.H. Song, I.K. Park, Y.S. Shin, J.H. Kim, S.W. Hong, B.T. Min, H.D. Kim, 2003, Fuel coolant interaction experiments in TROI using a UO2/ZrO2 mixture, Nuclear Engineering and Design, Volume 222, Issue 1, pp. 1-15.

[57] Mitja Uršič, Matjaž Leskovar, Borut Mavko, 2012, Simulations of KROTOS alumina and corium steam explosion experiments: Applicability of the improved solidification influence modelling, Nuclear Engineering and Design, Volume 246, pp. 163-174.

[58] S.J. Board, R.W. Hall, 1976, Recent Advances in Understanding Large Scale Vapour Explosions, In: Third Specialist Meeting on Sodium Fuel Interactions in Fast Reactors, Tokyo, March.

[59] D.F. Fletcher, 1995, Steam explosion triggering: a review of theoretical and experimental investigations, Nuclear Engineering and Design, Volume 155, Issues 1–2, pp. 27-36.

[60] L. Manickam, 2018, An Experimental Study on Melt Fragmentation, Oxidation and Steam Explosion during Fuel Coolant Interactions, KTH Royal Institute of Technology, Sweden, PhD Thesis.

[61] Roberta Concilio Hansson, 2010, An Experimental Study on the Dynamics of a Single Droplet Vapor Explosion, KTH Royal Institute of Technology, Sweden, PhD Thesis.

[62] Gaby Ciccarelli, David L. Frost, 1994, Fragmentation mechanisms based on single drop steam explosion experiments using flash X-ray radiography, Nuclear Engineering and Design, Volume 146, Issues 1–3, pp. 109-132.

[63] B. Kim, M.L. Corradini, 1988, Modeling of Small-Scale Single Droplet Fuel/Coolant Interactions, Nuclear Science and Engineering, Volume 98, Issue 1, pp. 16-28.

[64] Akira Inoue, Masanori Aritomi,Minoru Takahashi, Yoshiharu Tomita, 1992, An Analytical Model On Vapor Explosion Of A High Temperature Molten Metal Drop In Water Induced By A Pressure Pulse, Chemical Engineering Communications, Volume 118, Issue 1, pp. 189-206.

[65] Moon Kyu Hwang, Hee Dong Kim, 1999, Steam explosion studies review, KAERI/AR--534/99.

[66] I Huhtiniemi, D Magallon, H Hohmann, 1999, Results of recent KROTOS FCI tests: alumina versus corium melts, Nuclear Engineering and Design, Volume 189, Issues 1–3, pp. 379-389.

[67] Magallon, D, Huhtiniemi, I, Annunziato, A, Yerkess, A, Hohmann, Y H. 1996, Status of the FARO/KROTOS melt-coolant interactions tests, NUREG/CP--0149-VOL.2.

[68] Pavel Kudinov, Dmitry Grishchenko, Alexander Konovalenko, Aram Karbojian, 2017, Premixing and steam explosion phenomena in the tests with stratified melt-coolant

configuration and binary oxidic melt simulant materials, Nuclear Engineering and Design, Volume 314, pp. 182-197.

[69] Pavel Kudinov,Aram Karbojian,Weimin Ma, Truc-Nam Dinh, 2010, The DEFOR-S Experimental Study of Debris Formation with Corium Simulant Materials, Nuclear Technology, Volume 170, Issue 1, pp. 219-230.

[70] X Chen, W.W Yuen, T.G Theofanous, 1997, On the constitutive description of the microinteractions concept in steam explosions, Nuclear Engineering and Design, Volume 177, Issues 1–3, pp. 303-319.

[71] W.W. Yuen, T.G. Theofanous, 1995, The prediction of 2D thermal detonations and resulting damage potential, Nuclear Engineering and Design, Volume 155, Issues 1–2, pp. 289-309.

[72] C. Brayer, G. Berthoud, 1998, First vapor explosion calculations performed with MC3D thermal-hydraulic code, JAERI-Conf--97-011.

[73] Jian Tang, 1993, Modeling of the complete process of one-dimensional vapor explosions, The University of Wisconsin – Madison, PhD Thesis.

[74] Georges Berthoud, Luc Gros D'Aillon, 2009, Film boiling heat transfer around a very high temperature thin wire immersed into water at pressure from 1 to 210bar: Experimental results and analysis, International Journal of Thermal Sciences, Volume 48, Issue 9, pp. 1728-1740.

[75] Pavel Kudinov, Dmitry Grishchenko, Alexander Konovalenko, A. Karbojian, Sevostian Bechta, 2014, Investigation of Steam Explosion in Stratified Melt-Coolant Configuration, In: The 10th International Topical Meeting on Nuclear Thermal-Hydraulics, Operation and Safety (NUTHOS-10) Okinawa, Japan, December 14-18.

[76] Dmitry Grishchenko, Alexander Konovalenko, A. Karbojian, Valtyna Kudinova, Sevostian Bechta, Pavel Kudinov, 2013, Insight into steam explosion in stratified melt-coolant configuration, In: 15th International Topical Meeting on Nuclear Reactor Thermal Hydraulics, Italy.

[77] Saidur Rahman, 2013, Coolability of corium debris under severe accident conditions in light water reactors, University of Stuttgart, PhD Thesis.

[78] Sergey Yakush, Alexander Konovalenko, Simone Basso, Pavel Kudinov, 2015, Effect Of Particle Spreading On Coolability Of Ex-Vessel Debris Bed, In: 16th International Topical Meeting on Nuclear Reactor Thermal Hydraulics, Chicago.

[79] K. Hu, T.G. Theofanous, 1991, On the measurement and mechanism of dryout in volumetrically heated coarse particle beds, International Journal of Multiphase Flow, Volume 17, Issue 4, pp. 519-532.

[80] R.J. Lipinski, 1982, Model for boiling and dryout in particle beds (LMFBR), NUREG/CR—2646.

[81] Sachin Thakre, Liangxing Li, Weimin Ma, 2014, An experimental study on coolability of a particulate bed with radial stratification or triangular shape, Nuclear Engineering and Design, Volume 276, pp. 54-63.

[82] V.X. Tung, H.X. Vu, V.K. Dhir, 1985, Quenching of debris beds having variable permeability in the axial and radial directions, In: 3rd International Topical Meeting on Nuclear Reactor Thermal Hydraulics, Newport, USA.

[83] N.K. Tutu, T. Ginsberg, J. Klein, J. Klages, C.E. Schwarz, 1984, Debris bed quenching under bottom flood conditions (in-vessel degraded core cooling phenomenology), NUREG/CR—3850.

[84] Patrick Schäfer, Manfred Groll, Rudi Kulenovic, 2006, Basic investigations on debris cooling, Nuclear Engineering and Design, Volume 236, Issues 19–21, pp. 2104-2116.

[85] Nourdine Chikhi, F. Fichot, 2017, Experimental and theoretical study of large scale debris bed reflood in the PEARL facility, Nuclear Engineering and Design, Volume 312, pp. 48-58.

[86] G. Hofmann, On the Location and Mechanisms of Dryout in Top-Fed and Bottom-Fed Particulate Beds, Nuclear Technology, Volume 65, Issue 1, pp. 36-45.

[87] Manfred Bürger, Michael Buck, Werner Schmidt, Walter Widmann, 2006, Validation and application of the WABE code: Investigations of constitutive laws and 2D effects on debris coolability, Nuclear Engineering and Design, Volume 236, Issues 19–21, pp. 2164-2188.

[88] Weimin Ma, Nam Dinh, Michael Buck, Manfred Burger, 2007, Analysis Of The Effect Of Bed Inhomogeneity On Debris Coolability, In: The Proceedings of the International Conference on Nuclear Engineering (ICONE), ICONE15-10752.

[89] W. Schmidt, 2004, Influence of multidimensionality and interfacial friction on the coolability of fragmented corium, University of Stuttgart, PhD Thesis.

[90] Eveliina Takasuo, 2016, A summary of studies on debris bed coolability and multi-dimensional flooding, NKS-374.

[91] E. Takasuo, S. Holmstrom, T. Kinnunen, P.H. Pankakoski, V. Hovi, M. Ilvonen, S. Rahman, M. Burger, M. Buck, G. Pohlner, 2012, Experimental and computational studies of the coolability of heap-like and cylindrical debris beds, ERMSAR, Cologne, March 21-23.

[92] Eveliina Takasuo, Stefan Holmström, Tuomo Kinnunen, Pekka H. Pankakoski, 2012, The COOLOCE experiments investigating the dryout power in debris beds of heap-like and cylindrical geometries, Nuclear Engineering and Design, Volume 250, pp. 687-700.

[93] Eveliina Takasuo, Stefan Holmström, Tuomo Kinnunen, Pekka H. Pankakoski, Ensio Hosio, Ilona Lindholm, 2011, The effect of lateral flooding on the coolability of irregular core debris beds, Nuclear Engineering and Design, Volume 241, Issue 4, pp. 1196-1205.

[94] A. Karbojian, W.M. Ma, P. Kudinov, T.N. Dinh, 2009, A scoping study of debris bed formation in the DEFOR test facility, Nuclear Engineering and Design, Volume 239, Issue 9, pp. 1653-1659.

[95] Pavel Kudinov, Aram Karbojian, Chi-Thanh Tran, Walter Villanueva, 2013, Agglomeration and size distribution of debris in DEFOR-A experiments with Bi2O3–WO3 corium simulant melt, Nuclear Engineering and Design, Volume 263, pp. 284-295.

[96] Pavel Kudinov, A. Karbojian, Chi-Thanh Tran, Walter Villanueva, 2013, Experimental Data on Fraction of Agglomerated Debris Obtained in the DEFOR-A Melt-Coolant Interaction Tests with High Melting Temperature Simulant Materials, Nuclear Engineering and Design, Volume 263, pp. 284-295.

[97] P. Kudinov, M. Davydov, 2014, Development of Surrogate Model for Prediction of Corium Debris Agglomeration, In: International Congress on Advances in Nuclear Power Plants, pp. 1146-1155

[98] P. Kudinov, M. Davydov, 2013, Development and validation of conservative-mechanistic and best estimate approaches to quantifying mass fractions of agglomerated debris, Nuclear Engineering and Design, Volume 262, pp. 452-461.

[99] Eveliina Takasuo, 2015, Coolability of porous core debris beds: Effects of bed geometry and multi-dimensional flooding, VTT Technical Research Centre of Finland Ltd, PhD Thesis.

[100] Eveliina Takasuo, 2016, An experimental study of the coolability of debris beds with geometry variations, Annals of Nuclear Energy, Volume 92, pp. 251-261.

[101] S.E. Yakush, N.T. Lubchenko, Pavel Kudinov, 2012, Risk-informed approach to debris bed coolability issue, In: 20th International Conference On Nuclear Engineering And The ASME 2012 Power Conference, Volume 2, ASME Press, pp. 531-543.

[102] Sergey Yakush, Nazar Lubchenko, Pavel Kudinov, 2013, Surrogate Models for Debris Bed Dryout, In: 15th International Topical Meeting on Nuclear Reactor Thermal Hydraulics.

[103] Sergey Yakush, Pavel Kudinov, 2011, Effects of Water Pool Subcooling on the Debris Bed Spreading by Coolant Flow, In: International Congress on Advances in Nuclear Power Plants.

[104] Sergey Yakush, Pavel Kudinov, 2009, Simulation of Ex-Vessel Debris Bed Formation and Coolability in a LWR Severe Accident, In: Implementation of severe accident management measures, Paul Scherrer Institute.

[105] Sergey Yakush, Pavel Kudinov, Nam Truc Dinh, 2009, Multiscale Simulations of Self-organization Phenomena in the Formation and Coolability of Corium Debris Bed, In: 13th International Topical Meeting on Nuclear Reactor Thermal Hydraulics.

[106] E.L. Gluekler, L.Jr. Baker, 1977, Post-accident heat removal in LMFBRs, In: Winter annual meeting of the American Society of Mechanical Engineers, Atlanta, USA, GEFR-SP—023.

[107] Simone Basso, Alexander Konovalenko, Pavel Kudinov, 2014, Development of scalable empirical closures for self-leveling of particulate debris bed, In: International Congress on Advances in Nuclear Power Plants.

[108] Alvarez, D., Amblard, M., 1982, Fuel levelling, In: 5th Information Exchange Meeting on Post-Accident Debris Cooling, Karlsruhe, Germany.

[109] J.D. Gabor, 1974, Simulation Experiments for Internal Heat Generation, In: Reactor Development Program Progress Report ANL-RDP-32, Argonne, USA.

[110] Simone Basso, Alexander Konovalenko, S.E. Yakush, Pavel Kudinov, 2016, The effect of self-leveling on debris bed coolability under severe accident conditions, Nuclear Engineering and Design, Volume 305, pp. 246-259.

[111] Simone Basso, Alexander Konovalenko, Pavel Kudinov, 2016, Effectiveness of the debris bed self-leveling under severe accident conditions, Annals of Nuclear Energy, Volume 95, pp. 75-85.

[112] Alexander Konovalenko, Simone Basso, Aram Karbojian, Pavel Kudinov, 2012, Experimental and Analytical Study of the Particulate Debris Bed Self-leveling, In: 9th International Topical Meeting on Nuclear Thermal Hydraulics, Operation and Safety, Kaohsiung, Taiwan, September 9-13.

[113] P. Kudinov, A. Konovalenko, D. Grishchenko, S. Yakush, S. Basso, N. Lubchenko, A. Karbojian, 2013, Investigation of debris bed formation, spreading and coolability, NKS—287.

[114] Simone Basso, 2017, Particulate Debris Spreading and Coolability, KTH Royal Institute of Technology, Stockholm, PhD Thesis.

[115] Zheng Huang, 2019, Numerical Investigations on Debris Bed Coolability and Mitigation Measures in Nordic Boiling Water Reactors, KTH Royal Institute of Technology, Stockholm, PhD Thesis.

[116] Keiji Miyazaki, Kenji Murai, Toshihiro Ohama, Nobuo Yamaoka, Shoji Inoue, 1986, Dryout Heat Flux for Core Debris Bed, (I): Effects of System Pressure and Particle Size, Journal of Nuclear Science and Technology, Volume 23, Issue 8, pp. 702-710.

[117] D. Squarer, A.T. Pieczynski, L.E. Hochreiter, 1982, Effect of Debris Bed Pressure, Particle Size, and Distribution on Degraded Nuclear Reactor Core Coolability, Nuclear Science and Engineering, Volume 80, Issue 1, pp. 2-13.

[118] A.W. Reed, K.R. Boldt, E.D. Gorham-Bergeron, R.J. Lipinski, T.R. Schmidt, 1985, DCC-1/DCC-2 degraded core coolability analysis, NUREG/CR--4390-R3.

[119] T.N. Dinh, W.M. Ma, A. Karbojian, P. Kudinov, C.T. Tran, C.R. Hansson, 2008, Ex-Vessel corium coolability and steam explosion energetics in nordic light water reactors, NKS-160, Denmark.

[120] M. Rashid, R. Kulenovic, E. Laurien, A.K. Nayak, 2011, Experimental results on the coolability of a debris bed with multidimensional cooling effects, Nuclear Engineering and Design, Volume 241, Issue 11, pp. 4537-4543.

[121] M. Rashid, R. Kulenovic, E. Laurien, 2012, Experimental results on the coolability of a debris bed with down comer configurations, Nuclear Engineering and Design, Volume 249, pp. 104-110.

[122] K. Atkhen, G. Berthoud, 2006, SILFIDE experiment: Coolability in a volumetrically heated debris bed, Nuclear Engineering and Design, Volume 236, Issues 19–21, pp. 2126-2134.

[123] Weimin Ma, Truc-Nam Dinh, Michael Buck, Manfred Burger, 2007, Analysis of the effect of bed inhomogeneity on debris coolability, In: 15th International Conference on Nuclear Engineering.

[124] G. Hofmann, L. Barleon, 1986, Reduced coolability of particle beds as a result of capillary effects at horizontal phase boundaries, In: International ANS/ENS topical meeting on thermal reactor safety, San Diego, USA.

[125] S.E. Yakush, Pavel Kudinov, 2014, A model for prediction of maximum post-Dryout temperature in decay-heated debris BED, In: International Conference on Nuclear Engineering.

[126] B.R. Sehgal, 2012, Nuclear Safety in Light Water Reactors, Academic Press.

[127] Nuclear Energy Agency, 2017, State-of-the-Art Report on Molten Corium Concrete Interaction and Ex-Vessel Molten Core Coolability, NEA No. 7392.

[128] Hideo Nagasaka, Isao Sakaki, Masami Kato, Y. Vasilyev, A. Kolodeshnikov, V. Zhdanov, 2000, COTELS project (3): ex-vessel debris cooling tests, FZKA—6475.

[129] 2020, Chapter: Core Concrete Interaction, In: Comprehensive Nuclear Materials, Rudy Konings, Roger Stoller (Eds), Elsevier.

[130] D.A. Powers, F.E. Arellano, 1982, Large-Scale, Transient Tests of the Interaction of Molten Steel with Concrete, SAND 81-1753, NUREG/CR-2282.

[131] J.E. Gronager, A.J. Suo-Anttila, D.R. Bradley, J.E. Brockmann, 1986, TURC1: large scale metallic melt-concrete interaction experiments and analysis, NUREG/CR-4420; SAND-85-0707.

[132] E.R. Copus, J.E. Brockmann, R.B. Simpson, D.A. Lucero, R.E. Blose, 1992, Core-concrete interactions using molten urania with zirconium on a limestone concrete basemat, NUREG/CR-5443; SAND-90-0087.

[133] M.T. Farmer, W.S. Lomperski, Subhasis Basu, 2005, The results of the CCI-2 reactor material experiment investigating 2-D core-concrete interaction and debris coolability, In: 11th International Topical Meeting On Nuclear Reactor Thermal Hydraulics, Avignon, France.

[134] M.T. Farmer, W.S. Lomperski, Subhasis Basu, 2006, The Results of the CCI-3 Reactor Material Experiment Investigating 2-D Core-Concrete Interaction and Debris Coolability with a Siliceous Concrete Crucible, In: International Congress on Advances in Nuclear Power Plants, Reno, USA.

[135] Journeau, Ch., Piluso, P., Haquet, J.F., Aubert-Saldo, V., Brissonneau, L., 2007, Behaviour of nuclear reactor pit concretes under severe accident conditions, In: International Conference On Concrete Under Severe Conditions Of Environment And Loading, France.

[136] Hans Alsmeyer, Michel Cranga, Rene Fabianelli, Ivan Ivanov, Guena Doubleva, 2005, The COMET-L1 experiment on long-term concrete erosion and surface flooding, In: 11th International Topical Meeting On Nuclear Reactor Thermal Hydraulics, Avignon, France.

[137] J.K. Fink, D.H. Thompson, B.W. Spencer, B.R. Sehgal, 1995, Aerosol and melt chemistry in the ACE molten core-concrete interaction experiments, High Temperature and Materials Science, Volume 33, Issue 1.

[138] Bouyer, V., Journeau, C., Haquet, J. F., Piluso, P., Nakayoshi, A., Ikeuchi, H., Washiya, T., Kitagaki, T., 2019, Large scale VULCANO molten core concrete interaction test considering Fukushima Daiichi condition, ERMSAR, Prague, Czech Republic.

[139] D.R. Bradley, D.R. Gardner, J.E. Brockmann, R.O. Griffith, 1993, CORCON-MOD3: An integrated computer model for analysis of molten core-concrete interactions. User`s manual, NUREG/CR-5843; SAND-92-0167.

[140] M. Bottin, 2015, Molten Corium Concrete Interaction investigation of convective heat transfer in a pool with gas sparging, ERMSAR, Marseille, France.

[141] J.M. Bonnet, 2000, Thermal hydraulic phenomena in corium pools for ex-vessel situations: the BALI experiment, In: OECD Workshop on ex-vessel debris coolability, Karlsruhe, Germany.

[142] Christophe Journeau, Jean-François Haquet, 2009, Convection heat transfer anisotropy in a bubbling viscous pool—Application to molten core–concrete interaction, Nuclear Engineering and Design, Volume 239, Issue 2, pp. 389-394.

[143] T. Sevón, 2005, Molten core - Concrete interactions in nuclear accidents theory and design of an experimental facility, VTT TIEDOTTEITA ñ RESEARCH NOTES 2311.

[144] A.R. Marklund, S. Galushin, O. Bäckström, Scenarios and Phenomena Affecting Risk of Containment Failure and Release Characteristics (NKS-SPARC), NKS-428, ISBN 978-87-7893-518-2, 23 Oct 2019.

Bibliographic Data Sheet **NKS-461**

Title	Source Term And Timing Uncertainty in Severe Accidents
Author(s)	Sergey Galushin[1], Anders Riber Marklund[1] Dmitry Grischenko[2], Pavel Kudinov[2] Tuomo Sevón[3], Sara Ojalehto[3], Ilona Lindholm[3] Patrick Isaksson[4], Elisabeth Tengborn[4] Naeem Ul-Syed[5]
Affiliation(s)	[1] Vysus Sweden AB [2] KTH Royal Institute of Technology [3] VTT Technical Research Centre of Finland Ltd [4] SSM Swedish Radiation Safety Authority [5] DSA Norwegian Radiation and Nuclear Safety Authority
ISBN	978-87-7893-554-0
Date	July 2022
Project	NKS-R / STATUS
No. of pages	132
No. of tables	18
No. of illustrations	58
No. of references	144
Abstract max. 2000 characters	One set of representative accident scenarios and one set of relevant deterministic modelling parameters that can affect Nordic boiling water reactor (BWR) severe accident progression and the magnitude of the source term released to the environment were identified. To achieve this, a set of activities was performed, including review of the safety design of the Swedish and Finnish BWRs; review of the PSA L2 for a typical Nordic BWR and identification of risk significant accident sequences; review of severe accident phenomena and respective modelling in the MELCOR code as well as identification of epistemic modelling parameters that can affect severe accident progression and the source term. The scenario set was based on review of PSA L2 for a typical Nordic BWR design, as well as insights from the emergency preparedness and response and national regulators, including accident scenarios that lead to acceptable release (diffuse leakage from the intact containment, filtered containment venting in case of transient or LOCA), as well as scenarios that lead to unacceptable release (either due to containment rupture due to ex-vessel phenomena or unfiltered containment venting in case of failed containment isolation, or containment bypass sequences).

In total, 50 MELCOR code parameters were selected for further analysis based on the review of the MELCOR modelling of severe accident phenomena and uncertain epistemic (phenomenological) modelling parameters that can affect severe accident progression and the source term released to the environment. These parameters involved in the modelling of core degradation and relocation, fission products release from fuel, debris behaviour in the core region and vessel lower head, vessel lower head failure, fission products behaviour in the RCS and the containment, as well as modelling of the filter trapping, containment sprays and pool scrubbing.

Best-estimate and bounding assessments of the magnitude of fission products released to the environment were performed for the set of selected scenarios and parameters using MELCOR simulations performed at KTH, VTT and Vysus Group. A preliminary screening of the parameters and scenarios was performed using the obtained results and proposals for further study in phase two of the project were made.

Key words Severe accident, Source term, PSA L2, Boiling Water Reactor, MELCOR, Uncertainty analysis

Available on request from the NKS Secretariat, P.O.Box 49, DK-4000 Roskilde, Denmark.
Phone (+45) 4677 4041, e-mail nks@nks.org, www.nks.org